MUTUAL COUPLING REDUCTION IN MICROSTRIP ANTENNAS USING DEFECTED GROUND STRUCTURES

A THESIS

SUBMITTED TO THE DEPARTMENT OF ELECTRICAL AND

ELECTRONICS ENGINEERING

AND THE GRADUATE SCHOOL OF ENGINEERING AND SCIENCES

OF BILKENT UNIVERSITY

IN PARTIAL FULFILLMENT OF THE REQUIREMENTS

FOR THE DEGREE OF

MASTER OF SCIENCE

By

S. Melikşah Yayan

August 2012

I certify that I have read this thesis and that in my opinion it is fully adequate, in scope and in quality, as a thesis for the degree of Master of Science.

Assoc. Prof. Dr. Vakur B. Ertürk (Supervisor)

I certify that I have read this thesis and that in my opinion it is fully adequate, in scope and in quality, as a thesis for the degree of Master of Science.

Prof. Dr. Ayhan Altıntaş

I certify that I have read this thesis and that in my opinion it is fully adequate, in scope and in quality, as a thesis for the degree of Master of Science.

Prof. Dr. Özlem Aydın Çivi

Approved for the Graduate School of Engineering and Sciences:

Prof. Dr. Levent Onural
Director of Graduate School of Engineering and Sciences

ABSTRACT

MUTUAL COUPLING REDUCTION IN MICROSTRIP ANTENNAS USING DEFECTED GROUND STRUCTURES

S. Melikşah Yayan
M.S. in Electrical and Electronics Engineering
Supervisor: Assoc. Prof. Dr. Vakur B. Ertürk
August 2012

Mutual coupling between microstrip antenna elements (through space and surface waves) has a significant role in the performance merits of the microstrip antenna arrays. In many applications, low mutual coupling levels are desired such as bistatic radar systems where isolation is essential in order not to have any interference between the transmitter and receiver antennas. Furthermore, presence of mutual coupling among the antenna elements can affect the sidelobe levels, beam position and frequency bandwidth of arrays. Mutual coupling among the array elements usually occurs as a result of surface waves and space waves. Mutual coupling through the space waves are very strong if the array elements are very close to each other. However, they die out quickly as the separation between the array elements become larger. On the other hand, although the mutual coupling due to the surface waves are weaker than that of space waves when the array elements are close to each other, they remain as the only coupling mechanism when they are far away from each other, in particular for arrays of microstrip antennas.

In this thesis, the main goal is to reduce the mutual coupling between the microstrip antennas resulting from the surface waves by using a defected ground structure (DGS). The DGS is formed by etching either a dumbbell shape or a slotted complementary split ring resonator (SCSRR) to the part of the ground plane that remains between the microstrip antennas along their E-plane direction. It has been observed that although a considerable reduction in the mutual coupling can be achieved, the radiation patterns of the antennas are deteriorated due to a significant increase in the backlobe radiation. Hence, a reflector and a cavity combination is used to decrease the backlobe radiation to a certain level. Finally, to test the DGS in an array environment, the performance merits of a 2×2 microstrip antenna array is investigated in the presence of a dumbbell DGS, where each microstrip is backed with a cavity and a reflector. Based on both the simulations and the measurements, it has been concluded that despite the achieved mutual coupling reduction between the microstrip antennas in the array environment, the far-zone radiation patterns related merits have not been improved.

Keywords: Mutual Coupling, Space Waves, Surface Waves, Slotted Complementary Split Ring Resonators, Dumbbell, Defected Ground Structures.

ÖZET

MİKROŞERİT ANTENLERDE DEFORME TOPRAK YAPILARI KULLANARAK KARŞILIKLI BAĞLAŞIMIN AZALTILMASI

S. Melikşah Yayan
Elektrik ve Elektronik Mühendisliği Bölümü Yüksek Lisans
Tez Yöneticisi: Doç. Dr. Vakur B. Ertürk
Ağustos 2012

Mikroşerit anten elemanları arasındaki karşılıklı bağlaşımın (uzay ve yüzey dalgaları dolayısıyla) mikroşerit anten dizilerinin performansı üstüne önemli etkileri vardır. Birçok uygulamada, düşük karşılıklı bağlaşım seviyeleri istenen bir durumdur. Özellikle de bistatik radar sistemleri gibi alıcı ve verici antenlerinin birbirine yakın olduğu sistemlerde antenlerde parazit olmaması için antenler arasındaki izolasyonun yeterli seviyelerde olması gereklidir. Ayrıca, anten elemanları arasındaki karşılıklı bağlaşım, anten dizilerinin yan loplarını, huzme pozisyonunu ve frekans bant genişliğini olumsuz etkileyebilir. Dizi elemanları arasındaki karşılıklı bağlaşım genel olarak uzay ve yüzey dalgalarından kaynaklanmaktadır. Dizi elemanları birbirine çok yakın olduğu zaman, uzay dalgaları çok güçlü karşılıklı bağlaşıma yol açmaktadır fakat bu durum dizi elemanlarının arasındaki uzaklığın artmasıyla tersine dönerek uzay dalgalarının karşılıklı bağlaşıma olan etkisinin hızlıca yok olmasıyla sonuçlanmaktadır. Diğer taraftan, yüzey dalgalarının karşılıklı bağlaşıma etkisi anten elemanları birbirine yakın olduğu zaman uzay dalgalarından daha zayıf olsa da yüzey dalgaları, dizi elemanlarının arası açık olduğu zaman karşılıklı bağlaşıma etki eden dominant faktör haline gelmektedir. Bu durum özellikle mikroşerit anten dizileri için geçerlidir.

Bu tezin genel amacı, mikroşerit antenler arasındaki yüzey dalgalarının neden olduğu karşılıklı bağlaşımın deforme toprak yapıları (DTY) kullanılarak azaltılması. DTYler, mikroşerit antenler arasındaki toprak düzlemine dambıl şeklinin veya birleşik tümler yarıklı halka rezonatörünün (BTYHR) elektrik alan düzlemi yönünde kazınmasıyla oluşturuluyor. Bu yapıların antenler arasındaki bağlaşımı önemli ölçüde azaltmasına rağmen antenlerin uzak alan davranışlarının, arka lop seviyelerinin önemli ölçüde artması nedeniyle olumsuz yönde etkilendiği görüldü. Reflektör ve kavite kombinasyonu kullanılarak bu olumsuz etkilerin belli bir seviyeye kadar düşürülebildiği gözlemlendi. Son olarak da, DTYleri dizi ortamında test etmek için, 2×2'lik mikroşerit anten dizisine dambıl tipi DTY, reflektör ve kavite eklemenin anten performansına etkileri incelendi. Yapılan ölçüm sonuçları ve bilgisayar benzetimleri gösterdi ki, DTY, karşılıklı bağlaşım değerlerinde ciddi azalmalar sağlasa da, antenlerin uzak alan performanslarında bir gelişme sağlayamıyor.

Anahtar Kelimeler: Karşılıklı Bağlaşım, Uzay Dalgaları, Yüzey Dalgaları, Birleşik Tümler Yarıklı Halka Rezonatörü (BTYHR), Dambıl, Deforme Toprak Yapıları

ACKNOWLEDGEMENTS

I would like to express my endless gratitude to my supervisor Assoc. Prof. Vakur B. Ertürk for his guidance and supervision throughout the development of this thesis.

I would like to thank Prof. Dr. Ayhan Altıntaş and Prof. Dr. Özlem Aydın Çivi, the members of my jury, for reading and reviewing my thesis.

I would also like to express my gratitude to my company, Meteksan Defence Inc and especially Mehmet Altuntas, senior engineer at Meteksan Defence Inc., for his invaluable assistance throughout the measurement process of the antennas.

Finally, I would like to thank my family for their support and patience.

Contents

List of Figures

to my family . . .

Chapter 1

Introduction

Microstrip antennas and arrays have become one of the most widely used antennas and arrays over the last 30 years for many applications ranging from satellite and wireless communication to military and biomedical applications. The interest in these antennas and arrays comes directly from their advantages over the antennas such as low fabrication cost (especially for mass production), small volume, light weight, conformity to surface and easy integration with other microwave and solid-state devices. However, when a single microstrip antenna is considered, it mainly suffers from having a narrow bandwidth, low power handling capability and low gain [1]. Therefore, microstrip antenna arrays are preferred to improve the abovementioned performance merits. In spite of all the advantageous of microstrip antenna arrays, mutual coupling among the array elements which occurs as a result of space and surface waves, affects their operation and makes their design/analysis challenging.

In many applications such as bistatic radar systems, very low coupling levels are desired [2]. In such systems, isolation is essential in order not to have any interference between the transmitting and receiving antennas. In fact, in many applications where electromagnetic interference (EMI) deteriorates the system performance, mutual coupling reduction becomes a necessary study. Besides, excess amount of mutual coupling could increase the sidelobes, change the beam position and bandwidth [3],[4]. Thus, their elimination can lead to significant improvements in the performance merits of microstrip arrays.

When microstrip antenna arrays are considered, the mutual coupling among the array elements occurs as a result of space and surface waves. Space waves are usually stronger along the H-plane of the antennas and very strong if the array elements are close to each other. However, they die out quickly as the separation between array elements becomes larger. On the hand, the surface waves are usually stronger along the E-plane of the antennas and weaker than that of space waves when the array elements are close to each other. However, they remain as the only coupling mechanism when the array elements are far away from each other.

Keeping in mind the aforementioned mutual coupling mechanisms for microstrip antenna arrays, several techniques have been developed for mutual coupling reduction [3]-[9]. Most of these techniques aim to reduce the surface waves [4]-[9]. However, some studies may aim to reduce both space and surface waves [3]. Among them work in [3] aims to reduce the mutual coupling between two antennas by trying to decrease both space and surface waves. Therefore, they install two defected ground plane sidewall structures (DWS) between the adjacent patch antenna elements to attack the space waves while a pair of slits is also etched in the middle of the ground plane between the patch antennas to reduce the surface waves. Although the measurement results indicate an enhancement in isolation about 40 dB for an inter-element spacing of 0.272 λ_o (λ_o: free space wavelength) at 1 GHZ, the technique is not practical because of the vertically installed sidewalls between the patch antennas. Since measured farfield patterns without DWS are not given, effects of DWS on farfield patterns are not clear.

In [4], slotted complementary split ring resonators (SCSRR) are etched on the ground plane between the adjacent patch antenna elements to diminish the surface waves. The inter-element spacing between the antennas is 0.5 λ_o at 5 GHz and three SCSRR unit cells are etched in between the adjacent patch antennas. Simulation results show a 9 dB mutual coupling reduction at 5 GHz and simulated farfield results do not indicate any change in the farfield patterns. However, no fabrication results and no measurements are provided.

[5] and [6] aim to reduce the mutual coupling due to surface waves through electromagnetic band-gap structures. In [5], mushroom like EBG structures are inserted in between the microstrip antennas to reduce the mutual coupling between the adjacent microstrip patches. These EBG structures are consisted of small square patches that are connected to the ground plane by vias from their center. Measurement results show that an 8 dB mutual coupling reduction is achieved for an inter-element spacing of 0.88 λ_o at 5.8 GHz. However, integration of the EBG structures to the antenna requires the usage of vias and this results in a significantly increased production time and cost aside from the production problems with Teflon based dielectric materials. Besides, no farfield results are provided. [6] also aims to reduce the surface waves using EBG structures. In [6], multilayer dielectric substrates are used and vias are not used with the EBGs. Multilayer dielectric substrates are consisted of one high dielectric substrate at the bottom and a low dielectric substrate at the top. Microstrip patch antennas are constructed on the top substrate layer that has a low dielectric constant and the EBGs are constructed on the bottom substrate layer that has a higher dielectric constant. Center to center separation between the antennas is 0.75 λ_o. Measurement results indicate a 15 dB mutual coupling reduction at 3.05 GHz. However, farfield results are not provided for this technique. Besides, the cost of the multilayer dielectric substrates makes this technique less attractive.

Works in [7]-[9] focus on the use of different kinds of defected ground structures (DGS) in order to decrease the mutual coupling between the microstrip patch antenna elements by trying to kill the surface waves. In [7], dumbbell shapes are etched to the part of the ground plane that remains between the microstrip patch antennas to form a DGS. The edge-to-edge separation between the microstrip patch antennas is given as 0.5 λ_o at 6 GHz. According to the given simulation results, using the proposed dumbbell DGS, an 18.28 dB mutual coupling reduction is acquired. Moreover, this technique is also compared with other techniques such as substrate removal, cavity back and EBG by using the same antenna configurations. Comparison of the other three techniques with the proposed dumbbell DGS shows that dumbbell DGS provides a 14 dB more reduction than the use of the EBG, which has been the best technique among the abovementioned three techniques. However, simulated farfield results indicate that using DGS causes approximately a 10 dB increase in the backlobe levels although there is not any significant change in the frontlobe of the farfield patterns. However, no measurement results are provided to support these results. Work in [8] investigates the farfield and mutual coupling results after introducing H type DGS between the adjacent microstrip patch antennas where edge-to-edge separation between the microstrip patch antennas is 0.75 λ_o at 5.3 GHz. Measurement results indicate a 12 dB mutual coupling reduction at 5.3 GHz and the farfield results presents a 0.25 dB decrease in gain in addition to a slight increase in the backlobe radiation. Apart from the decreased gain and increased backlobe level, there is not a significant change in farfield patterns as also seen in [7]. In [9], in addition to the dumbbell and H type DGS, E shaped, back-to-back E shaped, H and inverted H and E shaped DGSs are used for the part between the microstrip patch antennas in a 2×2 planar array. The edge-to-edge separation between the microstrip patch antennas are set to 0.55 λ_o at 4.75 GHz. Measurement results indicate that insertion of the new DGS models shifts the resonant frequency of the patch antennas up to 500 MHz unlike the dumbbell

DGS which does not cause any frequency shift. Besides, simulated farfield results show increased backlobe radiations and severely affected farfield patterns after the insertion of DGSs to the antenna. However, there is not enough measurement data similar to the other studies.

Most of the abovementioned studies do not provide measurement results. Moreover, they have tried to reduce the mutual coupling between only two adjacent antennas along the E-plane. Thus, they are not tested in a full array environment. Therefore, our goal in this thesis is to consider many of these abovementioned techniques in a full array of microstrip antennas and provide some conclusions regarding their effects to the array performance merits based on the measurement results. In order to achieve this goal, first several DGS structures formed from dumbbells and SCSRRs are investigated considering two microstrip patch antennas, and the amount of mutual coupling reduction is investigated via some parametric tests. Simulation results are supported by some measurement results. Then, due to the increase at the backlobe levels of the farfield radiation pattern results, a reflector and a cavity combination is introduced to decrease the high backlobe levels. Finally, to test the DGS idea in a full array environment, the performance merits of a 2×2 microstrip antenna array is investigated in the presence of the dumbbell DGS, where each microstrip antenna is backed with a cavity and a reflector. It has been observed that (via simulations and measurements) despite a considerable amount of mutual coupling reduction can be achieved, the far-zone performance merits of the array have not been improved.

The outline of this thesis is as follows: In chapter 2, several DGS structures are investigated to reduce the mutual coupling between two microstrip antennas. For each proposed DGS structure, parametric studies are performed in the form of simulations and finally measurement results are provided. It has been observed that introducing a DGS between two-microstrip antenna increases the backlobe radiation significantly. Therefore, in chapter 3, a reflector and a cavity are introduced to decrease the backlobe radiation level. In chapter 4, final structure, optimized for 2 antennas, is extended to a 2×2 microstrip antenna array. Both simulation and fabrication results are provided regarding some of the array performance merits. Finally, conclusions are drawn in chapter 5.

Chapter 2

Mutual Coupling Reduction in 2-Element Antenna Arrays

Several techniques have been developed for mutual coupling reduction in the last decade as mentioned in Chapter 1. However, many of these techniques can be considered impractical and/or costly to implement in particular when the elimination of the space waves are considered. Therefore, in this thesis we focused on only to suppress the surface waves, by using DGSs.

DGS are widely used in microstrip circuits in order to change the characteristics of the transmission lines and acquire higher impedances, band rejection and/or slow wave characteristics [10]. Etching part of the ground plane and forming a DGS causes the disturbance of the current distribution when inserted under the microstrip transmission line, and changes the inductance and capacitance of the transmission line.

There are many DGS studies in the literature ranging from single rectangular slots to meander lines and dumbbell shaped variations [11]. Each of them varies based on the area they occupy, their equivalent circuit model, and their frequency response. For instance in [10], three different types of dumbbell shaped

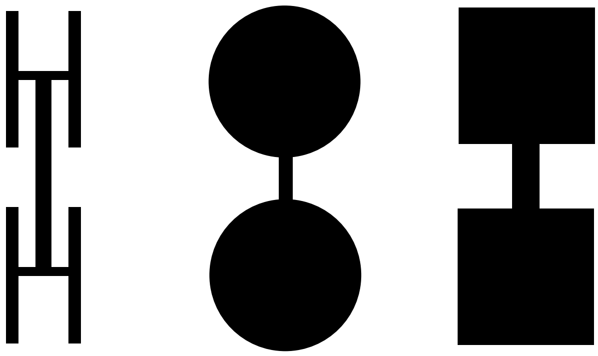

(a) (b) (c)

Figure 2.1: (a) H type DGS. (b) Circular head dumbbell DGS. (c) Square head dumbbell DGS. Solid lines in the middle of the DGSs indicate transmission lines.

DGSs resonating at 8.1 GHz are inserted under a transmission line which is on a substrate with 0.381 mm thickness and has a relative dielectric constant ϵ_r =2.2. It is seen from the measurement results that H type DGS (Fig. 1(a)) has narrower bandwidth with deeper suppression whereas circular head (Fig. 1(b)) and square head (Fig. 1(c)) dumbbell DGSs have very similar responses.

In this thesis, the main focus is the square head dumbbell and the SCSRR type DGSs. As a center frequency, we decided to work at 5 GHz in order to be able to tolerate production errors that can be more crucial for smaller structures resonating at higher frequencies. Besides, we also want to use less dielectric material during the production compared to the production of structures resonating at lower frequencies that usually result in consumption of more dielectric material.

2.1 Microstrip Antenna Design Procedure

There are different models in the literature such as cavity model, transmission line model, etc. to design a microstrip antenna. Among them, transmission line model is the easiest one. Although it does not account for the coupling and less accurate compared to the other models, it provides a good starting point for designing a microstrip antenna by using computer aided design (CAD) tools.

In [12] (pp. 819-820), a useful design procedure is given as follows:

1. The width (W) of the patch antenna is determined for the desired resonance frequency (f_r) provided that the substrate properties such as ϵ_r and the height (h) of the substrate are given. Thus W is given by

$$W = \frac{v_o}{2f_r}\sqrt{\frac{2}{\epsilon_r + 1}} \tag{2.1}$$

where (v_o) is the free-space speed of light.

2. The effective dielectric constant (ϵ_{reff}), that is defined to account for both the fringing fields and the propagating waves in microstrip line, is calculated as follows:

$$\epsilon_{reff} = \frac{\epsilon_r + 1}{2} + \frac{\epsilon_r - 1}{2}\sqrt{\frac{1}{1 + 12\frac{h}{W}}} \tag{2.2}$$

3. Extended length (ΔL) of the antenna due to the existence of the fringing fields is calculated as

$$\Delta L = 0.412h\frac{(\epsilon_{reff} + 0.3)(\frac{W}{h} + 0.264)}{(\epsilon_{reff} - 0.258)(\frac{W}{h} + 0.8)} \tag{2.3}$$

4. Finally, the length (L) of the patch antenna is determined by using the results coming from (2.2) and (2.3) as

$$L = \frac{v_o}{2f_r\sqrt{\epsilon_{reff}}} - 2\Delta L \tag{2.4}$$

Following this design procedure, the acquired parameters are used in the CAD tool CST Microwave Studio to design a patch antenna. In order to have good matching at the desired resonance frequency (i.e., 5GHz), the length and the feeding location are optimized. After the design of a single patch antenna is done,

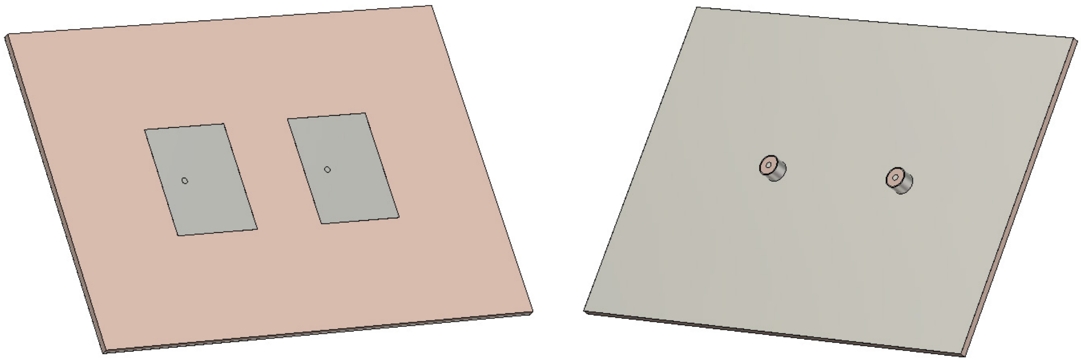

(a) (b)

Figure 2.2: (a) Perspective top-view of a 2×1 microstrip antenna array. (b) Perspective back-view of a 2×1 microstrip antenna array.

the final antenna dimensions are used to build the microstrip antenna arrays in CST Microwave Studio as illustrated in Fig. 2.2. Moreover, in order to acquire more consistent results between the simulated and the fabricated antennas, the SMA connectors are modelled and included in all simulations.

2.2 Analysis of the Dumbbell DGS

2.2.1 Band Rejection Characteristics of the Dumbbell DGS

One of the major characteristics of a dumbbell DGS is its band rejection. When placed under a transmission line, the dumbbell DGS acts like a band-stop filter. The band rejection properties of it are governed by the inter-element spacing between the etched dumbbells, the number of unit DGS elements (which are dumbbells) and the dimensions of the dumbbells.

Fig. 2.3 illustrates the simulation parameters that are used to govern the dimensions of a square head dumbbell DGS. In the rest of the thesis, the square

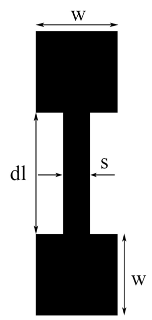

Figure 2.3: Dimensions of a square head dumbbell.

head dumbbell DGS will be referred to as only "dumbbell DGS" since no other type of dumbbell DGS is studied in this work.

Effects of the Inter-Element Spacing between the Dumbbells to the Frequency Response of the Dumbbell DGS

In order to understand the effects of the inter-element spacing between the dumbbells on the frequency response of the dumbbell DGS, simulations are made using CST Microwave Studio. As a substrate Rogers 5880 is chosen that has $\epsilon_r = 2.2$, tan$\delta = 0.0009$, thickness$s = 1.524$ mm, width $= 70$ mm and length $= 100$ mm. On this substrate a 50 Ω line having a width of 4.69 mm is defined and both ends of the microstrip line are terminated with waveguide ports as illustrated in Fig. 2.4(a).

In Fig. 2.4(b), it is shown that multiple dumbbells are etched to the ground plane under the microstrip line so that a DGS can be obtained. In order to comprehend the effect of the inter-element spacing (tx), are etched to the ground plane and the inter-element spacing is varied from 5 mm to 30 mm. In simulations, the parameter named tx is assigned to govern the inter-element spacing as shown in Fig. 2.4(b). The dumbbells are designed to resonate at 5 GHz. Hence, their dimensions are $w = 4.2$ mm, $s = 0.4$ mm and $dl = 7$ mm.

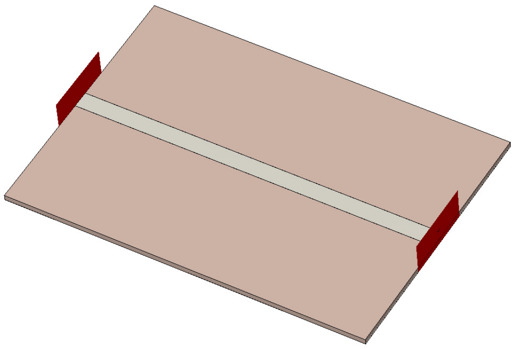

(a)

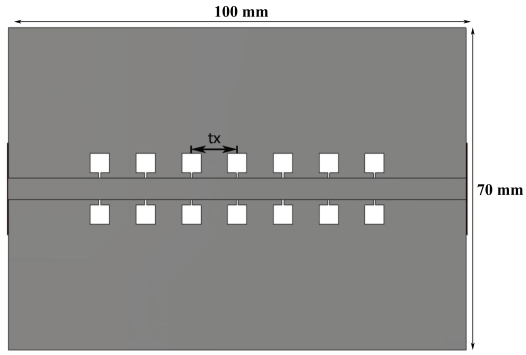

(b)

Figure 2.4: (a) Perspective view of a 50 Ω microstrip line on a substrate Rogers 5880 with $\epsilon_r = 2.2$, tan$\delta = 0.0009$, thickness $= 1.524$ mm with waveguide ports (multiple dumbbells are etched on the ground plane). (b) The dumbbells that form the DGS are illustrated together with the microstrip line.

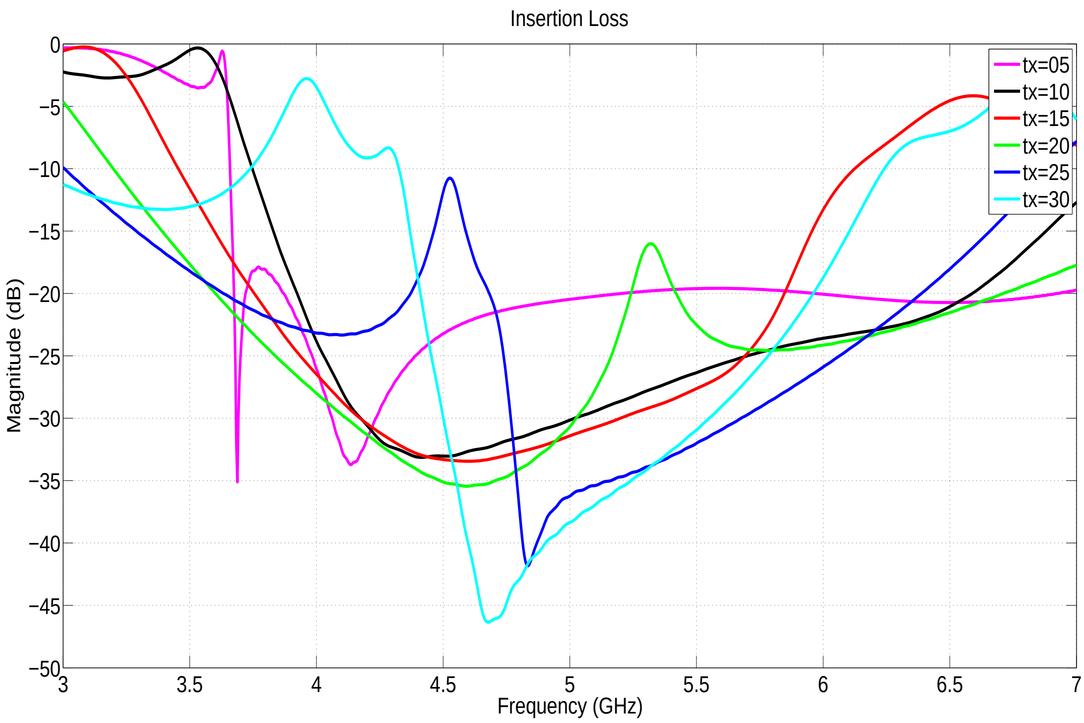

Figure 2.5: Frequency response of 3 dumbbell DGS as band-stop filter when the inter-element spacing tx is changed from 5 mm to 30 mm.

Fig. 2.5 shows the magnitude of the transmission characteristics ($|S_{21}|$dB) of a 3 dumbbell DGS structure versus frequency when the inter-element spacing tx is varied from 5 mm to 30 mm. It is seen from Fig. 2.5 that as tx increases the suppression at 5 GHz increases while the bandwidth of the rejection band decreases.

Effects of the Number of Dumbbells to the Frequency Response of the Dumbbell DGS

Effect of the number of unit DGS cells (i.e., number of dumbbells) on the frequency response of the dumbbell DGS is also investigated on the same substrate with the same 50 Ω microstrip line. The dumbbell dimensions are also kept the same. n denotes the number of dumbbells in the simulations, and the inter-element spacing (tx) is set to 7.5 mm. Magnitude of the transmission characteristics ($|S_{21}|$dB) of the dumbbell DGS structure versus frequency when the number of DGS elements is varied from 1 to 11 is shown in Fig. 2.6. It is seen from the simulation results (as shown in Fig. 2.6) that as the number of dumbbells increases both the bandwidth of the stop band and the suppression levels at 5 GHz increase.

Effects of the Dimensions of the Dumbbells to the Frequency Response of the Dumbbell DGS

A typical square head dumbbell DGS with its dimensions is illustrated in Fig. 2.3. As seen in Fig. 2.3, there are three parameters to optimize which are dl, s and w. It is expected that as the area of the etched structure increases (here it is dumbbell), the resonance frequency of the rejection band decreases. Therefore, the transmission characteristics ($|S_{21}|$dB) versus frequency of a single dumbbell DGS is investigated when dl, s and w are varied one at a time. The substrate

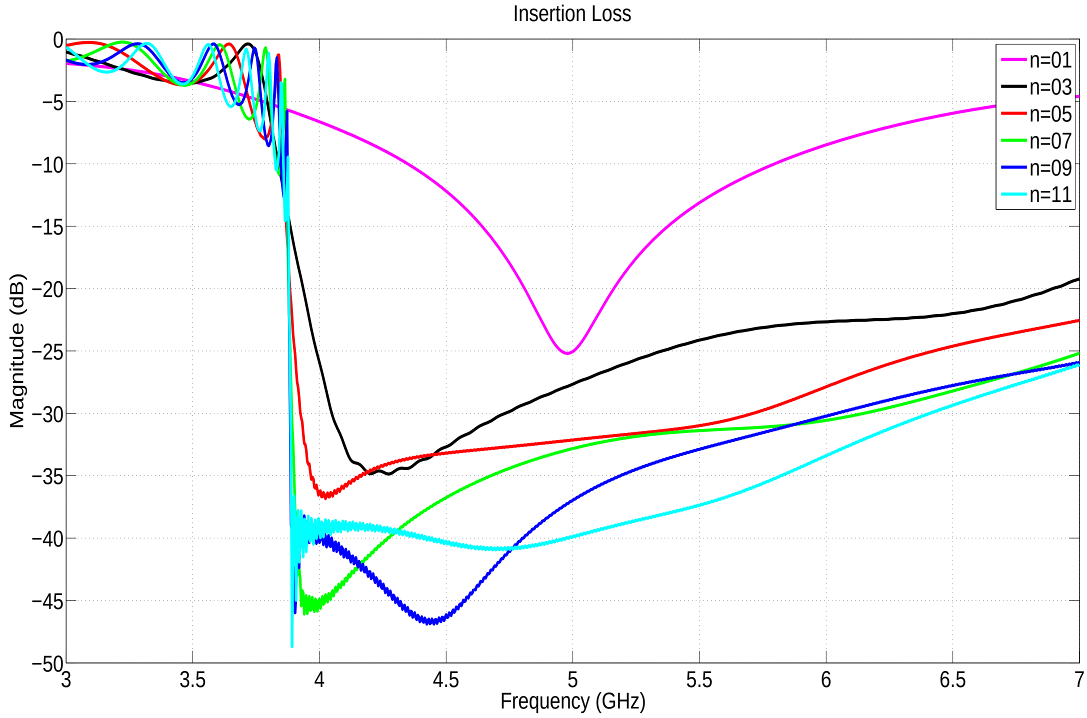

Figure 2.6: Frequency response of the dumbbell DGS as a band-stop filter when the number of unit dumbbell cells is varied.

and the 50 Ω transmission line are kept the same as before. In Fig. 2.7, the transmission characteristics versus frequency of a single dumbbell DGS, when the parameter w is varied, is given. Fig. 2.8 shows the transmission characteristics versus frequency of a single dumbbell DGS when the parameter s is varied. In Fig. 2.9, effect of the change in dl on the transmission characteristics of a single dumbbell DGS with respect to frequency is presented. As seen in Figs. 2.7, 2.8 and 2.9, all these dimension related parameters govern the resonance frequency of the stop band. However, as seen in Fig. 2.8, the parameter s is slightly more dominant than the others in controlling the suppression level.

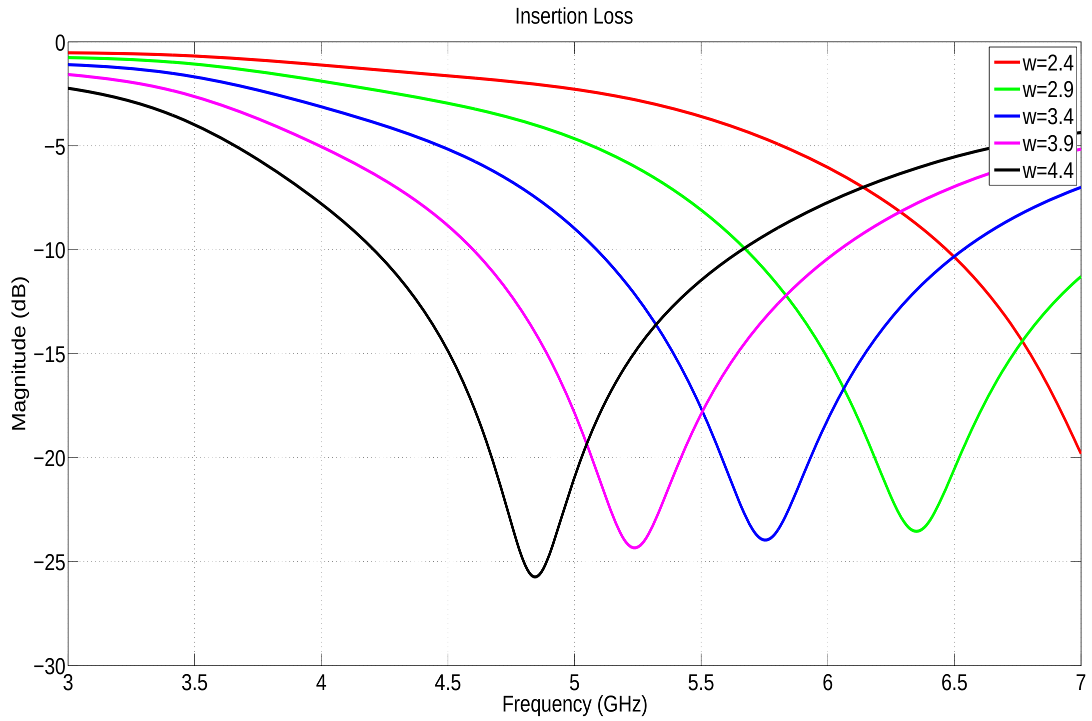

Figure 2.7: Frequency response of the dumbbell DGS when the parameter w is changed.

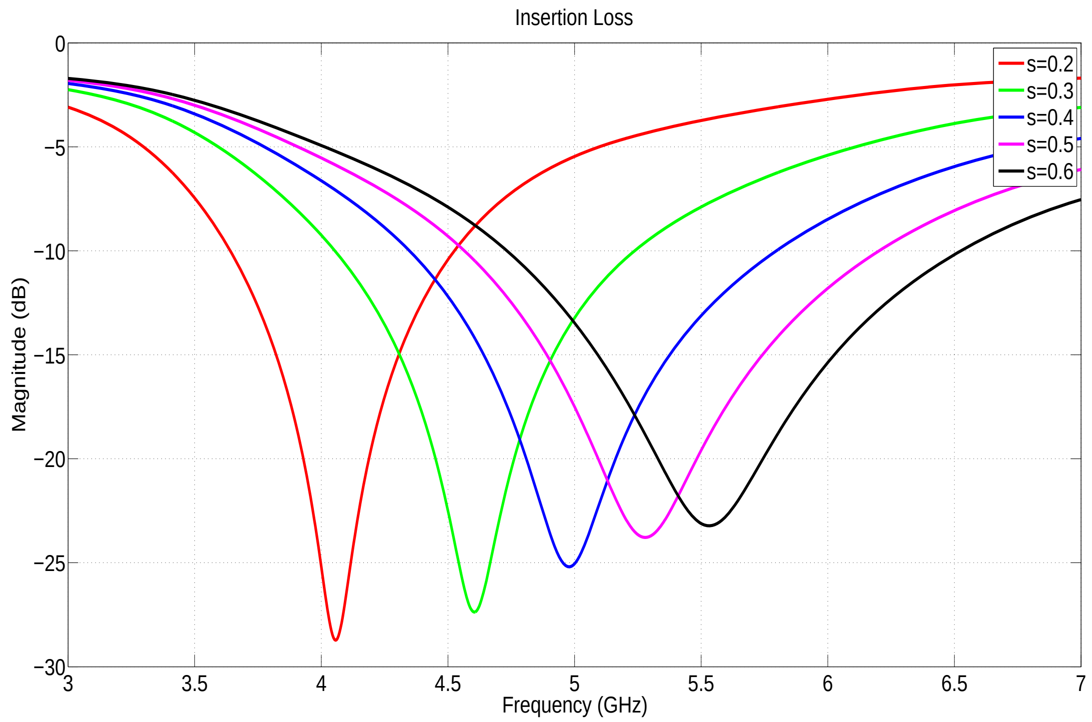

Figure 2.8: Frequency response of the dumbbell DGS when the parameter s is changed.

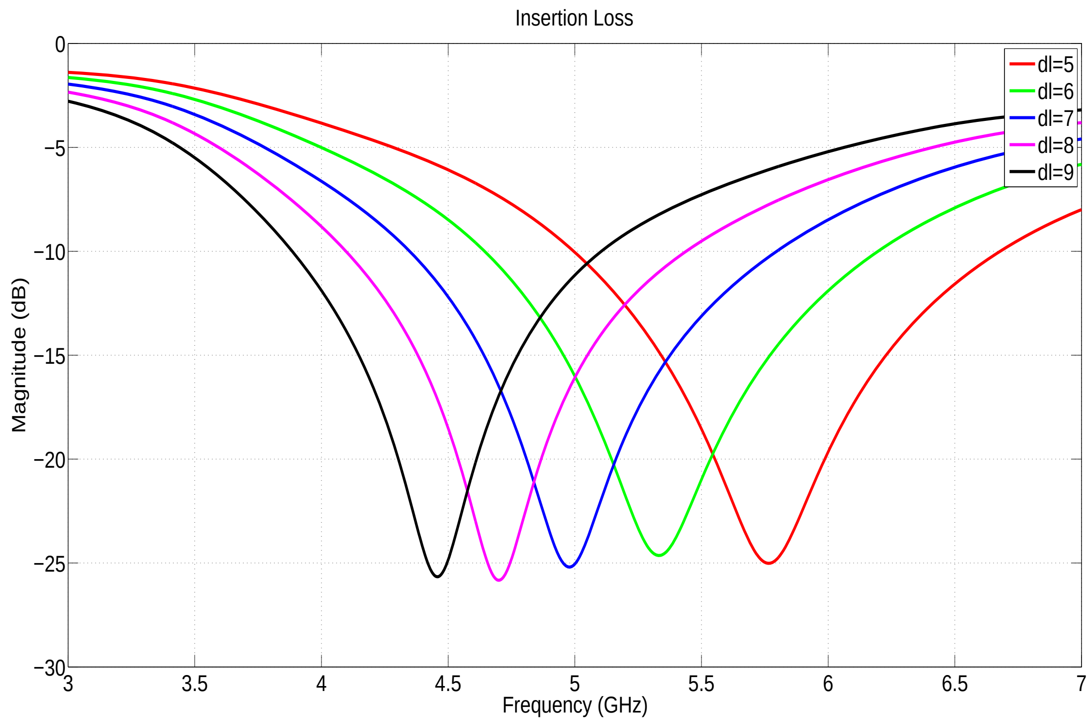

Figure 2.9: Frequency response of the dumbbell DGS when the parameter *dl* is changed.

2.2.2 Mutual Coupling Reduction with Dumbbell DGS

Mutual Coupling Reduction and Far-Zone Results Using a Single Dumbbell DGS with Different Substrates

In order to decide which dielectric material would be more appropriate so that the dumbbell DGS can provide maximum mutual coupling suppression without affecting the resonant frequency of the antennas, three different substrates with 1.524 mm thickness are used. These substrates are Rogers 5880 with $\epsilon_r = 2.2$ and tan$\delta = 0.0009$, ARLON TC600 with $\epsilon_r = 6.15$, tan$\delta = 0.002$ and ARLON AR1000 with $\epsilon_r = 10$ and tan$\delta = 0.003$. Two element antenna arrays resonating at 5 GHz are designed and then have been aligned collinearly along the E plane as shown in Fig. 2.10. Edge-to-edge separation between those microstrip antennas are chosen to be $\lambda_o/4$ which is 15 mm in this case.

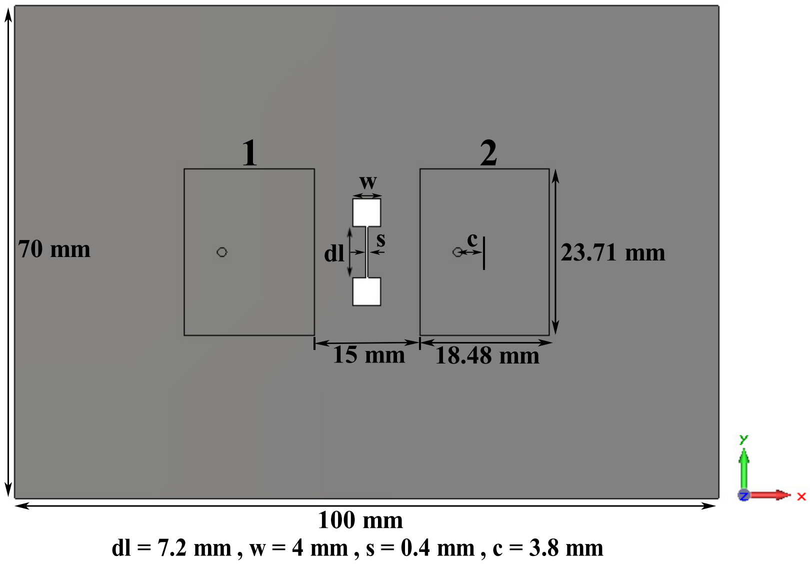

Figure 2.10: Top view of the 2-element array on Rogers 5880 with the antenna and substrate dimensions.

The first two-element microstrip array is designed on Rogers 5880. The dimensions of the board outline of the array are 100 mm × 70 mm and the thickness of the dielectric is 1.524 mm. Length and width of the antennas are 23.71 mm × 18.48 mm, respectively. The feed location of each antenna is at the middle of the length and c = 3.8 mm away from the center of the antenna along the width direction as shown in Fig. 2.10. The edge-to-edge separation is set to $\lambda_o/4$ (15 mm). Antennas and the etched dumbbell are aligned in the middle of the substrate. Moreover, during the simulations each antenna is fed one by one while the other antenna is terminated to a 50 Ω load. The dimensions of the dumbbell are given as dl = 7.2 mm, w = 4 mm and s = 0.4 mm, so that it resonates at 5 GHz.

Fig. 2.11 shows the magnitude of the return loss ($|S_{11}|$ and $|S_{22}|$ in dB) of the antennas versus frequency in the presence and absence of the dumbbell DGS. Similarly, Fig. 2.12 shows the magnitude of the mutual coupling ($|S_{21}|$ in dB) between the antennas versus frequency with and without the dumbbell DGS. It is seen from Fig. 2.12 that insertion of a single dumbbell DGS between the patch

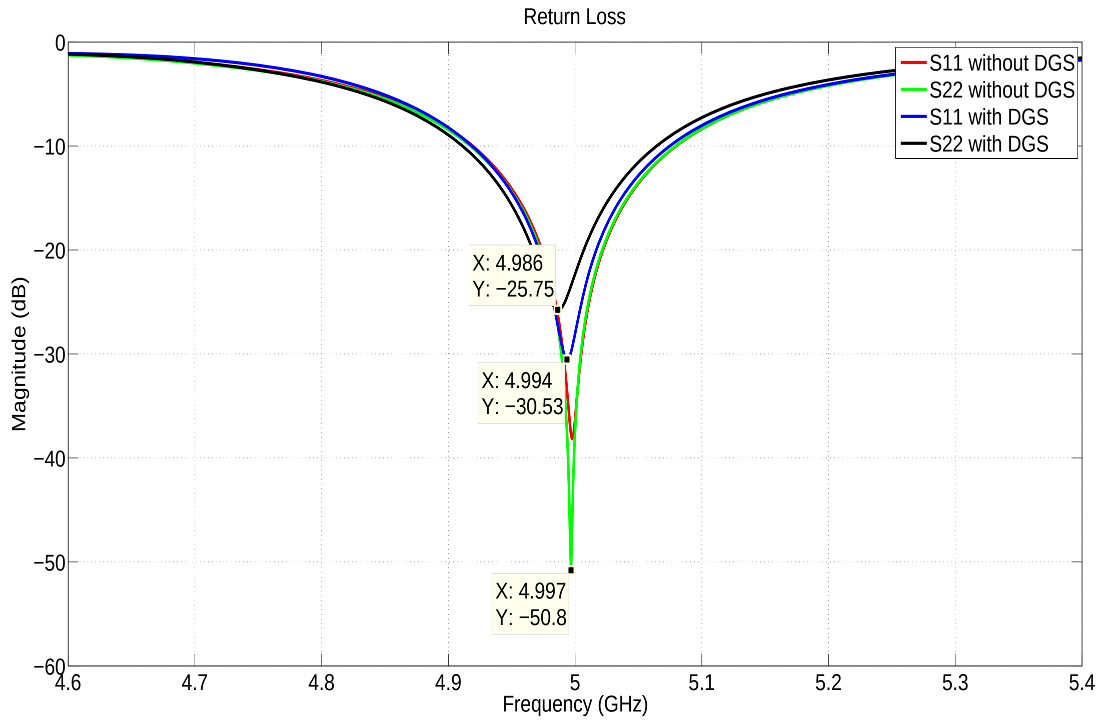

Figure 2.11: Simulated return loss results ($|S_{11}|$ and $|S_{22}|$ in dB) of the antennas with and without the dumbbell DGS versus frequency.

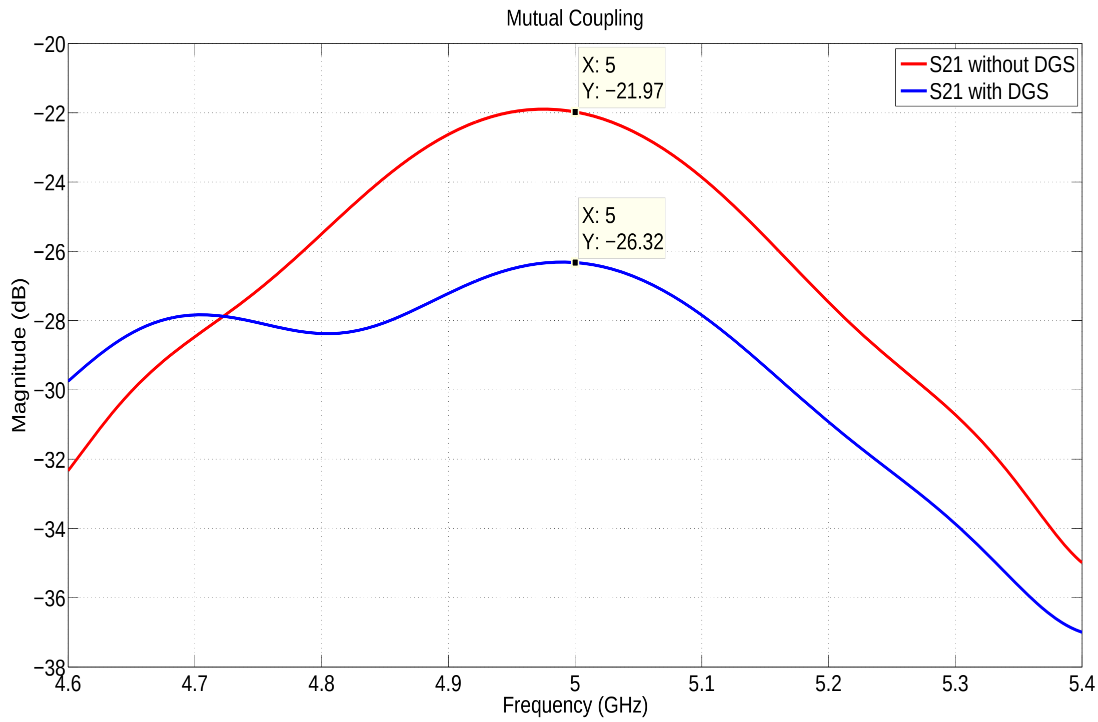

Figure 2.12: Simulated mutual coupling results ($|S_{21}|$ in dB) between the antennas with and without the dumbbell DGS versus frequency. The geometric parameters of the antennas and the dumbbell DGS are the same as those given in Fig. 2.10.

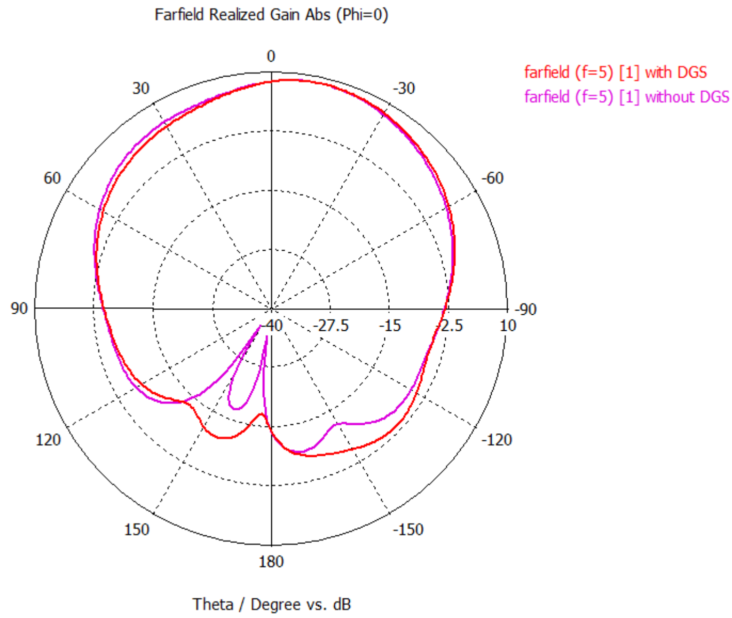

Figure 2.13: Simulated azimuth pattern of the first antenna with and without the dumbbell DGS.

antennas provides a 4.7 dB mutual coupling reduction at 5 GHz. Regarding the return loss, a slight frequency shift at the resonance frequency of the patch antennas (approximately 15 MHz) exists (which is acceptable) as seen in Fig. 2.11. On the other hand, it is also shown in 2.11 that the matching of the antennas is also degraded about 20 dB. However, because the return loss levels are about -25 to -30 dB, the matching is still acceptable.

Fig. 2.13 and Fig. 2.14 show the simulated azimuth patterns of the first and second antennas, respectively, with and without the dumbbell DGS. Similarly, Fig. 2.15 and Fig. 2.16 show the simulated elevation patterns of the first and second antennas, respectively, with and without the dumbbell DGS. When the farfield results are analysed it is seen that aside from minor changes at the backlobe of the patterns which are not more than 3 dB, the dumbbell DGS did not affect the farfield patterns of the first antenna while the sidelobe and the beamwidth of the second antenna are increased after the introduction of the dumbbell DGS. Moreover, the 3-dB beamwith narrows up to 5 degrees.

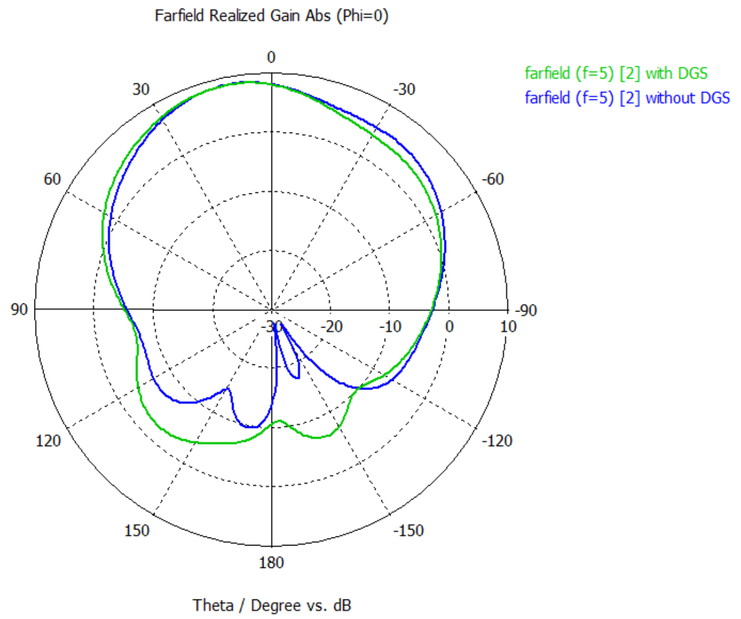

Figure 2.14: Simulated azimuth pattern of the second antenna with and without the dumbbell DGS.

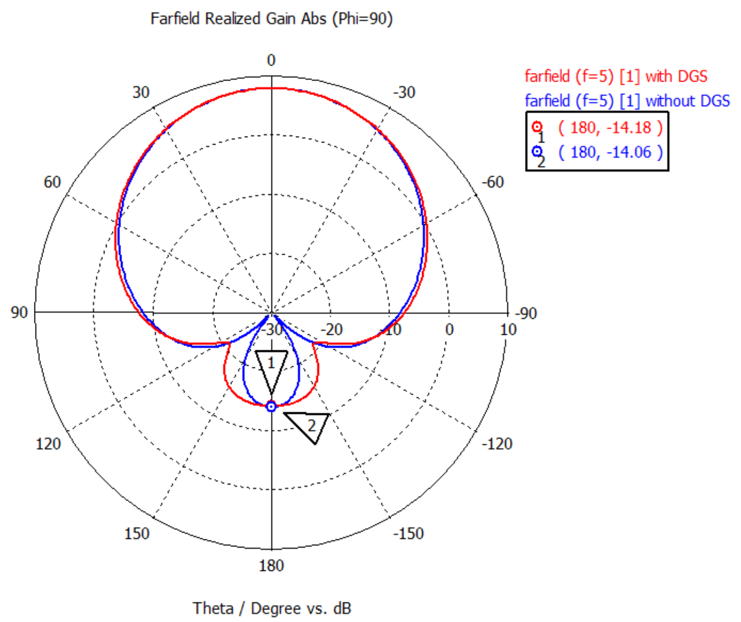

Figure 2.15: Simulated elevation pattern of the first antenna with and without the dumbbell DGS.

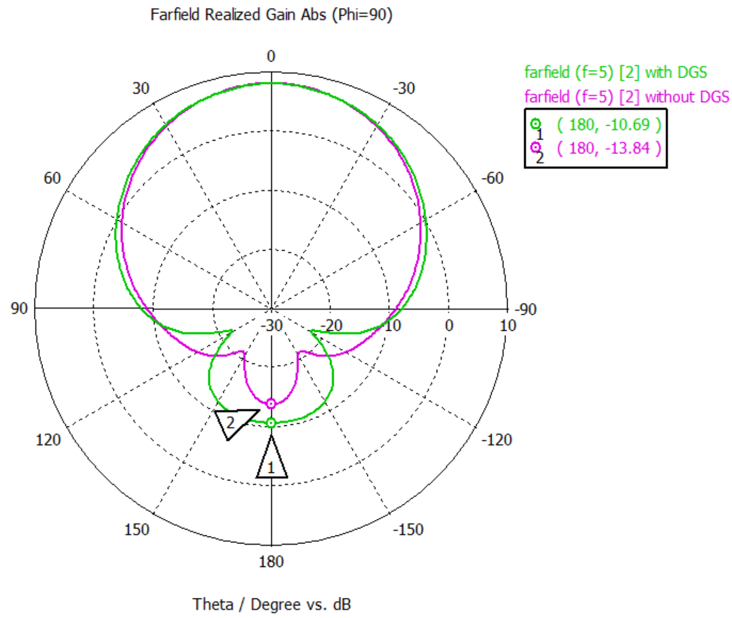

Figure 2.16: Simulated elevation pattern of the second antenna with and without the dumbbell DGS.

The second two-element microstrip array is designed on ARLON AR1000 (ϵ_r = 10 and tanδ = 0.003). Dimension of the board outline of the antenna is 60 mm × 35 mm and the thickness of the substrate is 1.574 mm. The length and width of the antennas are 12.4 mm × 8.04 mm, respectively. Similar to the first case, the feed location of each antenna is at the middle of the length and c = 1.57 mm away from the center of the antenna along the width direction as shown in Fig. 2.17. The edge-to-edge separation is set to $\lambda_o/4$ (15 mm). Note that because the permittivity of the substrate is higher, the whole geometry as well as the antennas have more compact size. Antennas and the etched dumbbell DGS are aligned at the middle of the substrate similar to the first case. Furthermore, during the simulations, antennas are fed one at a time while the other antenna is terminated to a 50 Ω load. The dimensions of the dumbbell are dl = 6.72 mm, w = 2.27 mm, s = 1.1 mm so that it can resonate at 5 GHz.

Fig. 2.18 shows the magnitude of the return loss ($|S_{11}|$ and $|S_{22}|$ in dB) of the antennas versus frequency in the presence and absence of the dumbbell DGS. Similarly, Fig. 2.19 shows the magnitude of the mutual coupling ($|S_{21}|$ in dB)

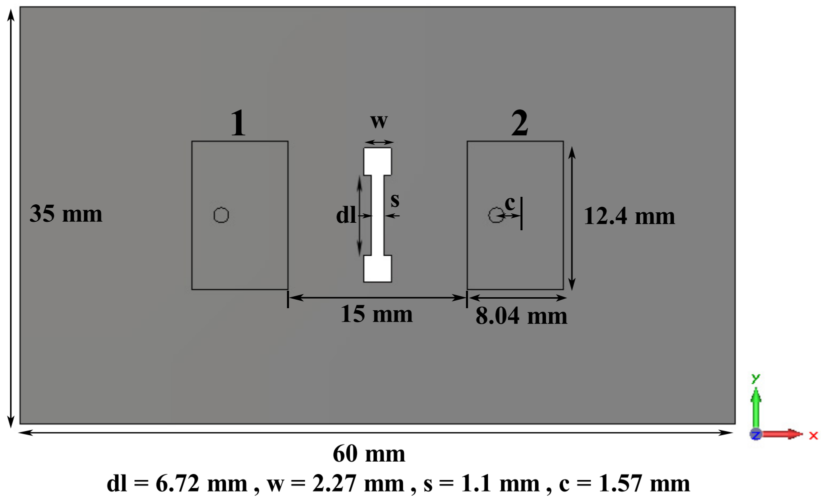

Figure 2.17: Top view of the 2-element array on ARLON AR1000 with the antenna and substrate dimensions.

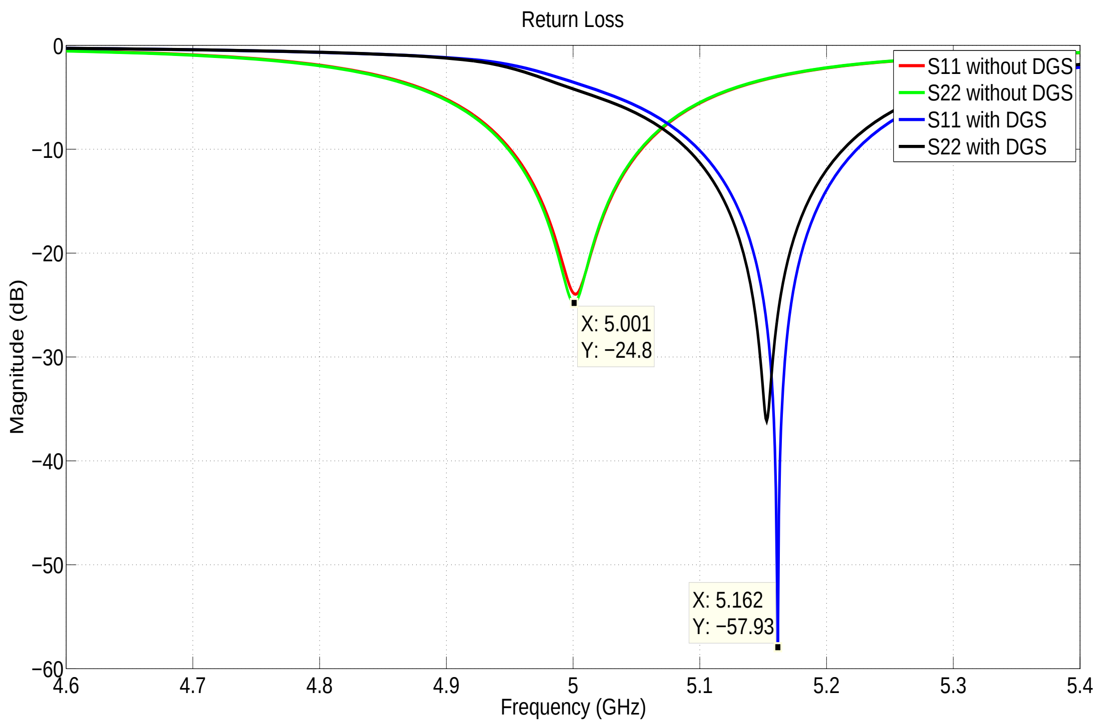

Figure 2.18: Simulated return loss ($|S_{11}|$ and $|S_{22}|$ in dB) of the antennas with and without the dumbbell DGS.

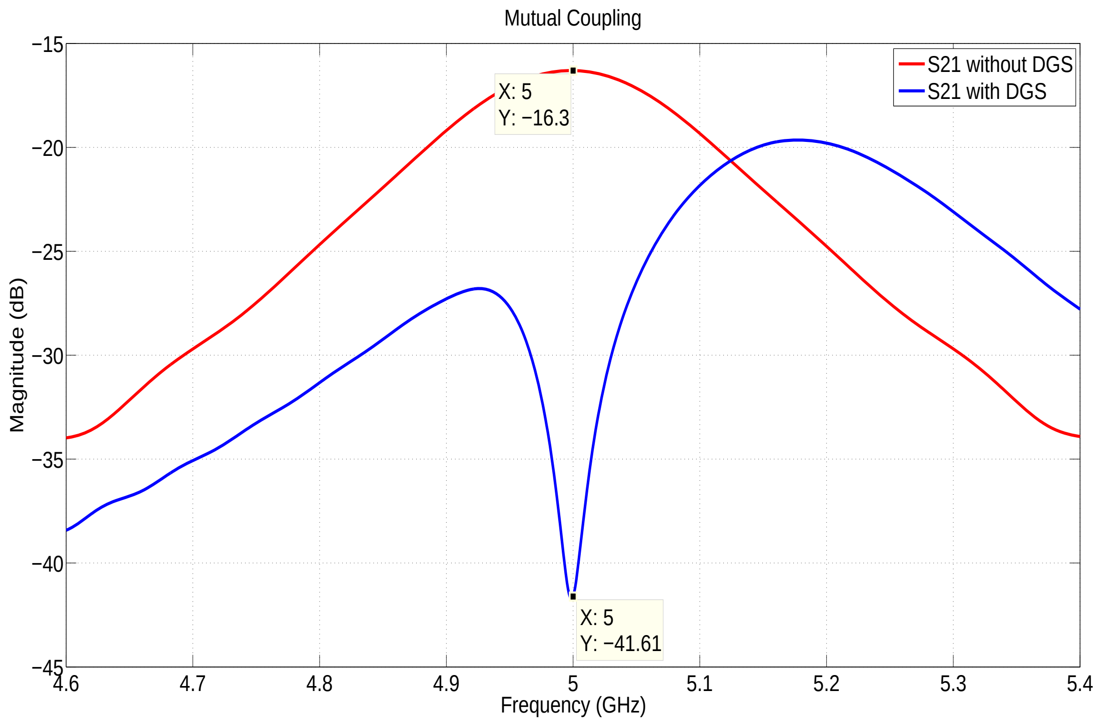

Figure 2.19: Simulated mutual coupling ($|S_{21}|$ in dB) results between the antennas with and without the dumbbell DGS.

between the antennas versus frequency with and without the dumbbell DGS. As seen in Fig. 2.19 approximately a 25 dB mutual coupling reduction is achieved around 5 GHz. However, such a change in $|S_{21}|$ (or $|S_{12}|$) affects the return loss results. There is approximately 150 MHz shift towards the low frequency side in the resonance frequency of the both antennas as illustrated in Fig. 2.18. It has been observed that the main reason for such a change is the reflection of the strong surface waves due to DGS as shown in Fig. 2.20. Note that, due to the high ϵ_r value ($\epsilon_r = 10$) ARLON AR1000 supports the surface waves significantly, and ideally, a DGS structure is supposed to kill the surface waves. However, as shown in Fig. 2.20, we have strong fields which are reflected from the dumbbell and travel towards the first antenna.

Fig. 2.21 and Fig. 2.22 show the simulated azimuth patterns of the first and second antennas, respectively, with and without the dumbbell DGS. Similarly, Fig. 2.23 and Fig. 2.24 show the simulated elevation patterns of the first and second antennas, respectively, with and without the dumbbell DGS. As seen

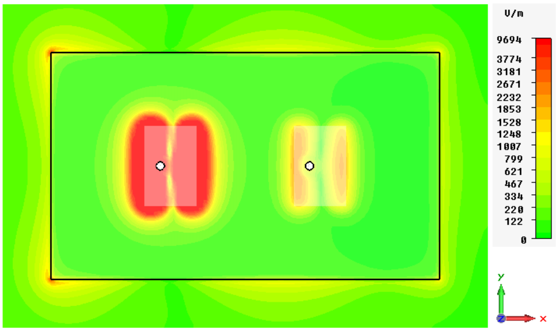

(a)

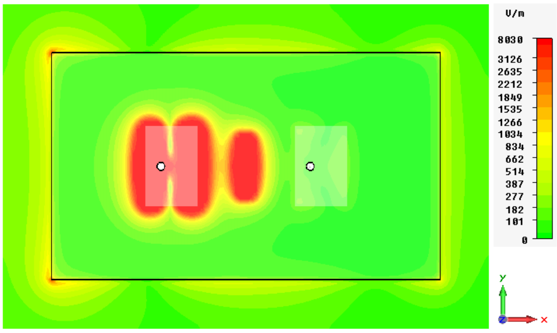

(b)

Figure 2.20: (a)Surface waves within the dielectric of the antenna array without the dumbbell DGS when the first antenna is excited and the second one is terminated to a 50 Ω load. (b)Surface waves within the dielectric of the antenna array with the dumbbell DGS when the first antenna is excited and the second one is terminated to a 50 Ω load.

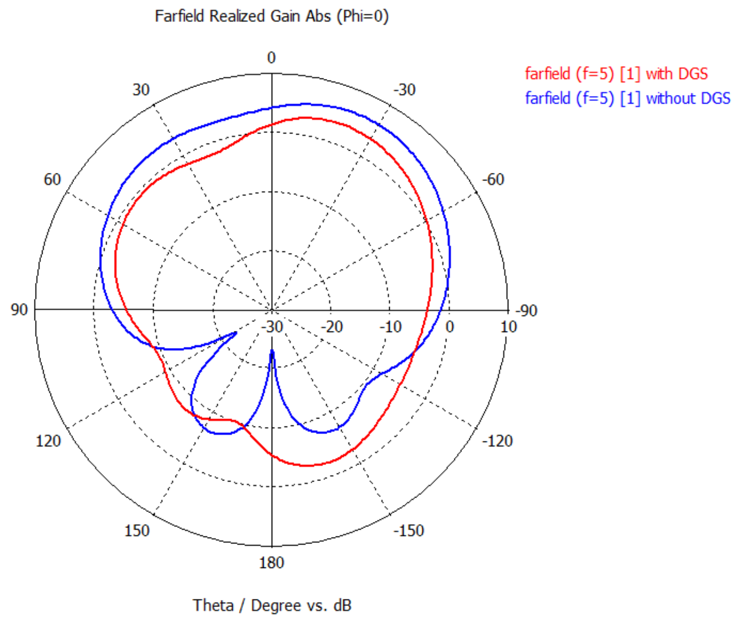

Figure 2.21: Simulated azimuth pattern of the first antenna with and without the dumbbell DGS.

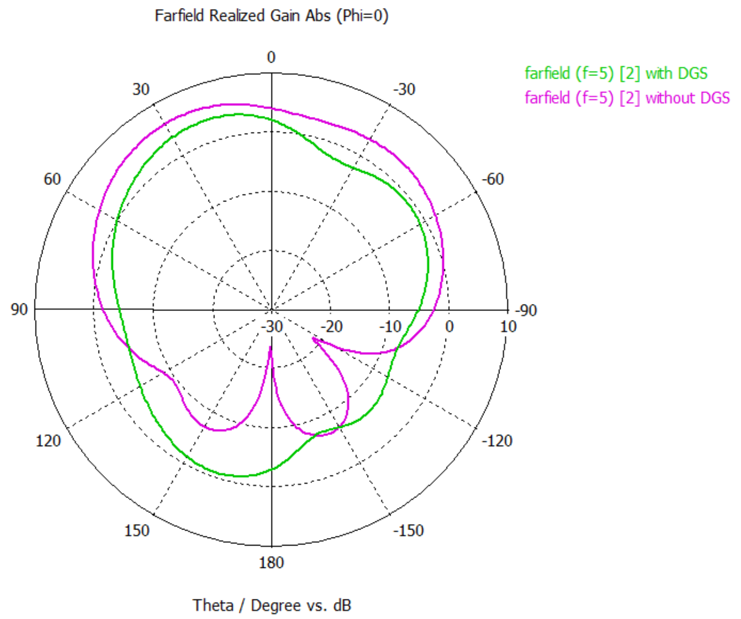

Figure 2.22: Simulated azimuth pattern of the second antenna with and without the dumbbell DGS.

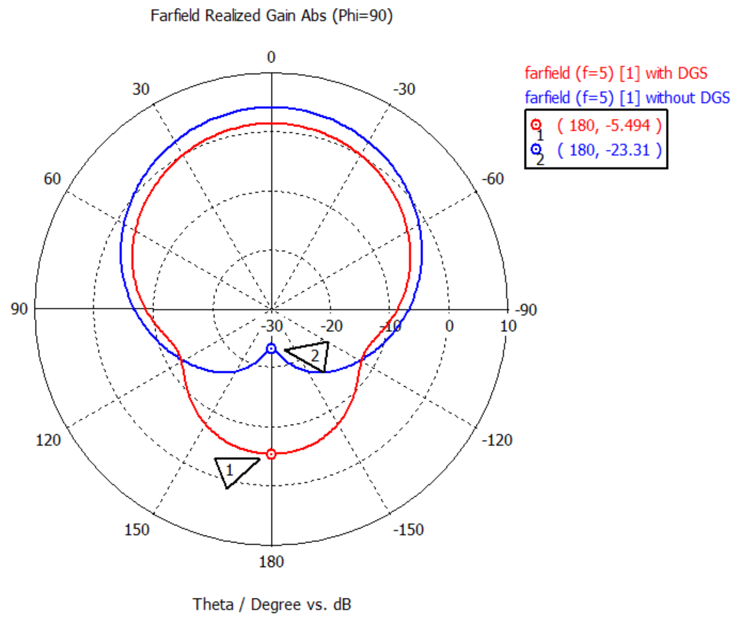

Figure 2.23: Simulated elevation pattern of the first antenna with and without the dumbbell DGS.

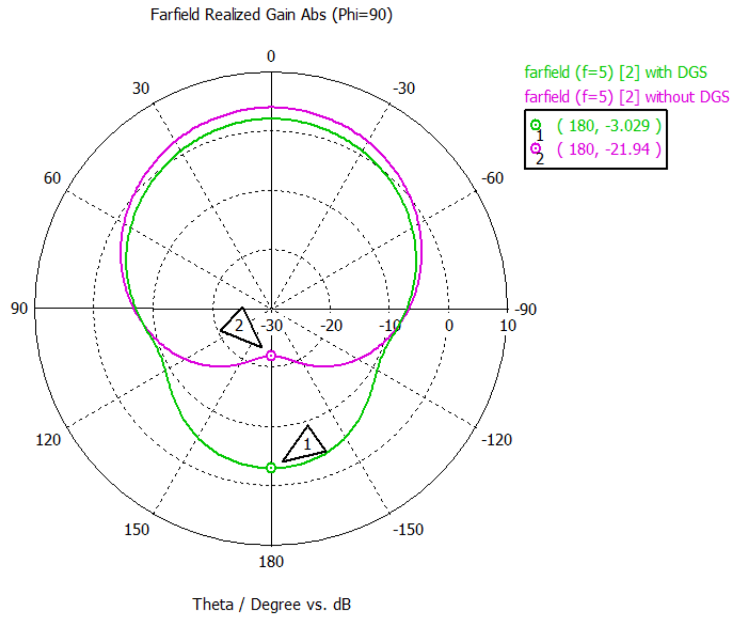

Figure 2.24: Simulated elevation pattern of the second antenna with and without the dumbbell DGS.

in Fig. 2.21 - Fig. 2.24, the presence of the dumbbell DGS results in increased backlobe and sidelobe in the both elevation and azimuth patterns of the antennas. It is seen from Fig. 2.21 and Fig. 2.22 that azimuth patterns of the antennas are negatively affected. Moreover, it is seen from Fig. 2.23 and Fig. 2.24 that the backlobe in the elevation pattern increases about 17-19 dB. The main reason behind this increase in the backlobe is because of the high ϵ_r of the substrate that leads to the very strong surface waves. When these surface waves reach to the etched dumbbell, they radiate significantly as the etched dumbbell behaves like a slot antenna and radiates strongly behind the ground plane.

The final two-element microstrip patch array-antenna is designed on ARLON TC600 ($\epsilon_r = 6.15$ and $\tan\delta = 0.002$). The board outline dimensions of the antenna are 66 mm $\times$ 50 mm and the thickness of the dielectric material is 1.524 mm. The length and width of the antennas are 15.86 mm $\times$ 10.84 mm, respectively. Similar to the previous cases, the feed location of each antenna is at the middle of the length and $c = 2$ mm away from the center of the antenna along the width direction as shown in Fig. 2.25. The edge-to-edge separation

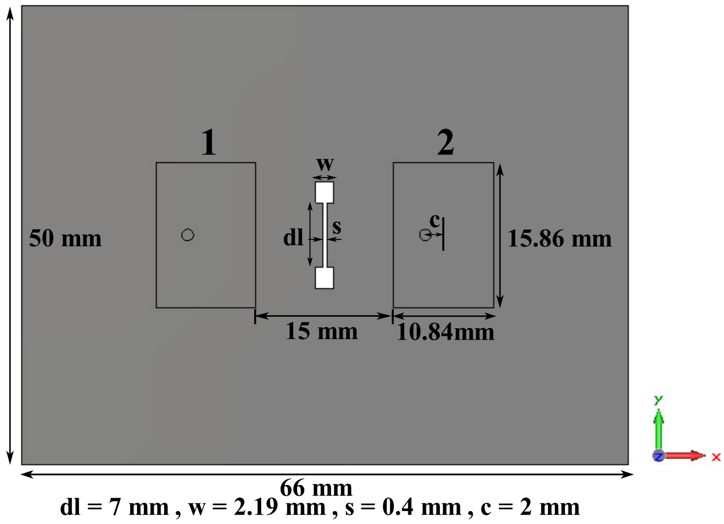

Figure 2.25: Top view of the 2 element array on ARLON TC600 with antenna and substrate dimensions.

is set to $\lambda_o/4$ (15 mm). Antennas and the etched dumbbell DGS are aligned at the middle of the substrate as in the other cases. Furthermore, during the simulations, antennas are fed one at a time while the other antenna is terminated to a 50 Ω load as previous simulations. The dimensions of the dumbbell are dl = 7 mm, w = 2.19 mm and s = 0.4 mm, so that it can resonate at 5 GHz.

Fig. 2.26 shows the magnitude of the return loss ($|S_{11}|$and $|S_{22}|$ in dB) of the antennas versus frequency in the presence and absence of the dumbbell DGS. Similarly, Fig. 2.27 shows the magnitude of the mutual coupling ($|S_{21}|$ in dB) between the antennas versus frequency with and without the dumbbell DGS. It is seen from Fig. 2.26 that the frequency shift in the resonance frequency of the both microstrip patch antennas is less than 20 MHz. On the other hand, as shown in Fig. 2.27, the mutual coupling reduction between the patch antennas is about 10 dB at 5 GHz. Since the relative dielectric constant of ARLON TC600 is less than that of ARLON 1000, reflected surface waves are reduced and hence their effect in shifting the resonance frequency is less significant. However, back radiation problem due to the etched dumbbell behaving like a slot antenna as

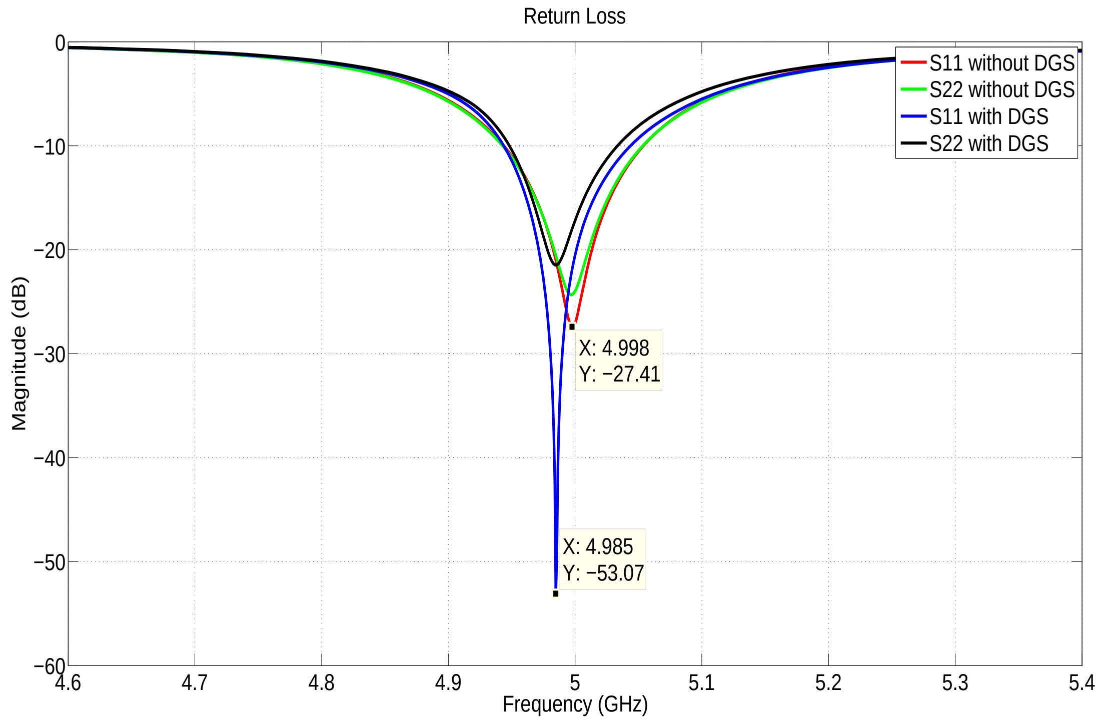

Figure 2.26: Simulated return loss ($|S_{11}|$ and $|S_{22}|$ in dB) results of antennas with and without the dumbbell DGS.

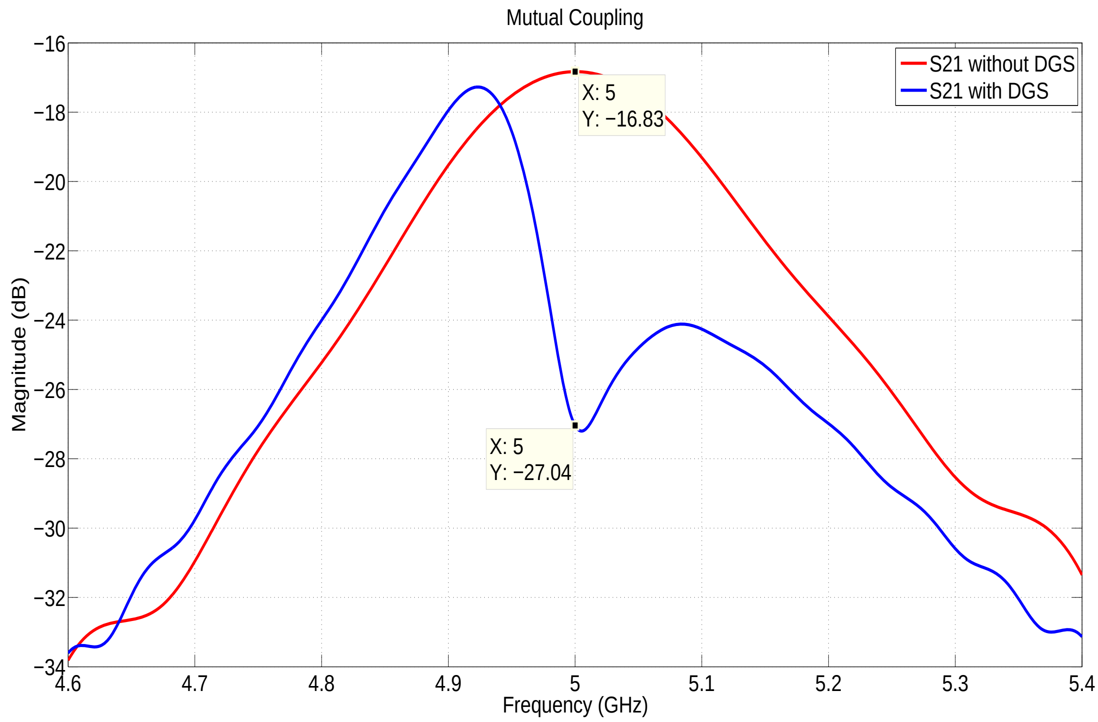

Figure 2.27: Simulated mutual coupling ($|S_{21}|$ in dB) results between antennas with and without the dumbbell DGS.

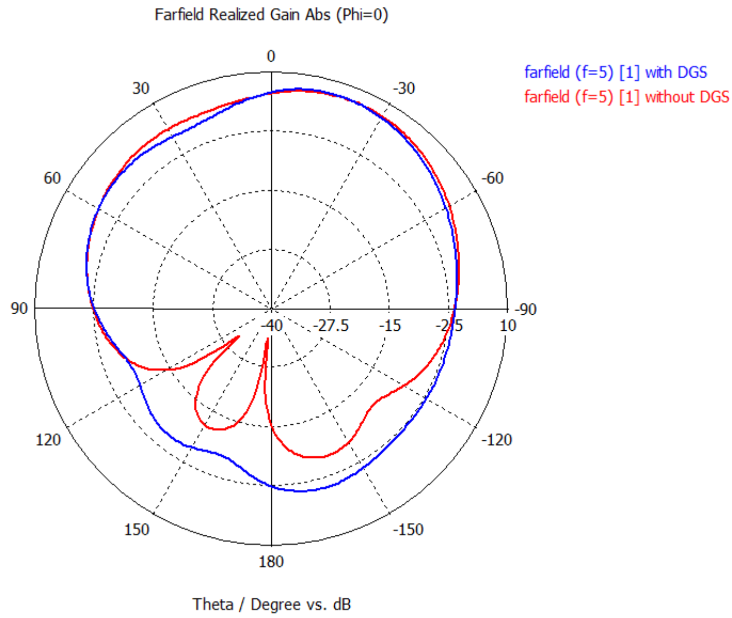

Figure 2.28: Simulated azimuth pattern of the first antenna with and without the dumbbell DGS.

well as the reflected surface waves still exists (compared to the Rogers 5880 case) as seen in the radiation pattern results illustrated in Fig. 2.28 - Fig. 2.31.

Fig. 2.28 and Fig. 2.29 show the simulated azimuth patterns of the first and second antennas, respectively, with and without the dumbbell DGS. Similarly, Fig. 2.30 and Fig. 2.31 show the simulated elevation patterns of the first and second antennas, respectively, with and without the dumbbell DGS. Similar to the previous case (i.e., ARLON 1000), presence of the dumbbell DGS results a backlobe especially more pronounced in the elevation patterns of the antennas and it also causes some minor changes in the sidelobes. Futhermore, the 3-dB beamwith narrows up to 12 degrees.

One final note regarding a single dumbbell DGS is that when the surface waves are stronger, a dumbbell DGS provides a significant mutual coupling reduction (see ARLON AR1000 results) despite a significant increase in the backlobe radiation; and the reverse is true when the surface waves are weaker (see Rogers 5880 results). Also note that the strength of the surface waves are related to the

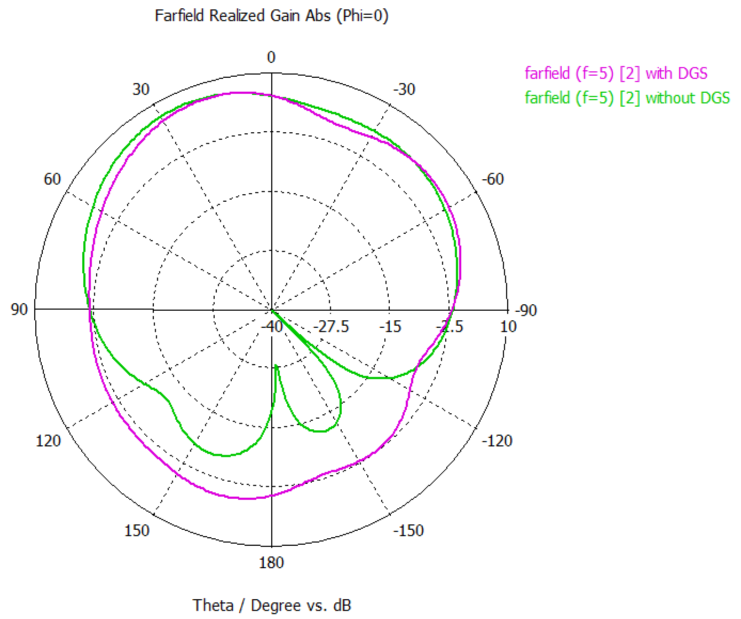

Figure 2.29: Simulated azimuth pattern of the second antenna with and without the dumbbell DGS.

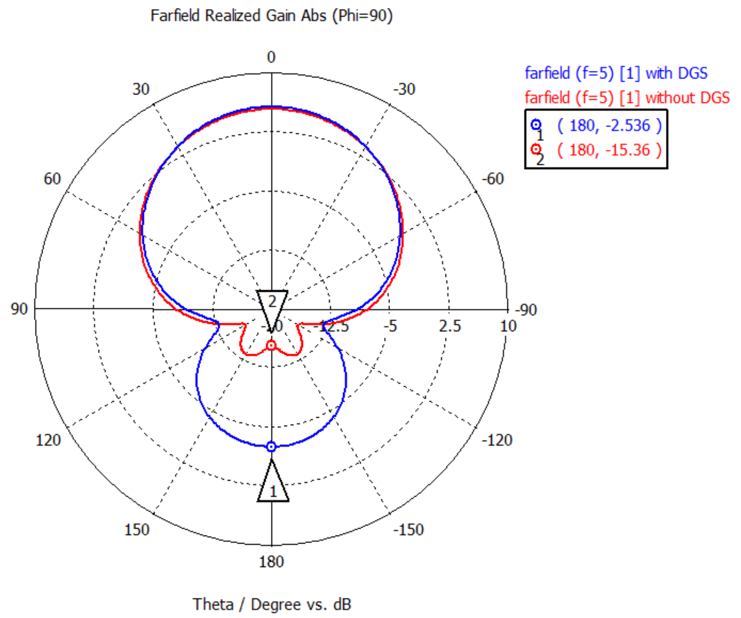

Figure 2.30: Simulated elevation pattern of the first antenna with and without the dumbbell DGS.

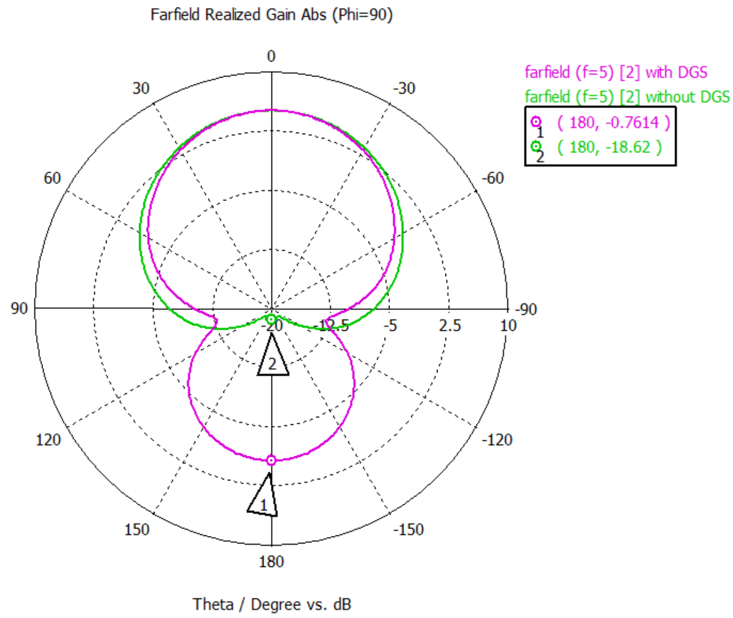

Figure 2.31: Simulated elevation pattern of the second antenna with and without the dumbbell DGS.

ϵ_r of the substrate. Because the thickness of all three substrates are very close to each other, the bigger the ϵ_r, the stronger the surface waves are.

Mutual Coupling Reduction with Multiple Dumbbell DGS

Since the backlobe radiation levels of the patch antennas on Rogers 5880 are lower and the mutual coupling reduction is inadequate, investigation of the effects of the multiple dumbbell based DGS is made on Rogers 5880 (ϵ_r = 2.2 and tanδ = 0.0009 with thickness of 1.574 mm). The board outline of the substrate is 100 mm $\times$ 70 mm which is the same as that of an antenna with a single dumbbell DGS. The dimensions of the microstrip patch antennas are kept the same (i.e., 23.71 mm $\times$ 18.45 mm). Each antenna is fed from the middle of its length and c = 3.8 mm away from its center along the width direction as shown in Fig. 2.30. The edge-to-edge separation remains the same (i.e., $\lambda_o/4$ = 15 mm). In order to increase the mutual coupling reduction levels, with an inter-element spacing of 6 mm are inserted on the ground plane of the two-element microstrip as shown in

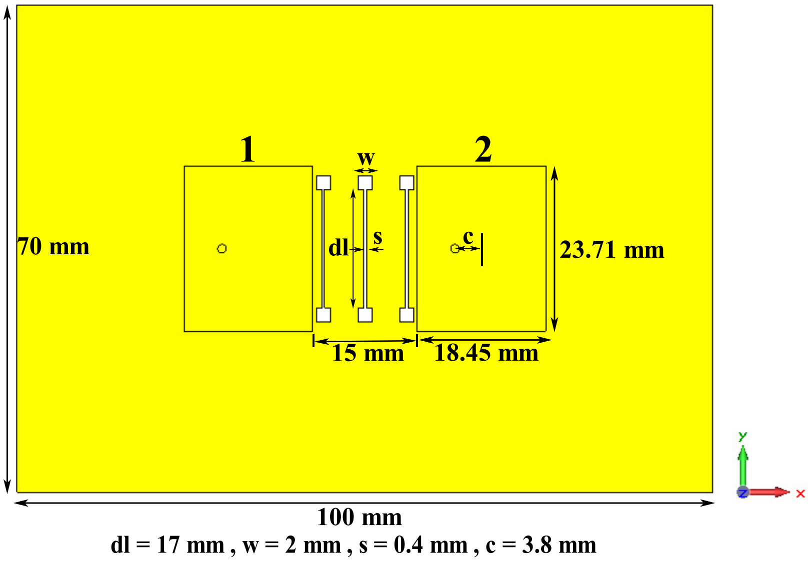

Figure 2.32: Top view of the 2-element array on Rogers 5880 with the antenna and substrate dimensions.

Fig. 2.32. The dimensions of each dumbbell are as follows: dl = 17 mm, w = 2 mm and s = 0.4 mm.

Fig. 2.33 shows the magnitude of the return loss ($|S_{11}|$and $|S_{22}|$ in dB) of the antennas versus frequency in the presence and absence of the three-dumbbell DGS. Similarly, Fig. 2.34 shows the magnitude of the mutual coupling ($|S_{21}|$ in dB) between the antennas versus frequency with and without the three-dumbbell DGS. As seen from Fig. 2.33, the frequency shift at the resonance frequency of the patch antennas increases about 80 MHz to 100 MHz. Since the feed location of the second antenna is closer to the dumbbells, its matching is affected more than the first antenna. However, as seen in Fig. 2.34, a reduction of 9 dB around 5GHz is obtained for the mutual coupling between antennas.

Fig. 2.35 and Fig. 2.36 show the simulated azimuth patterns of the first and second antennas, respectively, with and without the three-dumbbell DGS. Similarly, Fig. 2.37 and Fig. 2.38 show the simulated elevation patterns of the first and second antennas, respectively, with and without the three-dumbbell DGS. As seen from the radiation pattern results, although the front to backlobe ratio of

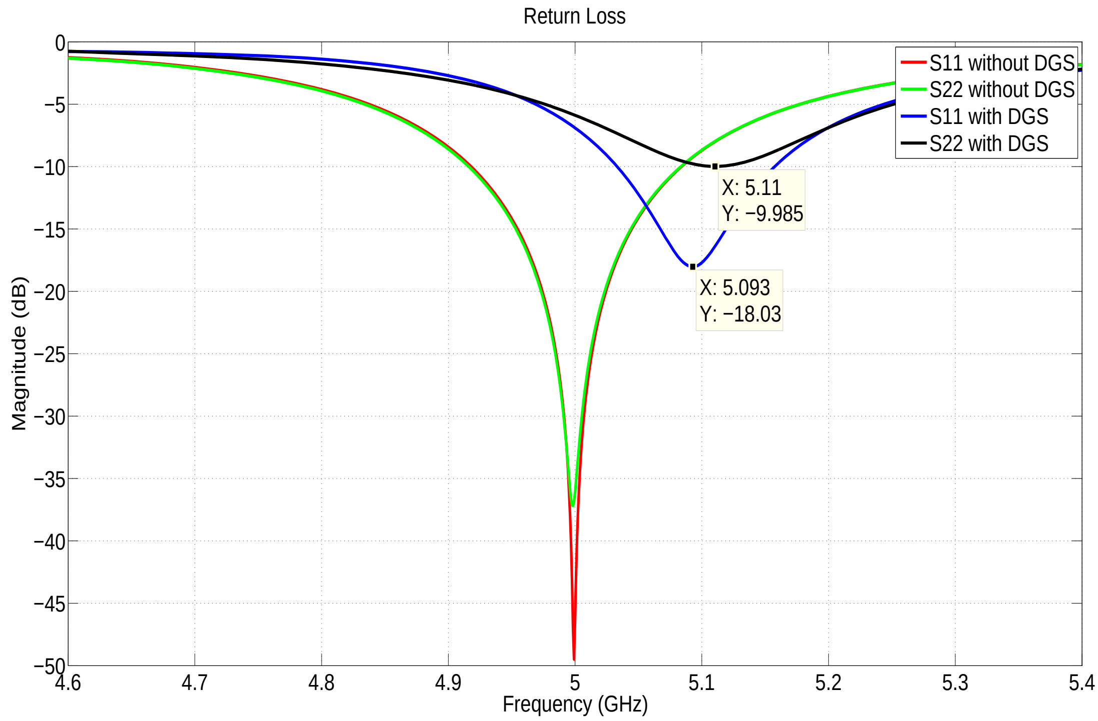

Figure 2.33: Simulated return loss ($|S_{11}|$ and $|S_{22}|$ in dB) of the antennas with and without the three-dumbbell DGS.

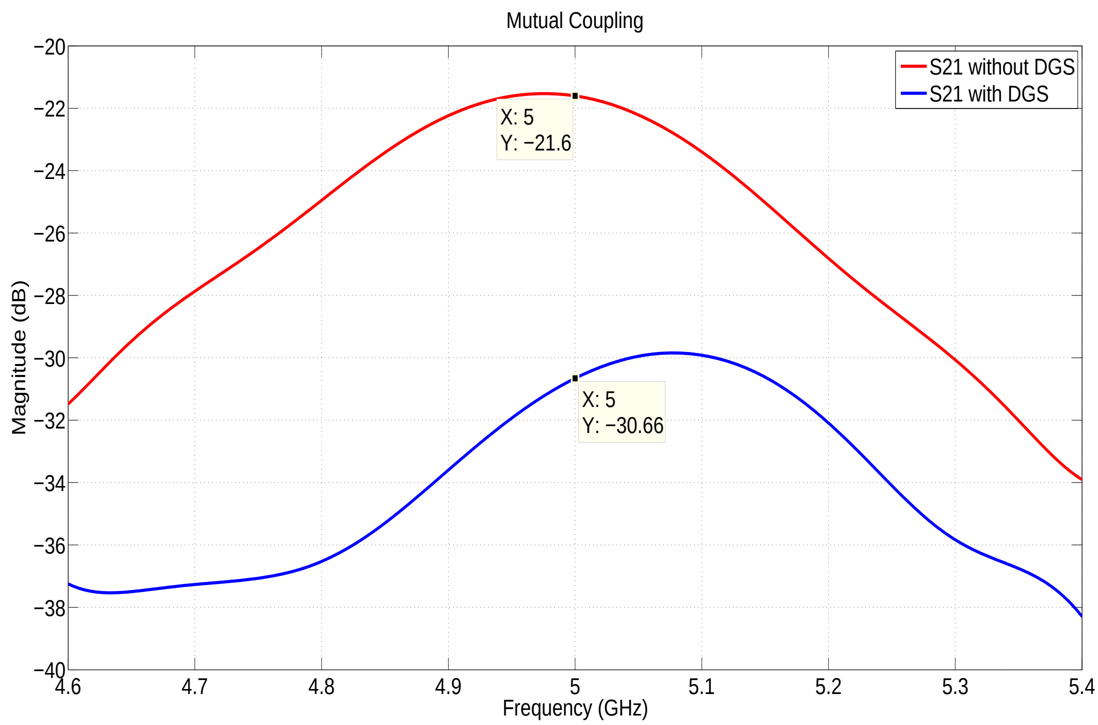

Figure 2.34: Simulated mutual coupling ($|S_{21}|$ in dB) results between antennas with and without the three-dumbbell DGS.

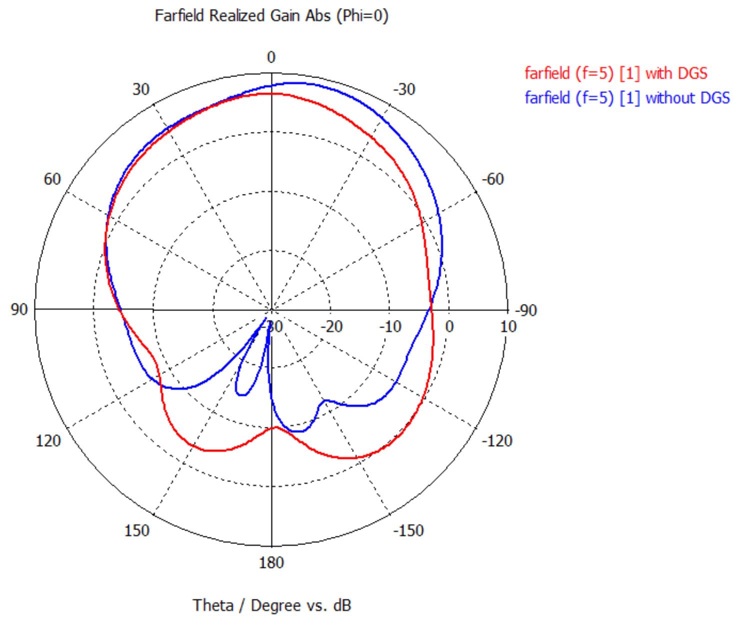

Figure 2.35: Simulated azimuth pattern of the first antenna with and without the three-dumbbell DGS.

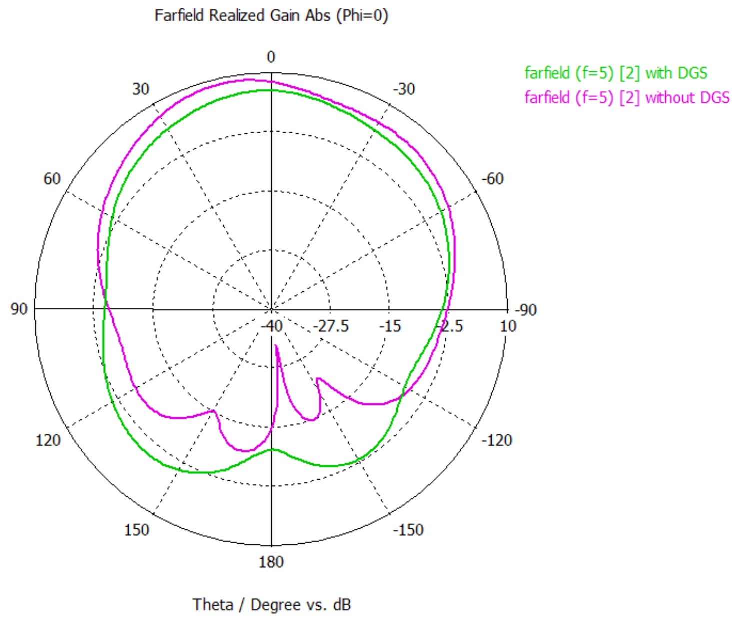

Figure 2.36: Simulated azimuth pattern of the second antenna with and without the three-dumbbell DGS.

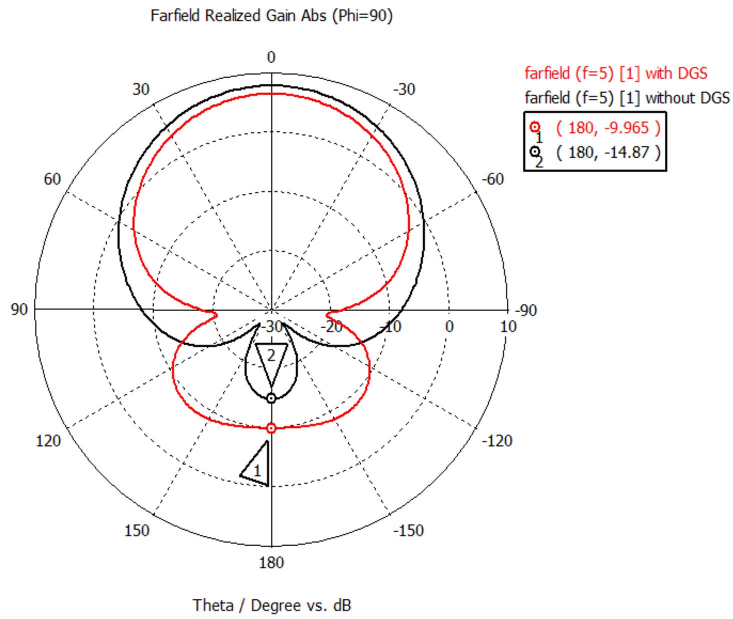

Figure 2.37: Simulated elevation pattern of the first antenna with and without the three-dumbbell DGS.

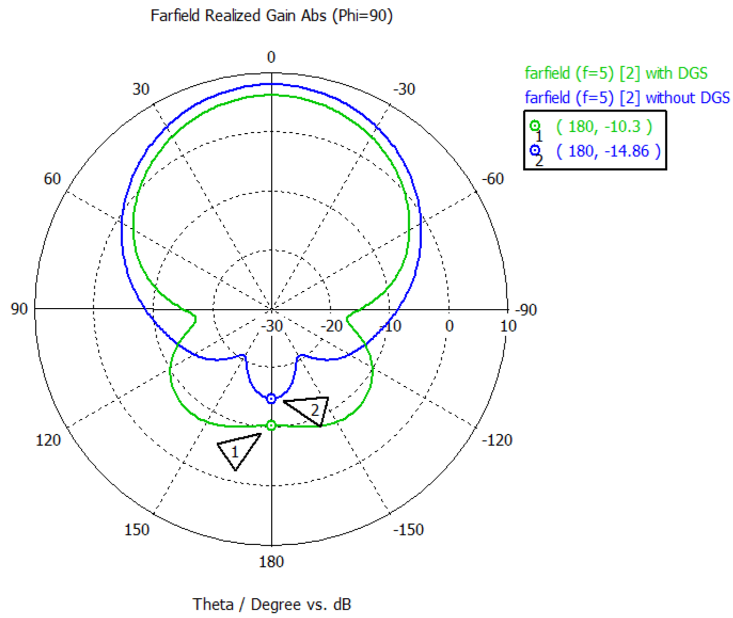

Figure 2.38: Simulated elevation pattern of the second antenna with and without the three-dumbbell DGS.

the antennas do not increase much (about 4 dB and 5dB, respectively), the sidelobes of the antennas increases significantly (about 8 dB and 3 dB, respectively). Since an increased beamwidth at the backlobe would cause more multipath signal propagation that occurs as a result of waves being reflected from the objects nearby the receiver antenna, data acquired from the transmitting antenna would be corrupted due to the multipath signal between the transmitting and the receiving antennas. Hence, the precision of the measurements would be degraded [13]. This problem is significant in the global positioning systems (GPS) . Therefore, it is decided not to use multiple dumbbell-based DGS between the adjacent microstrip patch antennas.

2.3 Analysis of Slotted Complementary Split Ring Resonator (SCSRR) DGS

2.3.1 Band Rejection Characteristics of SCSRR DGS

SCSRR is a more complicated structure than the dumbbell. In a SCSRR, there are six parameters (a, b, g, L, ws and Ls) to optimize as shown in Fig. 2.39. Hence, the optimization time is significantly longer compared to that of a dumbbell. Moreover, production of the SCSRR is more sensitive than that of a dumbbell because of the maze like geometry. However, notice that most of these parameters are optimized so that SCSRR can work at the desired frequency. Therefore, only the inter-element spacing between SCSRRs and the number of SCSRRs are investigated from the band rejection point of view.

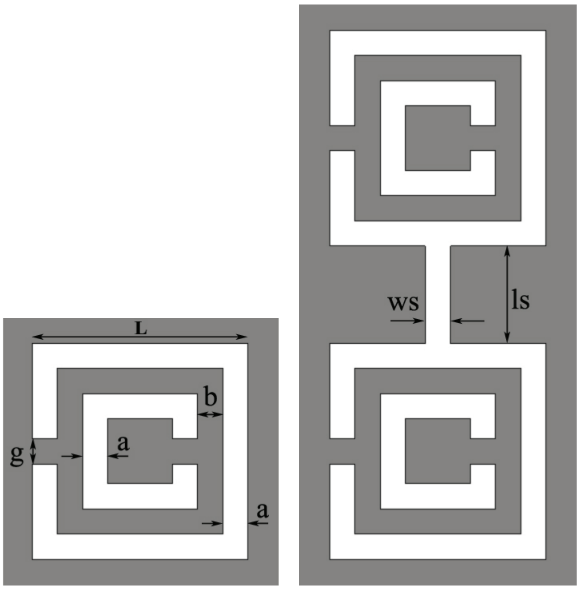

(a) (b)

Figure 2.39: (a) Complementary Split Ring Resonator (CSRR) unit cell (b) SCSRR unit cell

Effects of the Inter-Element Spacing between the SCSRRs to the Frequency Response of the SCSRR DGS

Same parametric setup that is used to determine the frequency response of the dumbbell DGS is used to find out the frequency response of the SCSRR type DGS. As a dielectric material again Rogers 5880 (ϵ_r = 2.2 and tanδ = 0.0009 with 1.524 mm thickness) is used. The board outline of the substrate is chosen to be same as in Section 2.1.1, that is 70 mm × 100 mm. The width of the 50 Ω line that is constructed on the dielectric material is 4.69 mm, and like the dumbbell DGS case, both ends of the microstrip line are terminated to waveguide ports as illustrated in Fig. 2.40(a).

In Fig. 2.40(b), multiple SCSRRs that are etched to the ground plane under the microstrip line are illustrated. In order to understand the effect of inter-element spacing on the frequency response of the SCSRR DGS, three SCSRRs are etched to the ground plane and the inter-element spacing is varied from 5

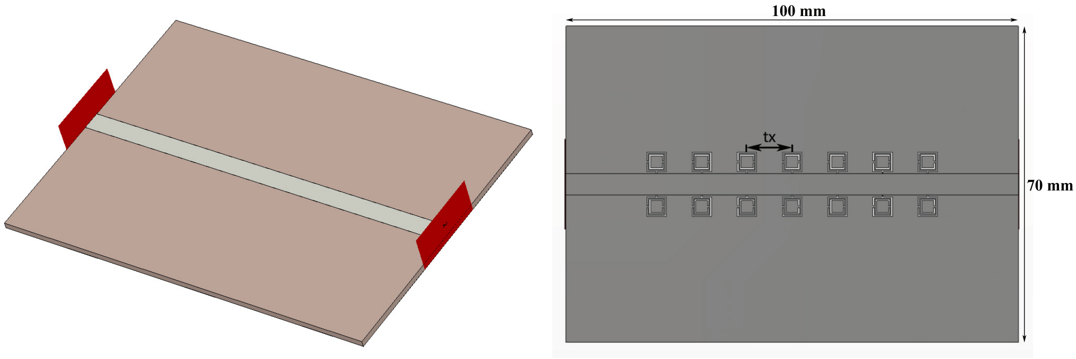

(a) (b)

Figure 2.40: (a) Perspective view of the 50 Ω microstrip line on a substrate Rogers 5880 with $\epsilon_r = 2.2$, tan$\delta = 0.0009$ and thickness 1.524 mm with waveguide ports (multiple SCSRRs are etched on the ground plane). (b) Top view of the SCSRRs that form the DGS as illustrated together with the microstrip line.

mm to 30 mm. In simulations, the parameter named tx is assigned to govern the inter-element spacing as shown in Fig. 2.41. The SCSRRs are designed to resonate at 5 GHz. Hence, their dimensions are ws = 0.22 mm, ls = 2.6 mm, L = 4.28 mm, g = 0.5 mm and a = b = 0.27 mm.

Fig. 2.41 indicates the magnitude of the transmission characteristics ($|S_{21}|$dB) of a three SCSRR structure versus frequency when the inter-element spacing tx is varied from 5 mm to 30 mm. It is seen from Fig. 2.41 that as tx increases suppression at 5 GHz increases while the bandwidth of the rejection band decreases as in the dumbbell DGS case. However, bandwidths of the suppression for tx = 5 mm to 30 mm seems to be narrower than that of the dumbbell DGS (see Fig. 2.5).

Effects of the Number of SCSRRs to the Frequency Response of the SCSRR DGS

Effects of the number of unit SCSRR cells to the frequency response of the SCSRR DGS is also examined on the same substrate with the same 50 Ω microstrip

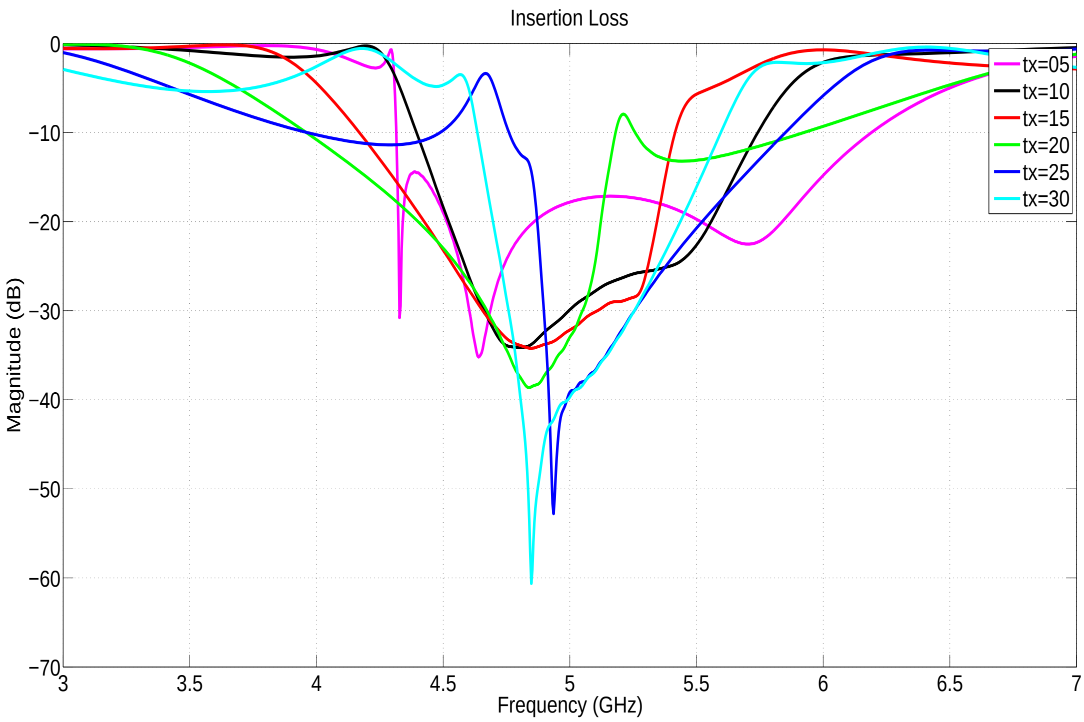

Figure 2.41: Frequency response of the three-SCSRR DGS as a band stop filter when the inter-element spacing tx is changed from 5 mm to 30 mm.

line. The SCSRR dimensions are kept the same as in the previous subsection of Section 2.3.1. n denotes the number of SCSRRs in the simulations and the inter-element spacing tx is set to 7.5 mm. Magnitude of the transmission characteristics ($|S_{21}|$dB) of the SCSRR structure versus frequency when the number of SCSRR elements are varied from 1 to 11 is shown in Fig. 2.42. It can be seen from the simulation results (see Fig. 2.42) that as the number of unit SCSRR cells increases, both the bandwidth of the stop band and the suppression levels at 5 GHz increase. However, when Fig. 2.42 and Fig. 2.6 are compared, the bandwidth of the suppression is wider when the dumbbell DGS is used instead of the SCSRR DGS.

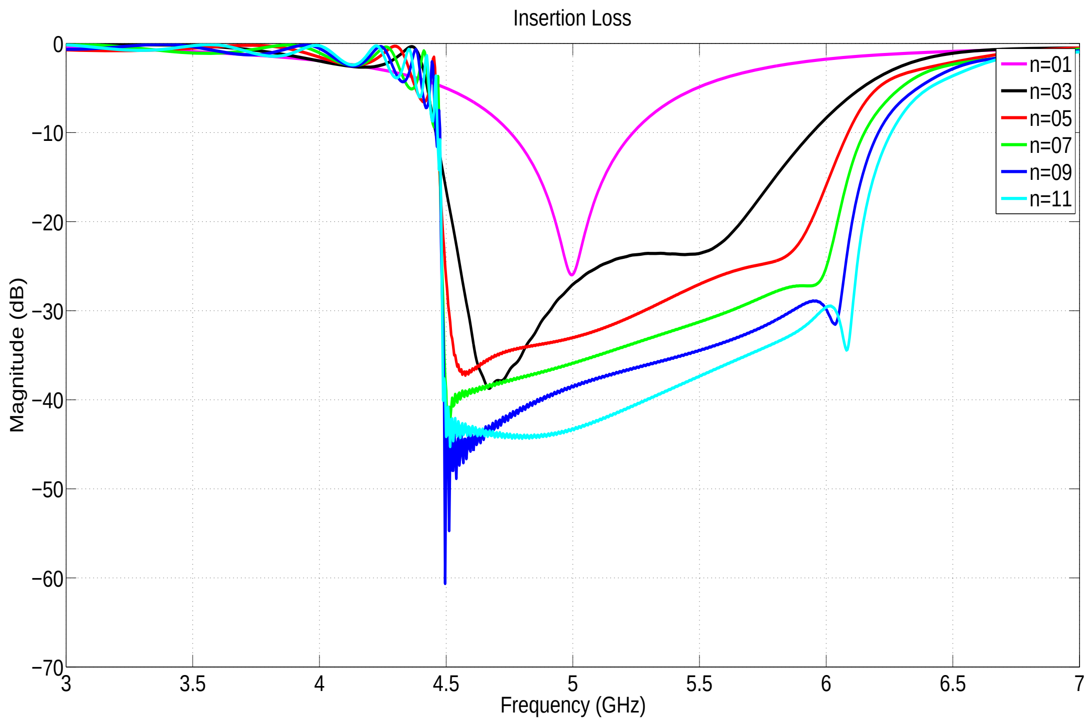

Figure 2.42: Frequency responses of the SCSRR DGS as a band stop filter when the number of unit SCSRR cells is varied.

2.3.2 Mutual Coupling Reduction and Far-Field Results Using a Single SCSRR DGS with Different Substrates

Recall that we have tested three different dielectric materials for the dumbbell DGS case where the dielectric constants have been ranging from 2.2 to 10. Based on the obtained results, the substrate AR1000 with $\epsilon_r = 10$ and $\tan\delta = 0.003$ is the worst choice since it shifts the return loss more than 150 MHz and the back-lobe radiation increases more than 20 dB. Despite having low suppression levels, the dumbbell DGS that is constructed on Rogers 5880 may still be attractive due to the minimal increase in the backlobe levels. Therefore, we have decided to use both Rogers 5880 and ARLON TC600.

As a first step, a single SCSRR is etched to the ground plane between the adjacent microstrip antennas on a Rogers 5880 ($\epsilon_r = 2.2$ and $\tan\delta = 0.0009$).

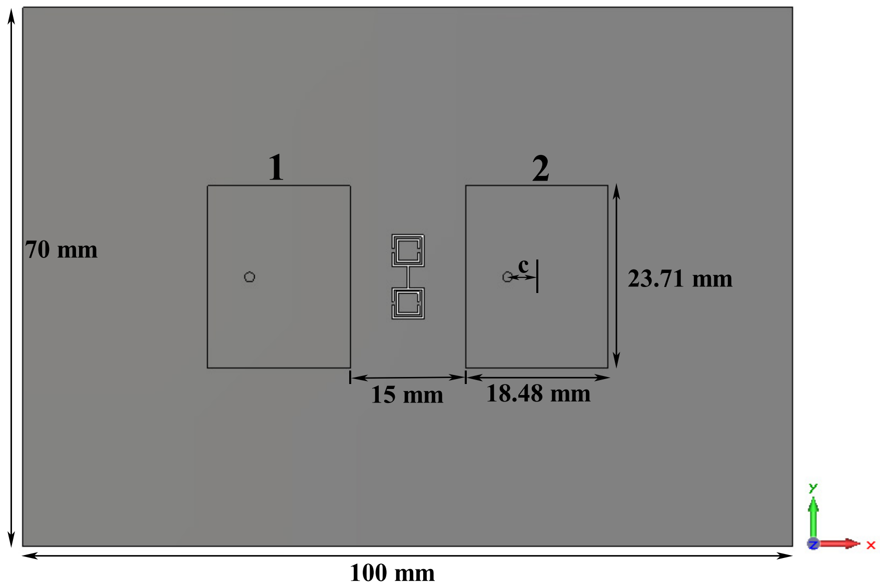

(a)

Figure 2.43: Top view of the two-element array on Rogers 5880 with the antenna and substrate dimensions.

The dimensions of the board outline of the antenna are 100 mm × 70 mm and the thickness of the substrate is 1.524 mm. The length and width of the antennas are, 23.71 mm × 18.48 mm, respectively. The feed location of each antenna is at the middle of the length and c = 3.8 mm away from the center of the antenna along the width direction as shown in Fig. 2.43. The edge-to-edge separation is kept the same ($\lambda_o/4$ = 15 mm). Antennas and the etched SCSRR are aligned at the middle of the substrate. Moreover, during the simulations each antenna is fed one at a time while the other antenna is terminated to a 50 Ω load. The dimensions of the SCSRR are L = 4.12 mm, ws = 0.22 mm, ls = 2.7 mm, g = 0.5 and $a = b$ = 0.27 mm, so that it resonates at 5 GHz.

Fig. 2.44 shows the magnitude of the return loss ($|S_{11}|$and $|S_{22}|$ in dB) of the antennas versus frequency in the presence and absence of the SCSRR DGS. Similarly, Fig. 2.45 shows the magnitude of the mutual coupling ($|S_{21}|$ in dB) between the antennas versus frequency with and without the SCSRR DGS. Fig. 2.44 indicates that the frequency shift in center frequency of the patch antenna

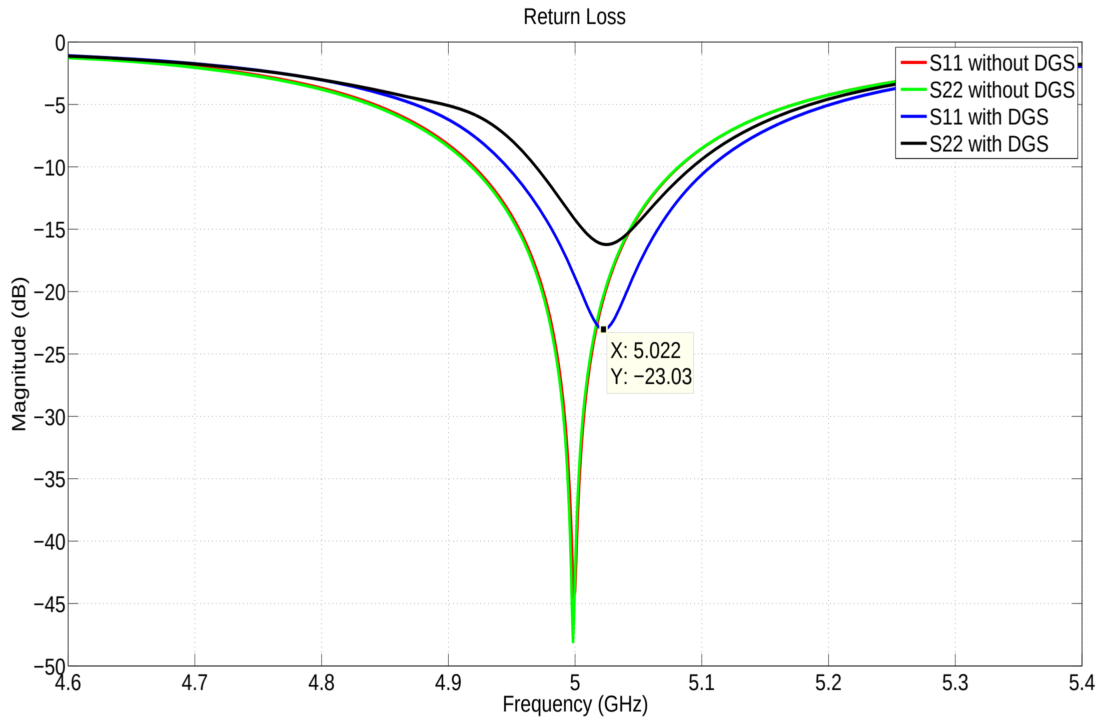

Figure 2.44: Simulated return loss results ($|S_{11}|$and $|S_{22}|$ in dB) of the antennas with and without the SCSRR DGS versus frequency

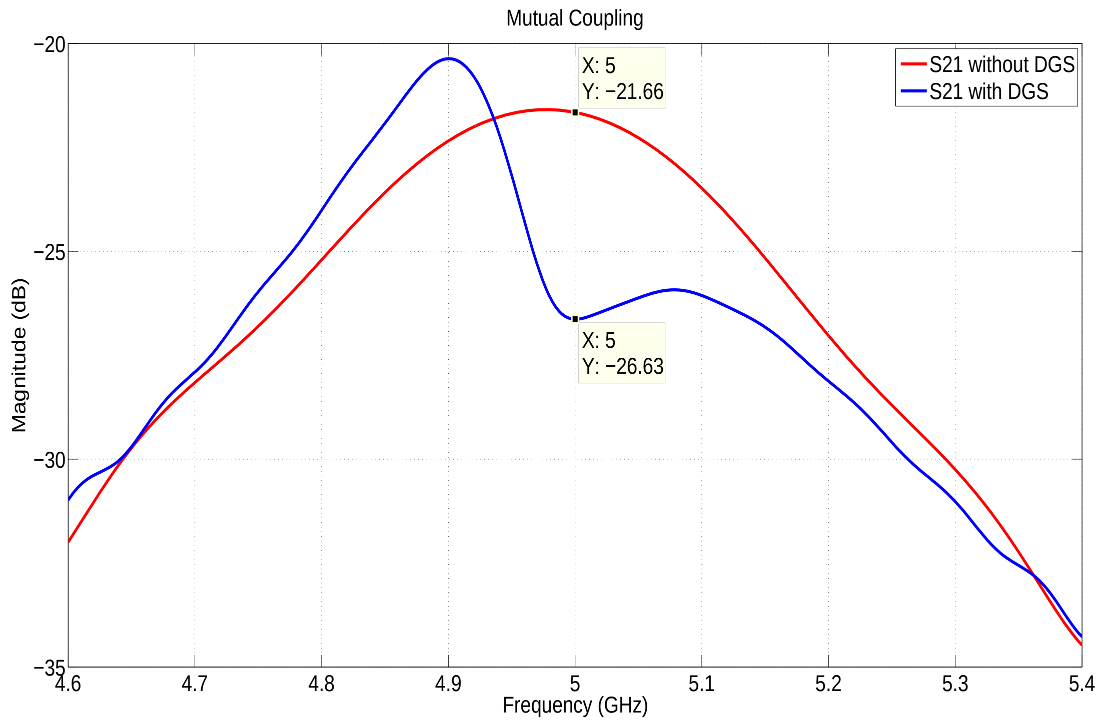

Figure 2.45: Simulated mutual coupling results ($|S_{21}|$ in dB) between the antennas with and without the SCSRR DGS versus frequency. The geometric parameters of the antennas and SCSRR are the same as those given in Fig. 2.43(b)

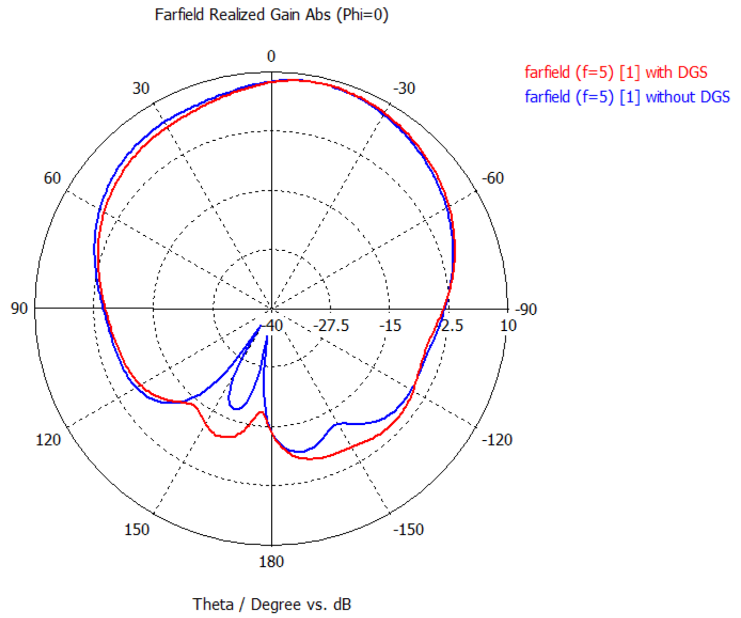

Figure 2.46: Simulated azimuth pattern of the first antenna with and without the SCSRR DGS.

is around 25 MHz and close to the value which is obtained with the dumbbell DGS on the same substrate. As in the case of the dumbbell DGS, matching of the antennas is degraded by 20 dB. In addition to that, a 5 dB mutual coupling reduction is acquired after introducing the SCSRR DGS as can be seen in Fig. 2.45.

Fig. 2.46 and Fig. 2.47 show the simulated azimuth patterns of the first and second antennas, respectively, with and without the SCSRR DGS. Additionally, Fig. 2.48 and Fig. 2.49 show the simulated elevation patterns of the first and second antennas, respectively, with and without the SCSRR DGS. Based on these farfield results (Fig. 2.46 - 2.49), the changes in the farfield patterns of the first antenna due to the SCSRR DGS are less than 3 dB as in the case of the dumbbell DGS whereas the sidelobe and the beamwidth of the second antenna are increased after the introduction of the SCSRR DGS. Futhermore, the 3-dB beamwith narrows up to 6 degrees after the introduction of SCSRR DGS. Hence, it can be concluded that the effect of the SCSRR DGS is not much different from the dumbbell DGS for this substrate.

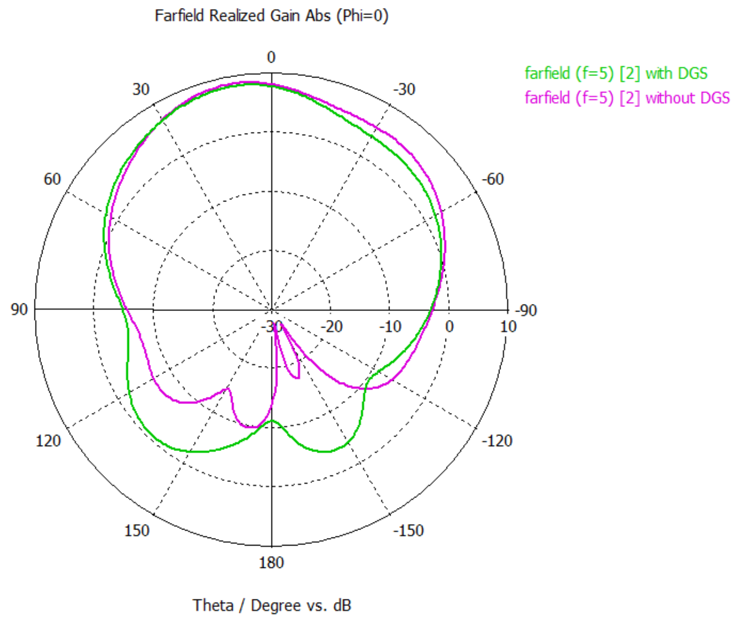

Figure 2.47: Simulated azimuth pattern of the second antenna with and without the SCSRR DGS.

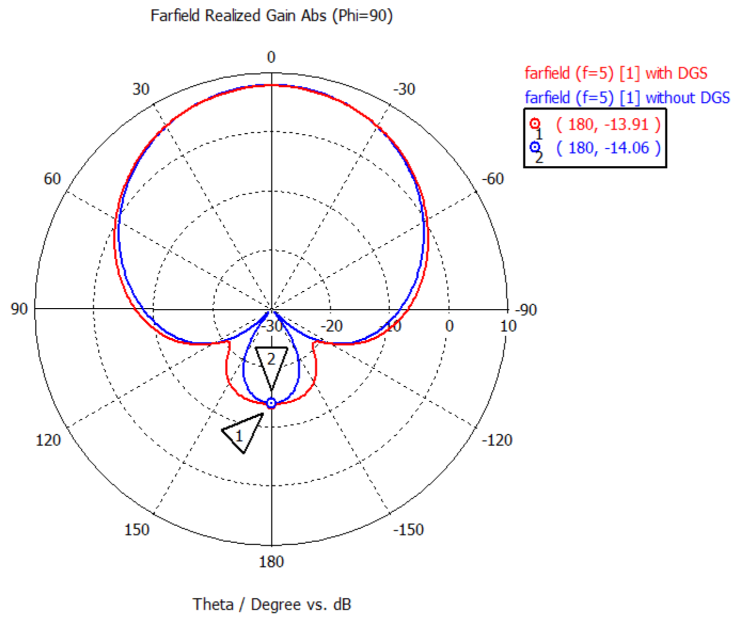

Figure 2.48: Simulated elevation pattern of the first antenna with and without the SCSRR DGS.

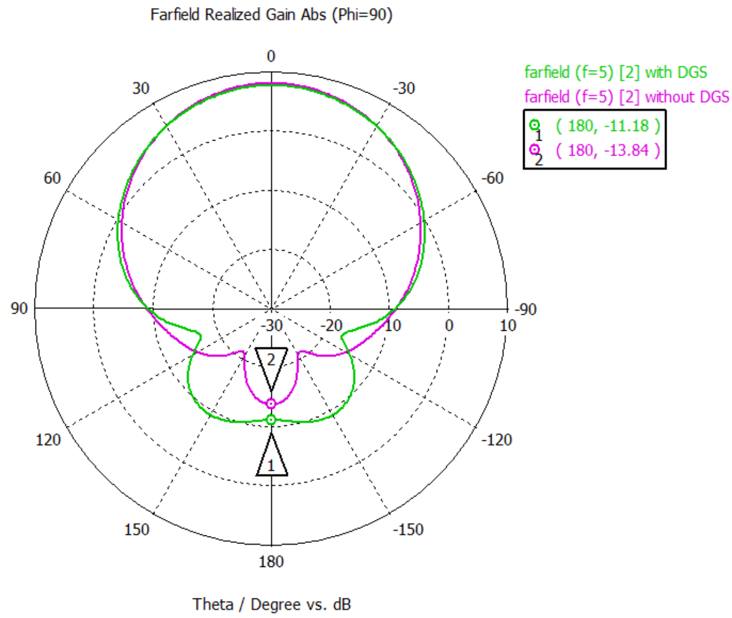

Figure 2.49: Simulated elevation pattern of the second antenna with and without the SCSRR DGS.

The second two-element microstrip array with a single SCSRR etched at the middle of the ground plane of the substrate is constructed on ARLON TC600 (ϵ_r = 6.15 and tanδ = 0.002). The board outline dimensions of the antenna are 66 mm $\times$ 50 mm and the thickness of the dielectric material is 1.524 mm. The length and width of the patch antennas are 15.86 mm $\times$ 10.84 mm, respectively. Each antenna is fed from the middle of its length and $c = 2$ mm away from its center along the width direction as shown in Fig. 2.50. The edge-to-edge separation between the antennas is still $\lambda_o/4 = 15$ mm. Antennas and the etched SCSRR are aligned at the middle of the substrate as in the previous cases. Moreover, during the simulations, antennas are fed one at a time while the other antenna is terminated to a 50 Ω load similar to the previous simulations. The dimensions of the SCSRR are $L = 4.17$ mm, $ws = 0.17$ mm, $ls = 3.7$ mm, $g = 0.5$ and $a = b = 0.17$ mm, so that it can resonate at 5 GHz.

Fig. 2.51 shows the magnitude of the return loss ($|S_{11}|$and $|S_{22}|$ in dB) of the antennas versus frequency in the presence and absence of the SCSRR DGS. Similarly, Fig. 2.52 shows the magnitude of the mutual coupling ($|S_{21}|$ in dB) between

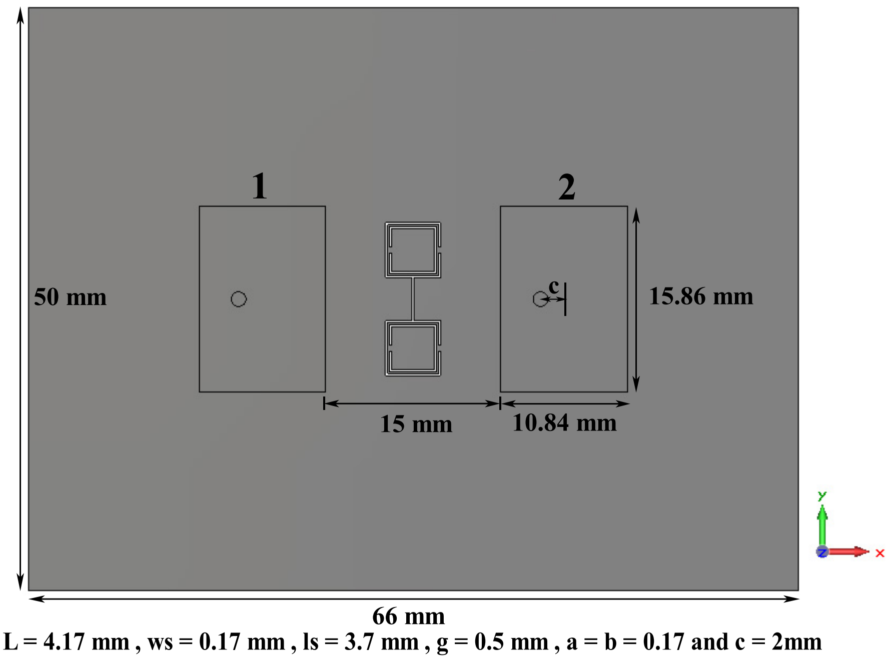

(a)

Figure 2.50: Top view of the two-element array on ARLON TC600 with the antenna and substrate dimensions.

the antennas versus frequency with and without the SCSRR DGS. Figure 2.51 indicates that the frequency shift in the resonance frequency of the microstrip patch antennas is less than 25 MHz. Furthermore, it is seen from Fig. 2.52 that insertion of the SCSRR to the ground plane provides an additional 13 dB isolation between the microstrip patch antennas.

Fig. 2.53 and Fig. 2.54 show the simulated azimuth patterns of the first and the second antennas, respectively, with and without the SCSRR DGS. Additionally, Fig. 2.55 and Fig. 2.56 show the simulated elevation patterns of the first and the second antennas, respectively, with and without the SCSRR DGS. Farfield results in Fig. 2.53 - 2.56 show that the backlobe radiation level of the patterns of the patch antennas increases by 13 dB to 18 dB, which is similar to what is observed for the dumbbell DGS case whereas azimuth patterns in Fig. 2.53 and Fig. 2.54 becomes more isotropic. Moreover, 3-dB beamwith narrows up to 10 degrees after the introduction of SCSRR DGS.

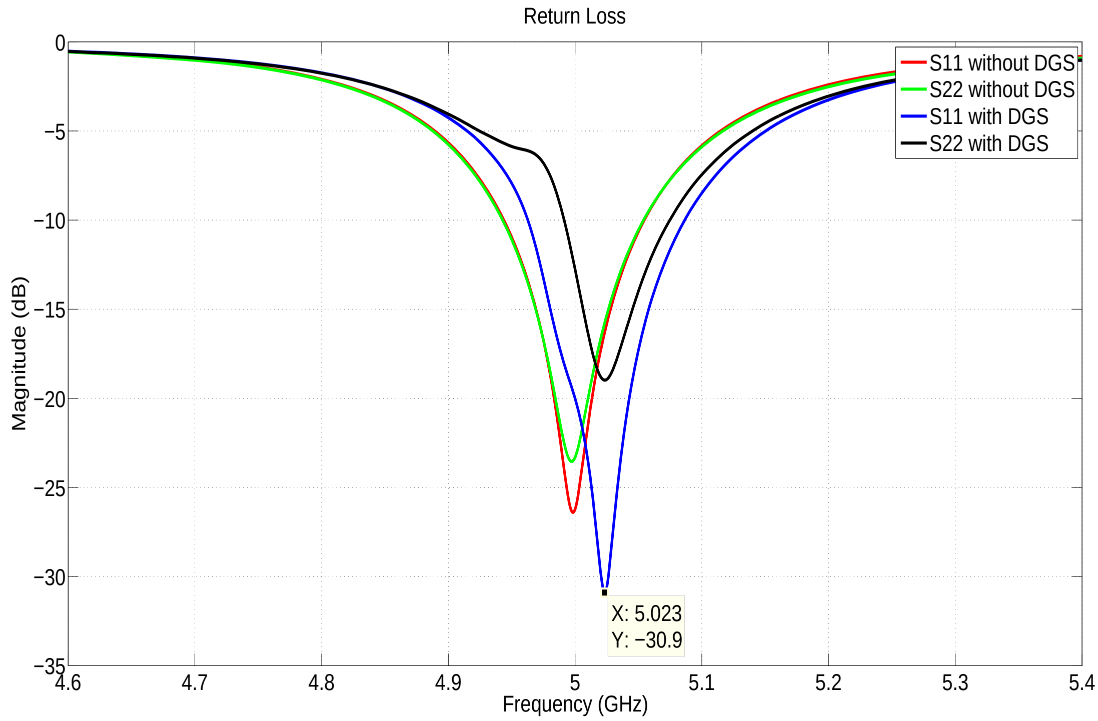

Figure 2.51: Simulated return loss ($|S_{11}|$ and $|S_{22}|$ in dB) results of the antennas with and without the SCSRR DGS.

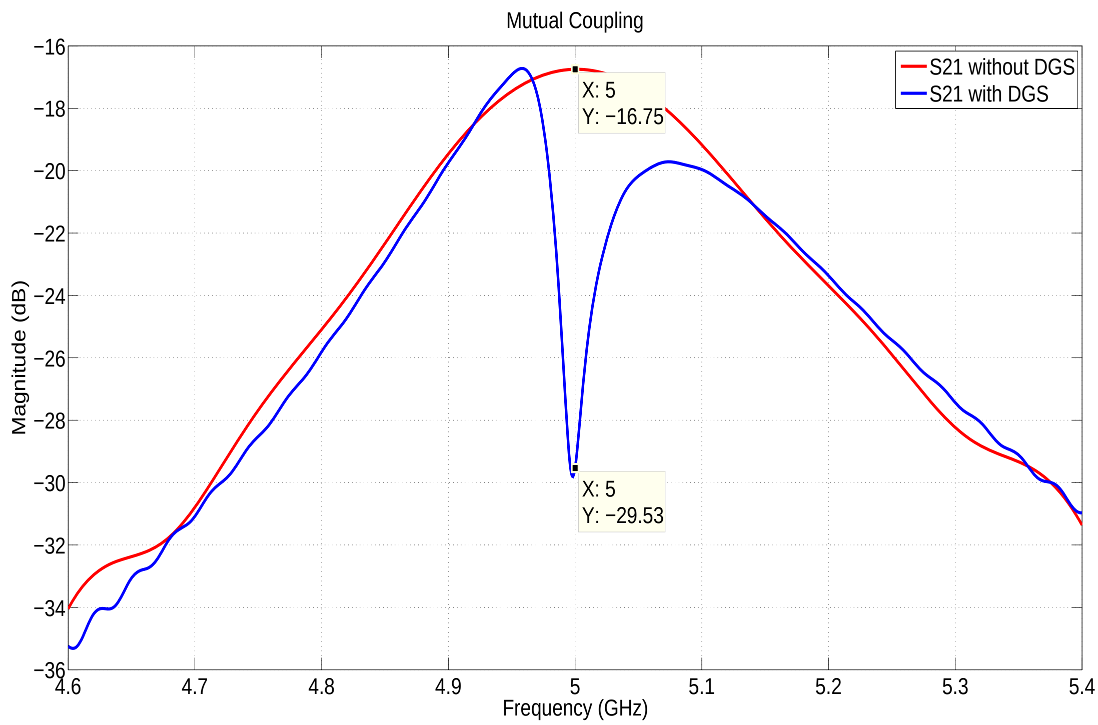

Figure 2.52: Simulated mutual coupling ($|S_{21}|$ in dB) results between the antennas with and without the SCSRR DGS.

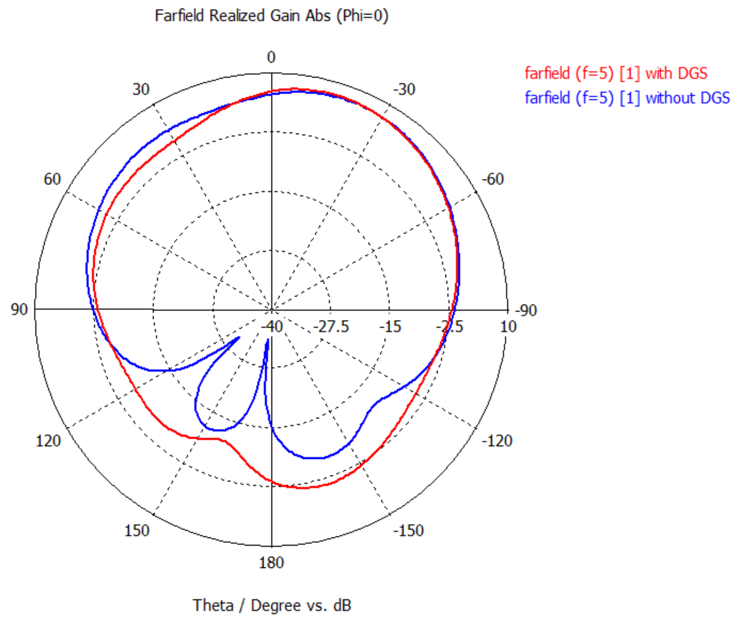

Figure 2.53: Simulated azimuth pattern of the first antenna with and without the SCSRR DGS.

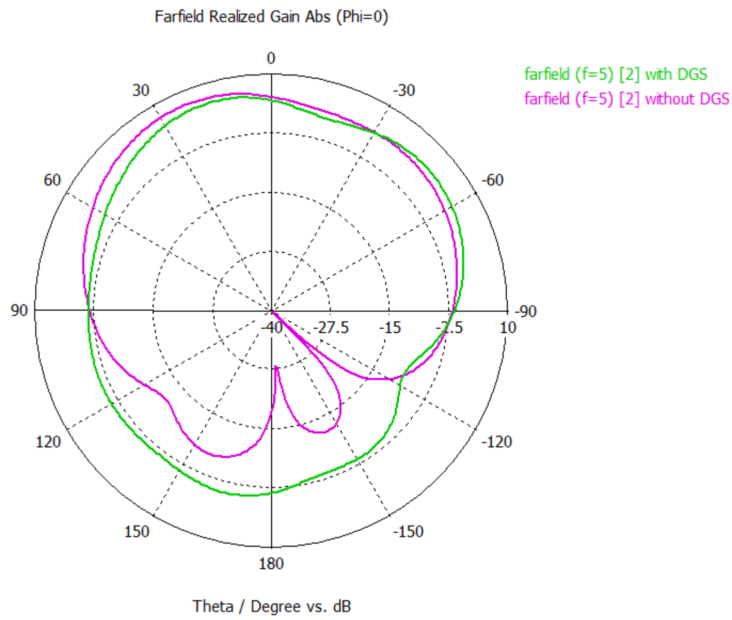

Figure 2.54: Simulated azimuth pattern of the second antenna with and without the SCSRR DGS.

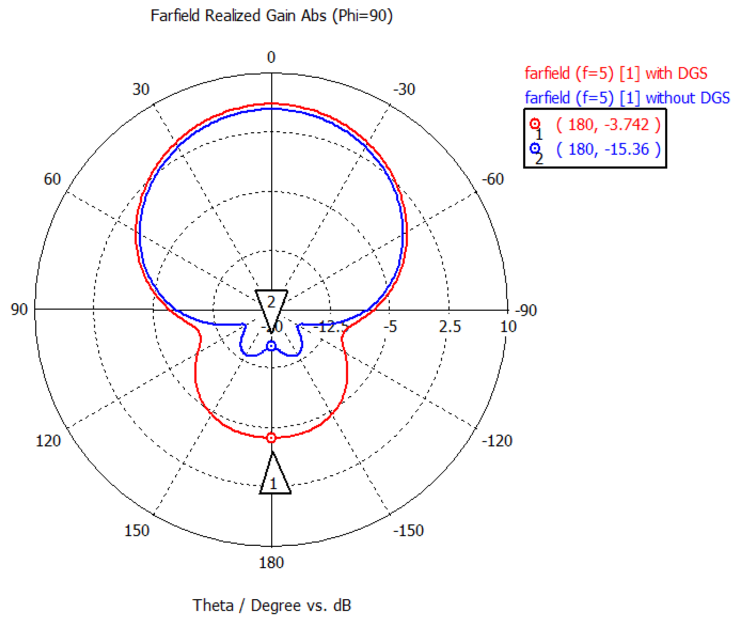

Figure 2.55: Simulated elevation pattern of the first antenna with and without the SCSRR DGS.

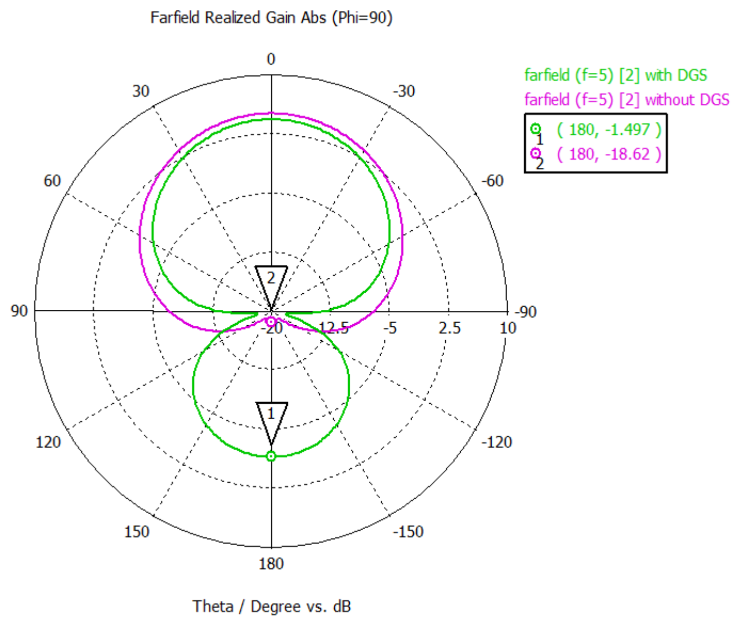

Figure 2.56: Simulated elevation pattern of the second antenna with and without the SCSRR DGS.

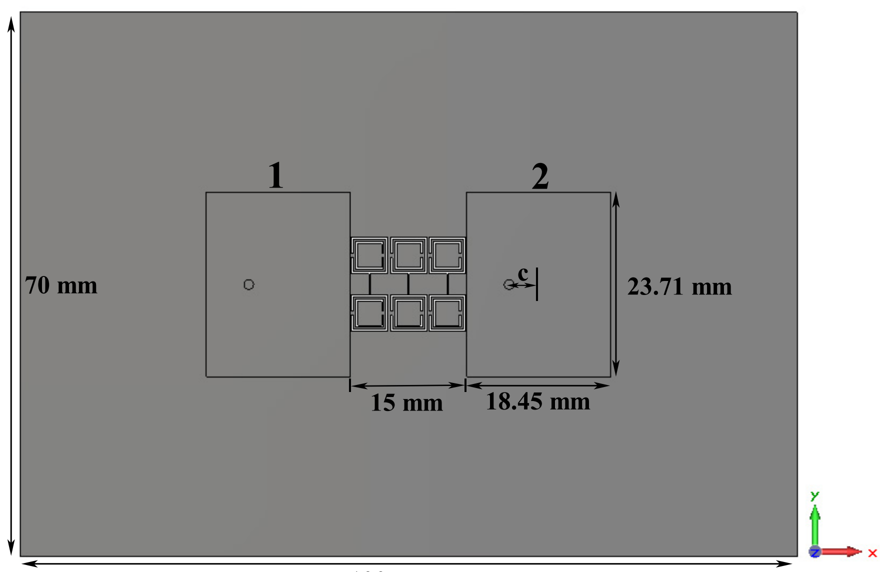

(a)

Figure 2.57: Top view of the two- element array on Rogers 5880 with the antenna and substrate dimensions.

Mutual Coupling Reduction with Multiple SCSRR DGS

As in the dumbbell DGS case, three SCSRRs resonating at 5 GHz are etched between the adjacent microstrip patch antennas. As a substrate again Rogers 5880 ($\epsilon_r = 2.2$ and tan$\delta = 0.0009$) is used. The dimensions of the board outline of the antenna are 100 mm $\times$ 70 mm and thickness of the substrate is 1.574 mm. The length and width of the antennas are 23.71 mm $\times$ 18.45 mm, respectively. Similar to the single SCSRR case, each antenna is fed from the middle of its length and $c = 3.8$ mm away from its center along the width direction as shown in Fig. 2.57. The edge-to-edge separation is kept the same (i.e., $\lambda_o/4 = 15$ mm). Antennas and the etched three SCSRRs are aligned at the middle of the substrate as shown in Fig. 2.57. Moreover, during the simulations each antenna is fed one at a time while the other antenna is terminated to a 50 Ω load. The dimensions of the SCSRRs are $L = 4.7$ mm, $ws = 0.17$ mm, $ls = 2.72$ mm , $g =$ 0.5 and $a = b = 0.27$ mm.

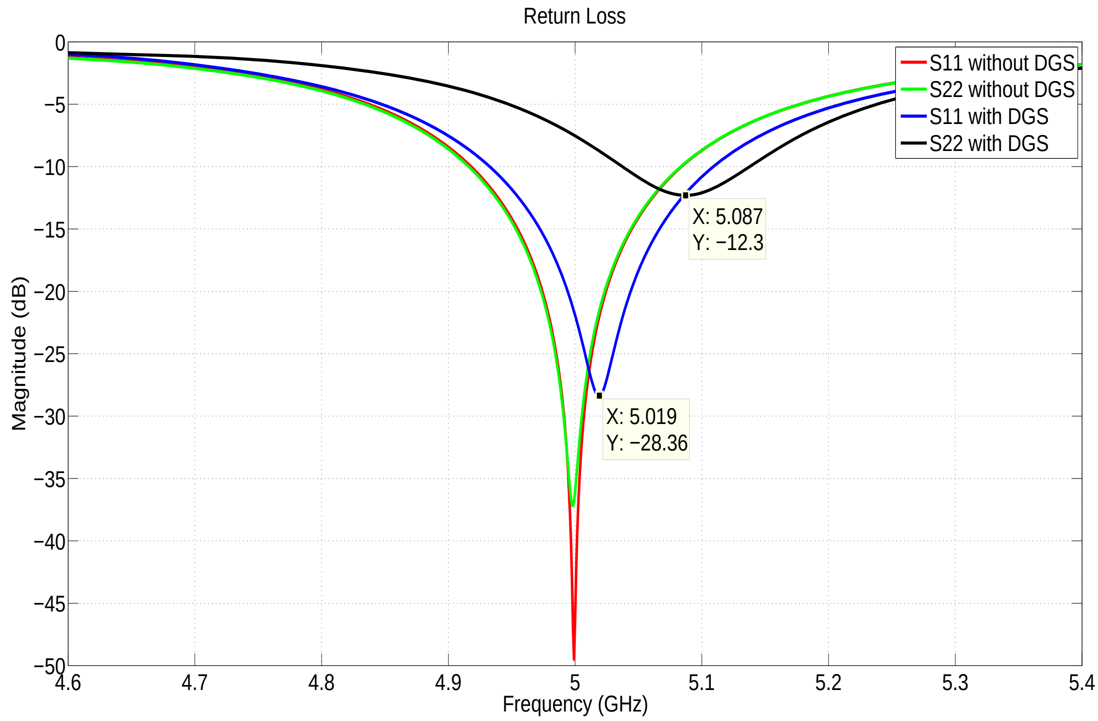

Figure 2.58: Simulated return loss ($|S_{11}|$ and $|S_{22}|$ in dB) results of the antennas with and without the three-SCSRR DGS.

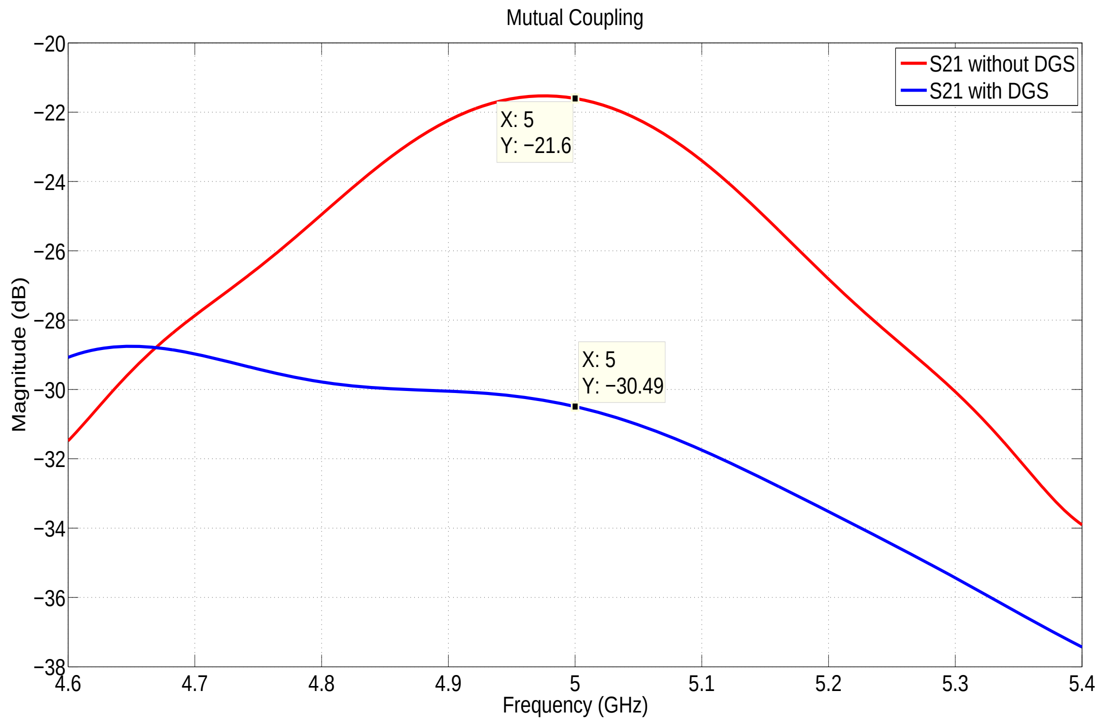

Figure 2.59: Simulated mutual coupling ($|S_{21}|$ in dB) results between the antennas with and without the three-SCSRR DGS.

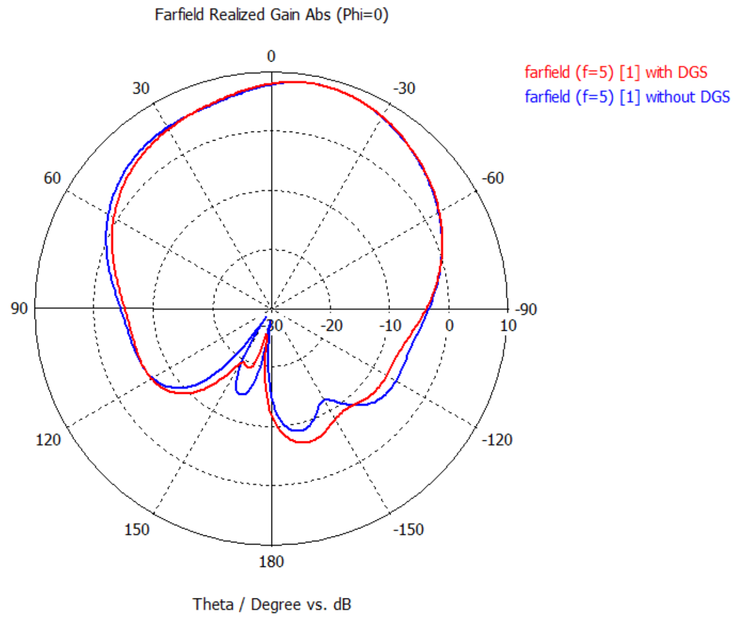

Figure 2.60: Simulated azimuth pattern of the first antenna with and without the three-SCSRR DGS.

Fig. 2.58 shows the magnitude of the return loss ($|S_{11}|$and $|S_{22}|$ in dB) of the antennas versus frequency in the presence and absence of the SCSRR DGS. Similarly, Fig. 2.59 shows the magnitude of the mutual coupling ($|S_{21}|$ in dB) between the antennas versus frequency with and without the SCSRR DGS. It is seen from Fig. 2.58 that the matching of the second antenna is severely harmed and its center frequency is shifted about 90 MHz although the first antenna is not affected much. Besides, similar to the dumbbell DGS case, Fig. 2.59 indicates that insertion of the multiple SCSRRs improves the bandwidth of the suppression and the level of the suppression is similar to that of the multiple dumbbell DGS case (see Fig. 2.34). Approximately 9 dB mutual coupling reduction is acquired at 5 GHz

Fig. 2.60 and Fig. 2.61 show the simulated azimuth patterns of the first and the second antennas, respectively, with and without the three-SCSRR DGS. Similarly, Fig. 2.62 and Fig. 2.63 show the simulated elevation patterns of the first and the second antennas, respectively, with and without the three-SCSRR DGS. It is seen from farfield patterns in Fig. 2.60-Fig. 2.63 that 3-dB beamwith

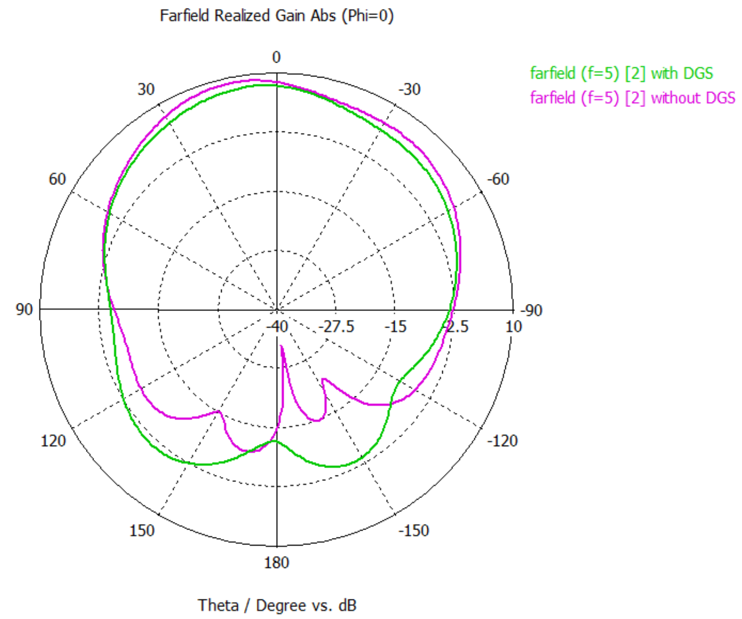

Figure 2.61: Simulated azimuth pattern of the second antenna with and without the three-SCSRR DGS.

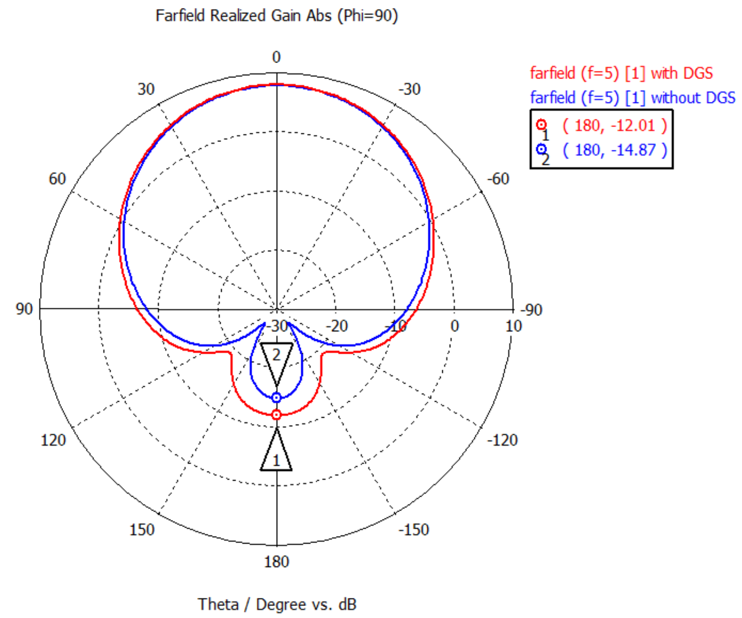

Figure 2.62: Simulated elevation pattern of the first antenna with and without the three-SCSRR DGS.

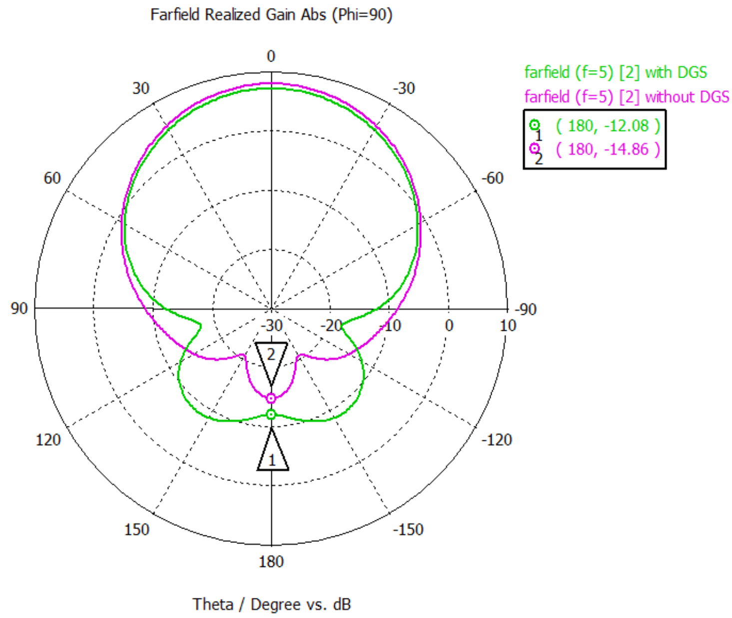

Figure 2.63: Simulated elevation pattern of the second antenna with and without the three-SCSRR DGS.

narrows up to 7 degrees after the introduction of SCSRR DGS. Similar to the previous cases, azimuth patterns shown in Fig. 2.60 and Fig. 2.61 are not affected significantly aside from some minor changes in the sidelobes. However, it is seen from the radiation pattern results provided in Fig. 2.62 and Fig. 2.63 that, although the backlobe radiation levels in the elevation pattern do not increase much (about 4 dB to 5dB), the beamwidth of the backlobe increases significantly. Since an increased beamwidth may cause more multipath signal propagation leading to inaccurate data transmission, multiple SCSRRs is not preferable to use.

2.4 Fabrication and Measurement Results

Based on the abovementioned simulations, it has been concluded that when the surface waves are very strong (high ϵ_r case), significant reduction in mutual coupling can be achieved. Unfortunately, this achievement comes with an expense of very significant increase in the backlobe radiation and a significant shift at the resonant frequency. Besides, high ϵ_r substrates are not preferable for microstrip antenna applications. On the other hand, when the surface waves are weak (low ϵ_r case) it is not possible to obtain a reasonable reduction in mutual coupling. However, it should be kept in mind that low ϵ_r materials are preferred for microstrip antenna applications.

In this thesis, bacause we want to explore the ups and downs of the microstrip antenna arrays, we decided to proceed with ARLON TC600. It has a medium ϵ_r. Therefore, as shown in single dumbbell and single SCSRR DGS cases, it can provide enough mutual coupling reduction for the proof of the concept while the increase in the backlobe radiation and the shift at the resonance frequency are at resonable levels. Consequently, all fabrications are performed on ARLON TC600.

2.4.1 Measurement Results of the Two Microstrip Patch Antennas Fabricated on ARLON TC600: No DGS Case

The first fabrication is the two microstrip antennas on ARLON TC600. The accuracy of the simulations was increased in order to have better agreement between the simulation and fabrication results. After the accuracy of the simulations was increased, the resonant frequency of the antennas shifted slightly to the higher frequencies. Therefore, the width of the antennas is slightly increased so a resonance at 5 GHz can be achieved. Hence, the length and width of the patch antennas are 15.86 mm $\times$ 10.91 mm, respectively. The dimensions of the board outline are 50 mm $\times$ 66 mm and the thickness of the substrate is 1.524 mm. The feeding is the same as that of the simulations. Each antenna is fed from the middle of its length and c = 2 mm away from its center along the

(a) (b)

Figure 2.64: (a) Top view of the fabricated 2 microstrip antennas on ARLON TC600 without DGS. (b) Back view of the produced antennas without DGS.

width direction. The edge-to-edge separation between antennas is 15 mm (same as before).

Fig. 2.65 shows the magnitude of the return loss ($|S_{11}|$and $|S_{22}|$ in dB) of the simulated and the fabricated antennas versus frequency in the absence of DGS. Similarly, Fig. 2.66 shows the magnitude of the mutual coupling ($|S_{21}|$ in dB) results of the simulated and the fabricated antennas versus frequency without DGS. Fig. 2.65 indicates that the resonance frequency of the fabricated antennas is 20 MHz higher than the simulated case and the matching of the fabricated antennas are about 5 dB less than that of the simulated antennas due to the production errors. Moreover, it is seen from Fig. 2.66 that although the mutual coupling results of the simulated and the fabricated antennas are close to each other, there is approximately 0.5 dB difference between each other.

Fig. 2.67 shows the simulated and the measured azimuth patterns of the first and the second antennas without DGS. Similarly, Fig. 2.68 shows the simulated and the measured elevation patterns of the first and the second antennas without DGS. It is seen from the Fig. 2.67 that although shape of the azimuth patterns

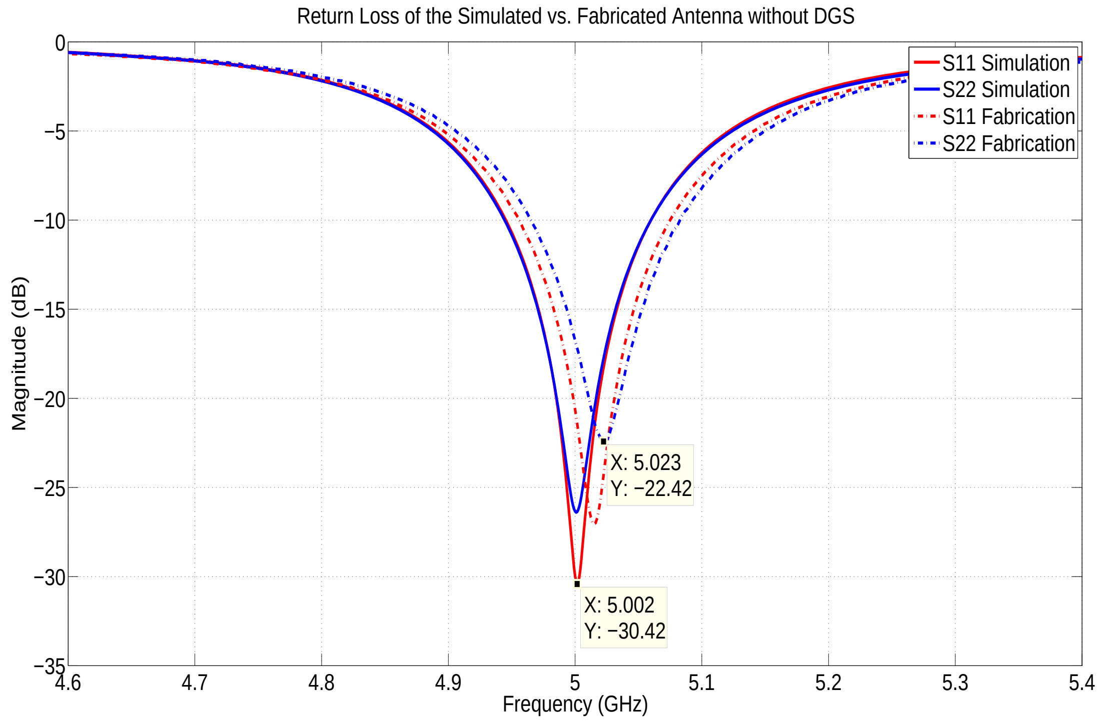

Figure 2.65: Return loss ($|S_{11}|$ and $|S_{22}|$ in dB) results of the simulated and the fabricated antennas without DGS.

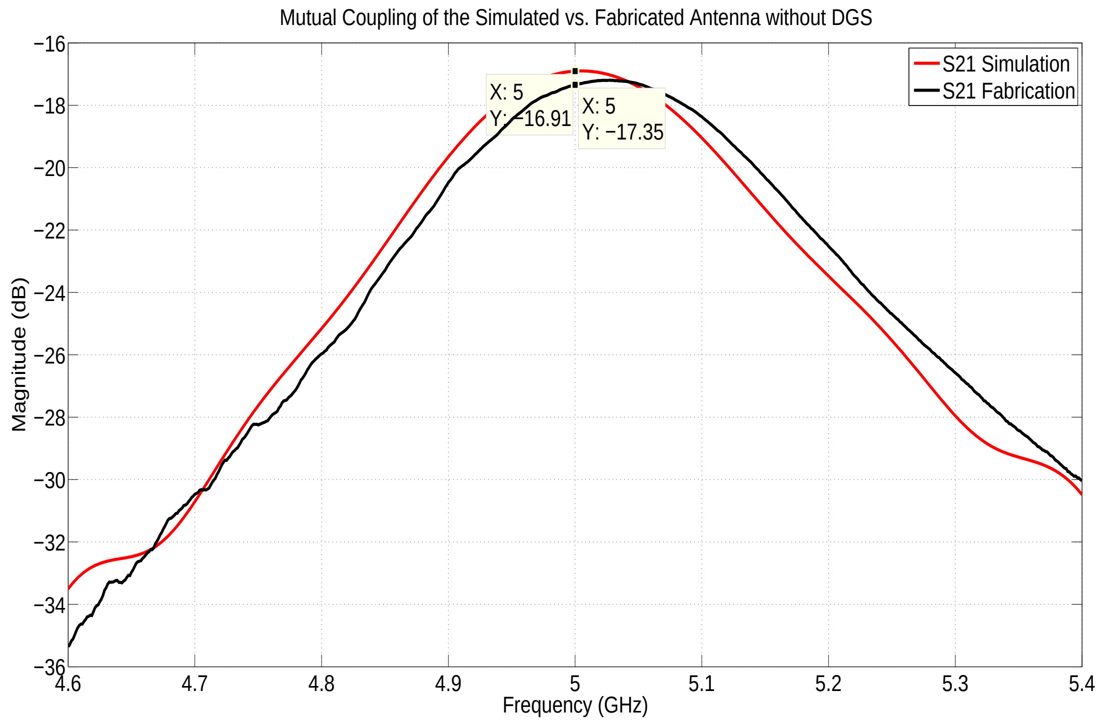

Figure 2.66: Mutual coupling ($|S_{21}|$ in dB) results of the simulated and the fabricated antennas without DGS.

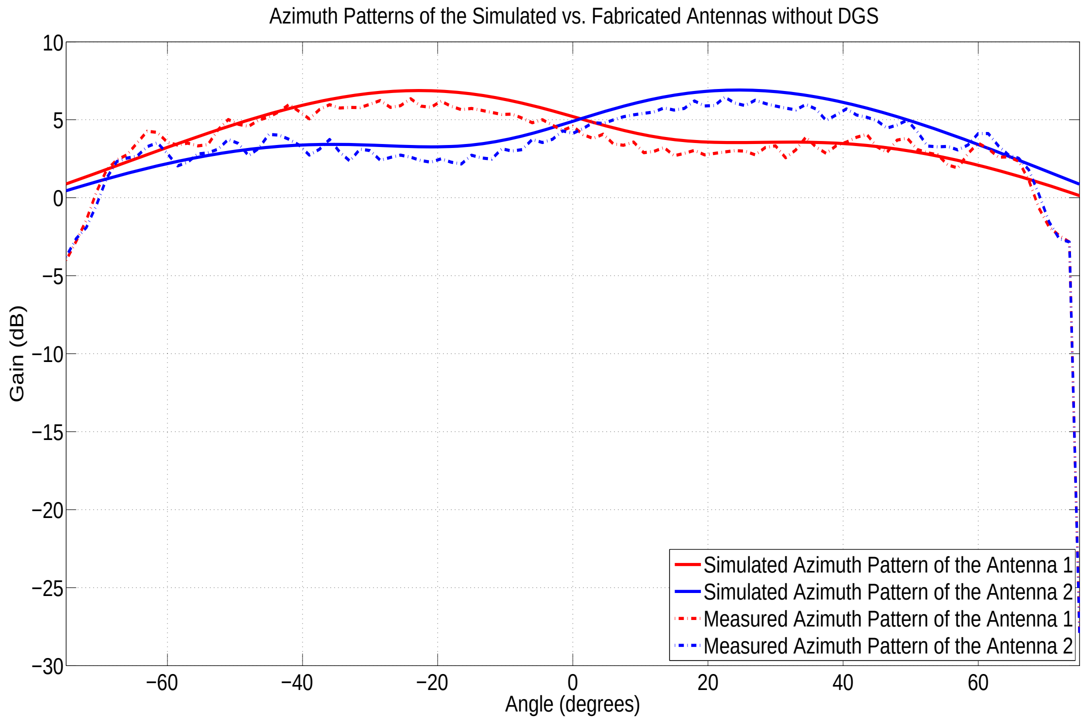

Figure 2.67: Azimuth patterns of the simulated and the fabricated antennas without DGS.

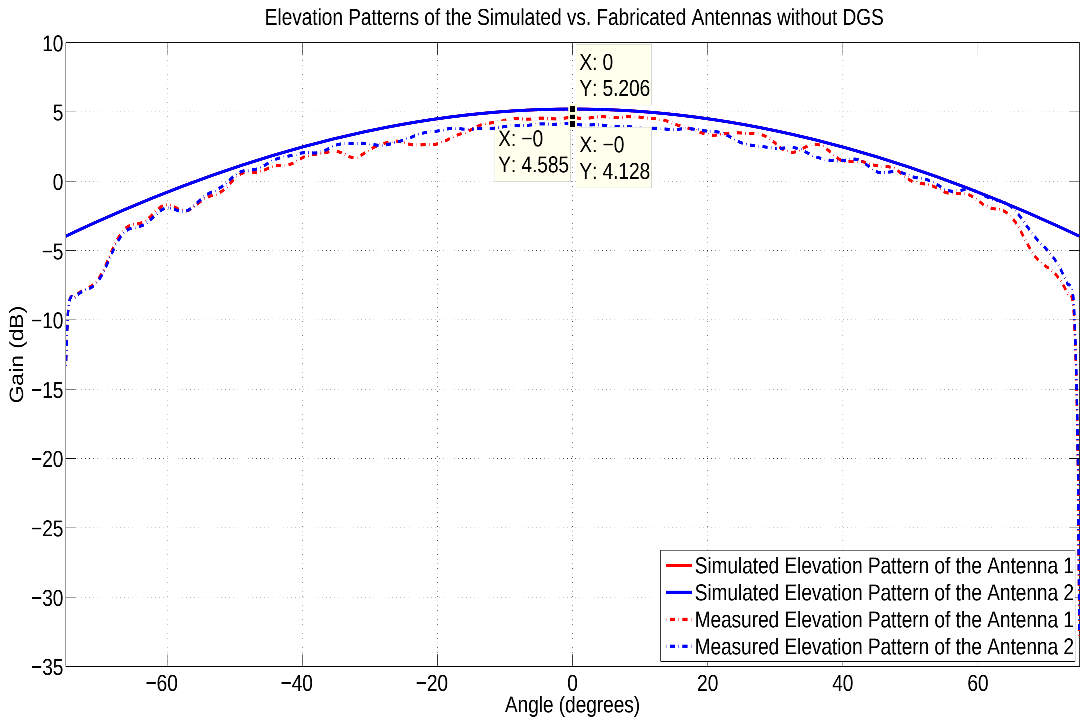

Figure 2.68: Elevation patterns of the simulated and the fabricated antennas without DGS.

of the simulated and the measured antennas agree well with each other, the gains of the measured antennas are about 0.7 dB less than the simulation results. In a similar fashion, Fig. 2.68 indicates that the gains of the measured antennas are 0.7 to 1 dB less than that of the simulation results, and a difference of 4 degrees appears in 3 dB beamwidth of both antennas compared to the simulations. However, such levels of errors are expected because the planar nearfield systems are designed to measure high gain antennas with small beam widths. Therefore, measurements of antenna gains less than 10 dB are inaccurate due to the mechanical limitations. Moreover, backlobe gain measurements are not possible in this system since the backlobe gain ranges from 0 dB to -20 dB for the antennas of this study. Besides, because the nearfield chamber has a finite volume, the maximum farfield angle is limited. In our case, we can span maximum 150 degrees for the antennas that are fabricated.

2.4.2 Measurement Results of the Two Microstrip Patch Antennas Fabricated on ARLON TC600: Dumbbell DGS Case

The second fabrication is the two element microstrip array with a dumbbell etched to the ground plane in between the patch antennas to form a DGS on ARLON TC600. The dimensions of the board outline are the same (i.e., 50 mm $\times$ 66 mm) and the thickness of the substrate is 1.524 mm. The length and width of the patch antennas are 15.86 mm $\times$ 10.91 mm, respectively. The feeding location of each antenna and the edge-to- edge separation between the two are unchanged. The dimensions of the dumbbell DGS are $dl = 6.5$ mm, $w = 2.5$ mm and $s = 0.4$ mm.

Fig. 2.70 shows the magnitude of the return loss ($|S_{11}|$and $|S_{22}|$ in dB) of the simulated and the fabricated antennas versus frequency in the presence of the

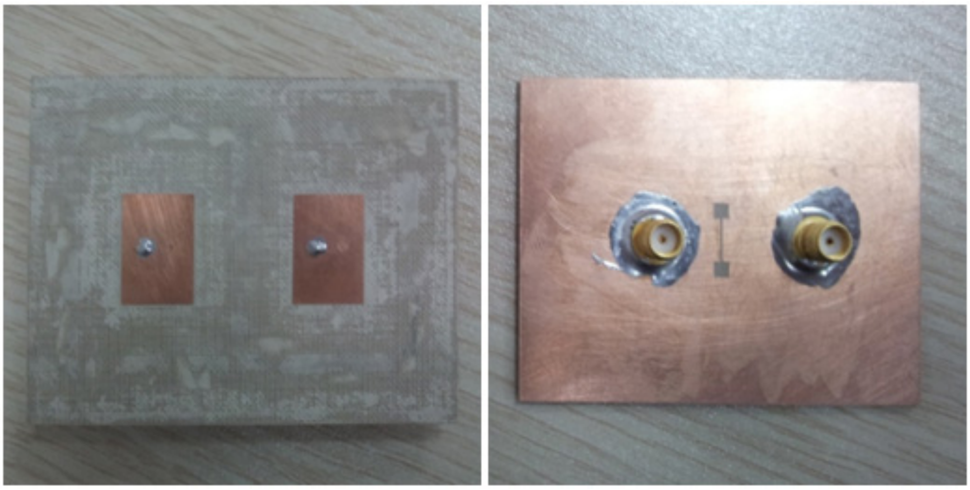

(a) (b)

Figure 2.69: a) Top view of the fabricated two microstrip antennas on ARLON TC600 with a single dumbbell DGS. (b) Back view of the fabricated antennas with a single dumbbell DGS.

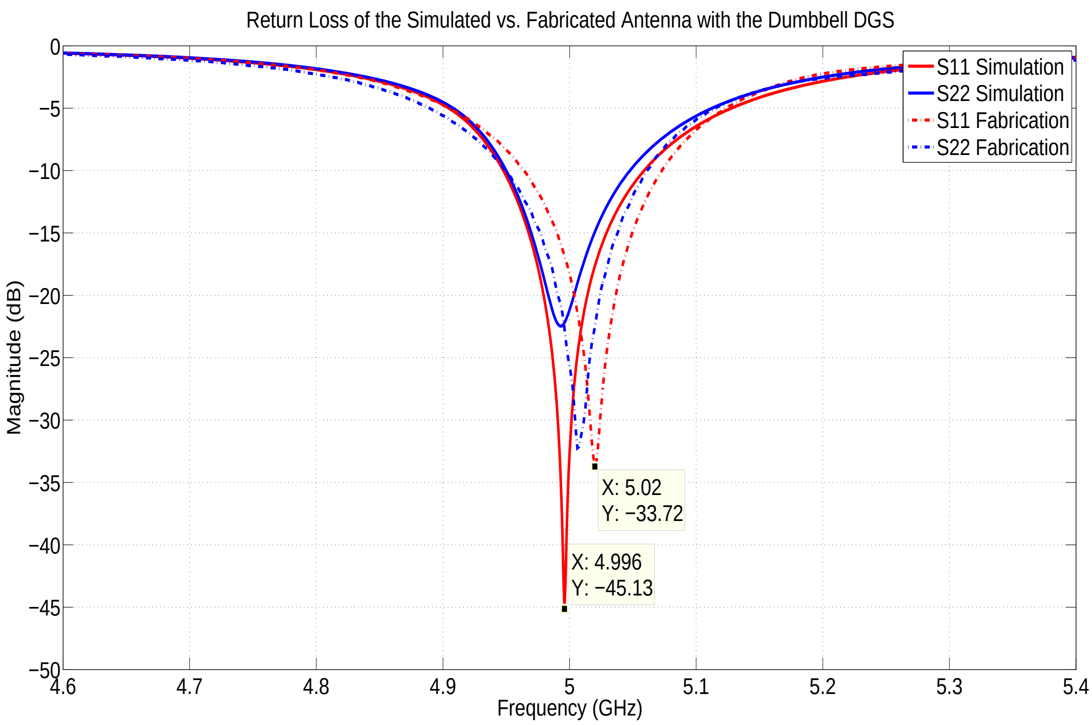

Figure 2.70: Return loss ($|S_{11}|$ and $|S_{22}|$ in dB) results of the simulated and the fabricated antennas with a dumbbell DGS.

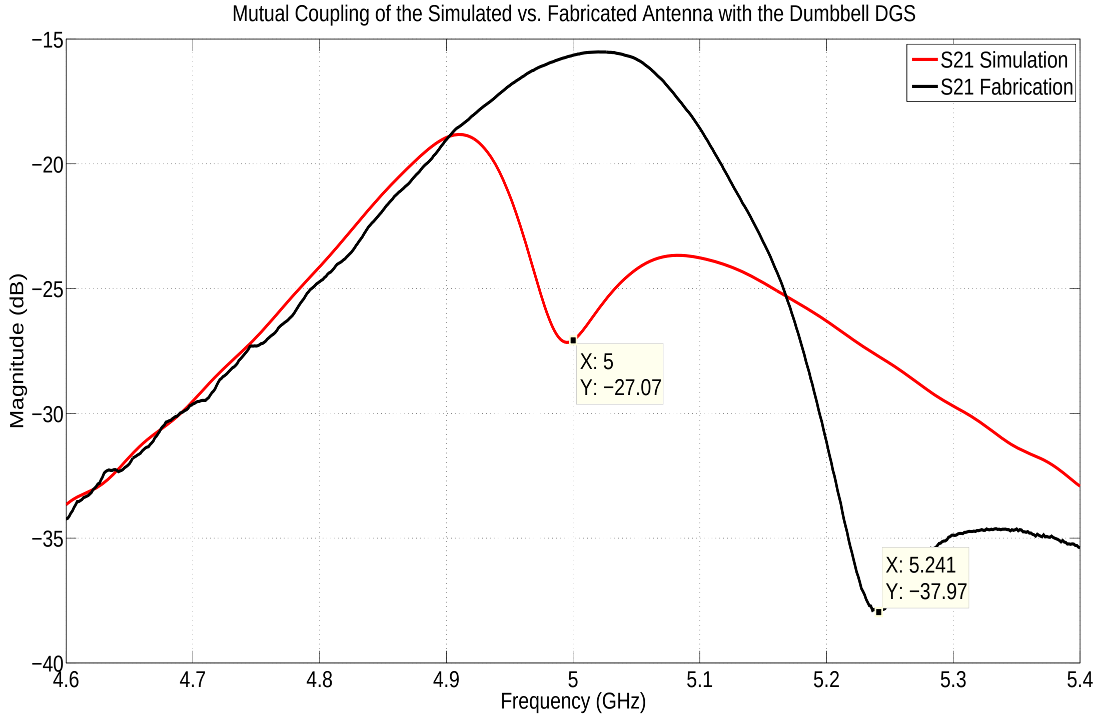

Figure 2.71: Mutual coupling ($|S_{21}|$ in dB) results of the simulated and the fabricated antennas with a dumbbell DGS.

dumbbell DGS. Similarly, Fig. 2.71 shows the magnitude of the mutual coupling ($|S_{21}|$ in dB) results of the simulated and the fabricated antennas versus frequency with the dumbbell DGS. Figure 2.70 shows that the resonance frequency of the fabricated antennas is shifted by 25 MHz compared to the simulated antennas which is acceptable. However, it is seen from Fig. 2.71 that the resonance frequency of the stop band of the fabricated DGS is about 5 percent, in other words it is 250 MHz, larger than the results obtained from the simulations. Such discrepancies are due to the fabrication errors. Therefore, to compensate the fabrication errors, dimensions of the dumbbells are slightly modified so that the resonance frequency of the dumbbell DGS matches with the simulations.

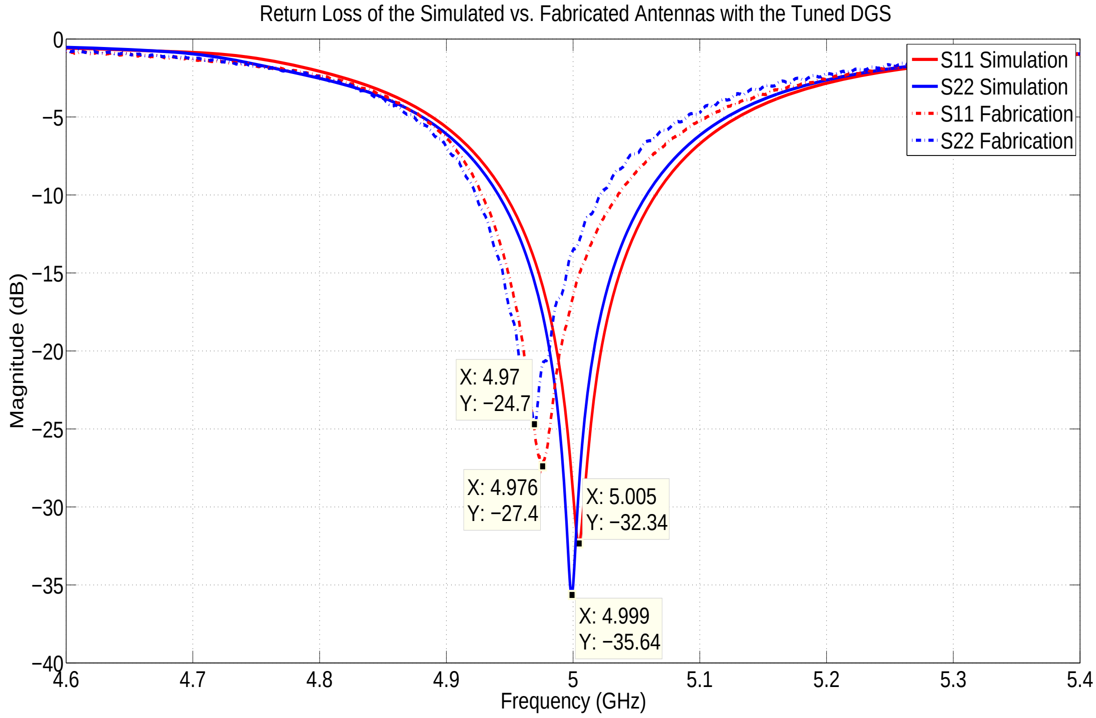

Figure 2.72: Return loss ($|S_{11}|$ and $|S_{22}|$ in dB) results of the simulated and the fabricated antennas with the tuned dumbbell DGS.

2.4.3 Measurement Results of the Two Microstrip Patch Antennas Fabricated on ARLON TC600: Tuned dumbbell DGS Case

The third fabrication is the two microstrip antennas with the tuned dumbbell etched to the ground plane in the between patch antennas that are on ARLON TC600. The dimensions of the board outline, the thickness of the substrate, the length and width of the patch antennas and the feed location of the antennas are kept the same as the previous case. Similarly, the edge-to-edge separation between the antennas is still $\lambda_o/4$ (15 mm). The dimensions of the dumbbell DGS are modified as follows: dl = 7.15 mm, w = 2.5 mm and s = 0.4 mm. As seen from these dimensions only dl is varied.

Fig. 2.72 shows the magnitude of the return loss ($|S_{11}|$and $|S_{22}|$ in dB) of the simulated and the fabricated antennas versus frequency in the presence of

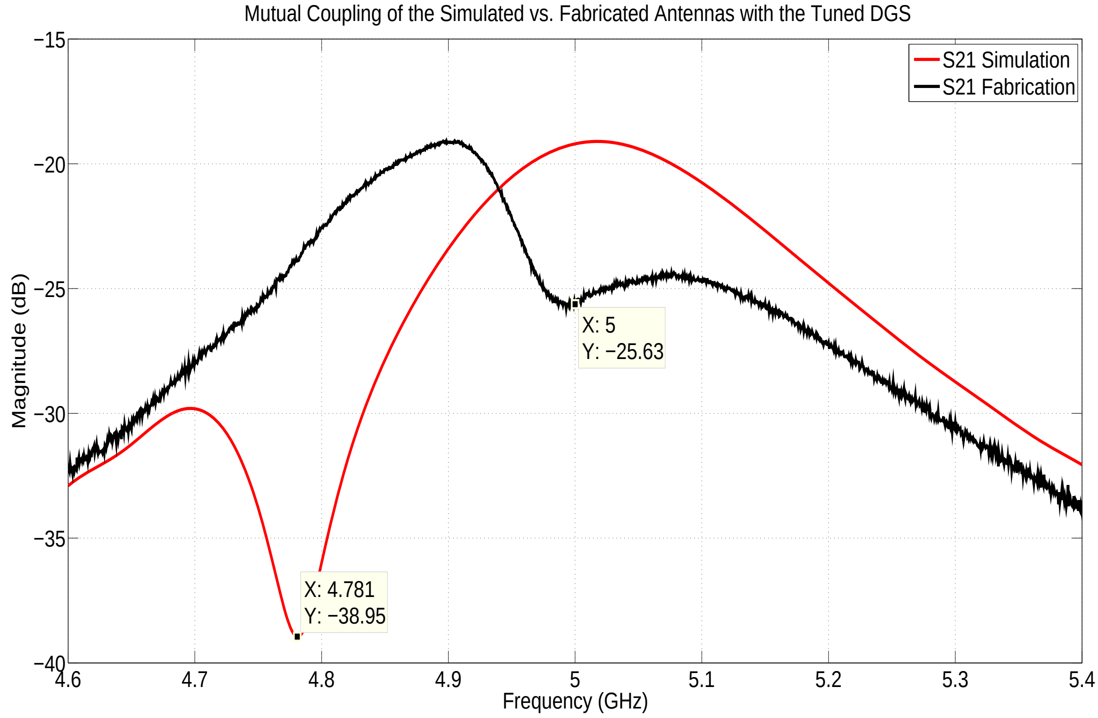

Figure 2.73: Mutual coupling ($|S_{21}|$ in dB) results of the simulated and the fabricated antennas with the tuned dumbbell DGS.

the tuned dumbell DGS. Similarly, Fig. 2.73 shows the magnitude of the mutual coupling ($|S_{21}|$ in dB) results of the simulated and the fabricated antennas versus frequency with the tuned dumbbell DGS. Moreover, we also provide the mutual coupling ($|S_{21}|$ in dB) results of all the fabricated antennas in Fig. 2.74. It shows the correction of the stop band frequency of $|S_{21}|$ after the dumbbell is tuned. As is seen from Fig. 2.72, the resonance frequencies of the fabricated patch antennas are 50 MHz lower than that of the simulated ones. However, Fig. 2.73 indicates that after the modification made on the dumbbell DGS, the resonance frequency of the stop band for the dumbbell DGS is shifted to 5 GHz. Finally, as seen from Fig. 2.74, there is a 8 dB mutual coupling suppression at 5 GHz.

Fig. 2.75 shows the simulated and the measured azimuth patterns of the first and the second antennas with the tuned dumbbell DGS and Fig.2.76 shows the simulated and the measured elevation patterns of the first and the second antennas with the tuned dumbbell DGS. Additionally, Fig. 2.77 illustrates the

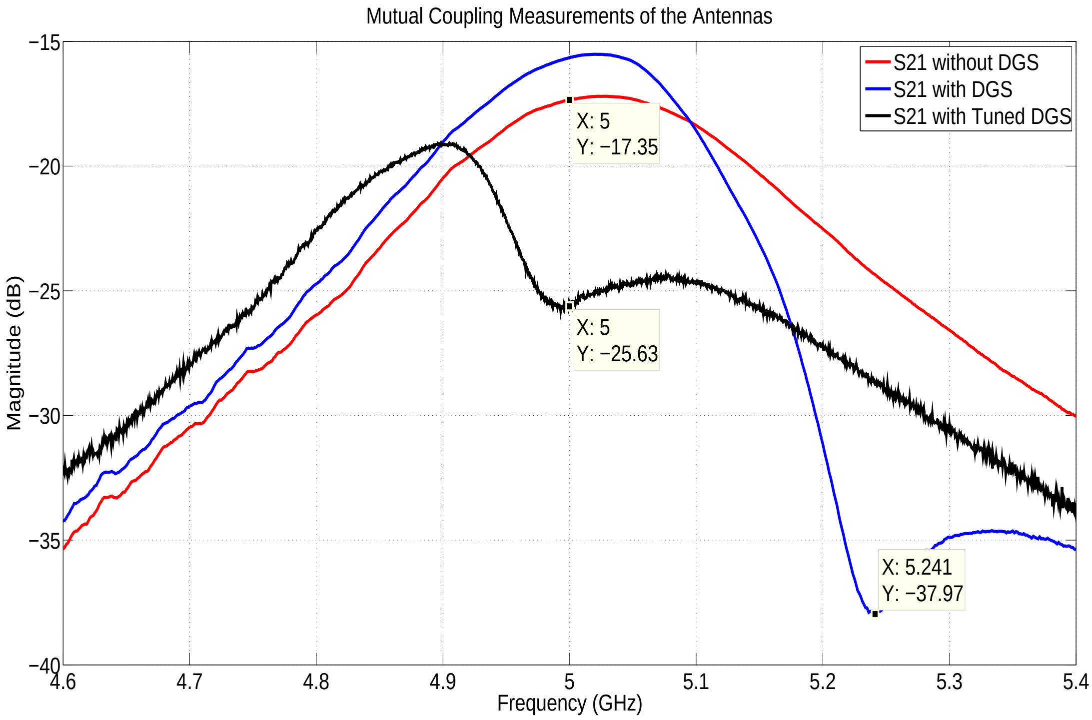

Figure 2.74: Mutual coupling ($|S_{21}|$ in dB) results of all the fabricated antennas.

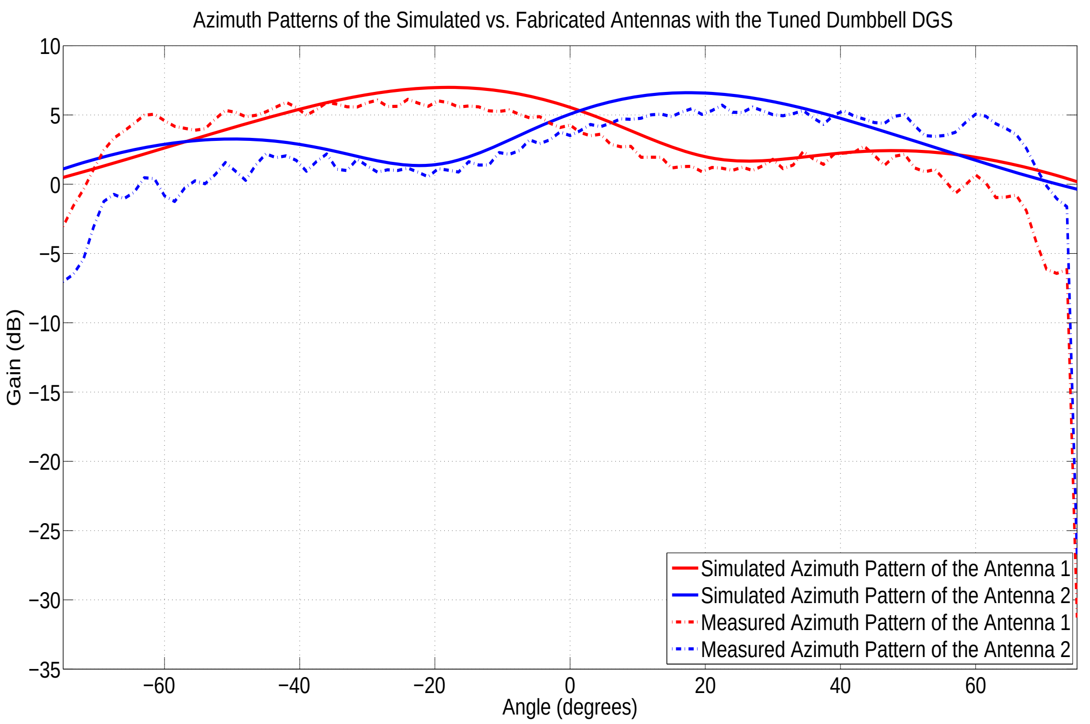

Figure 2.75: Azimuth patterns of the simulated and the fabricated antennas with the tuned dumbbell DGS.

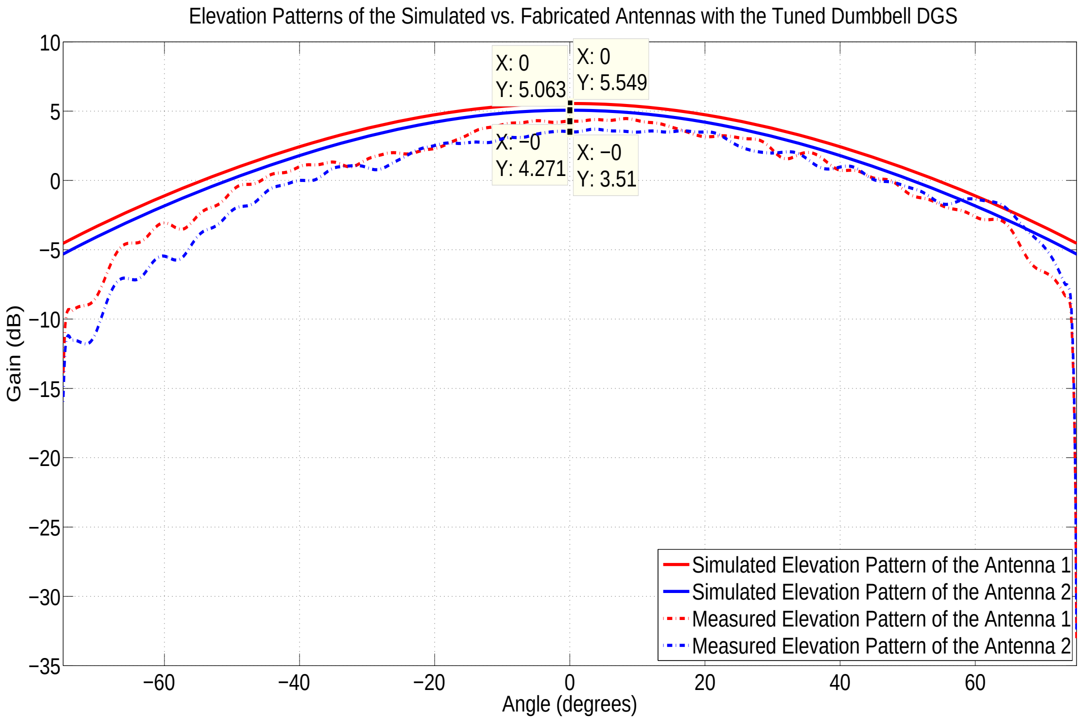

Figure 2.76: Elevation patterns of the simulated and the fabricated antennas with the tuned dumbbell DGS.

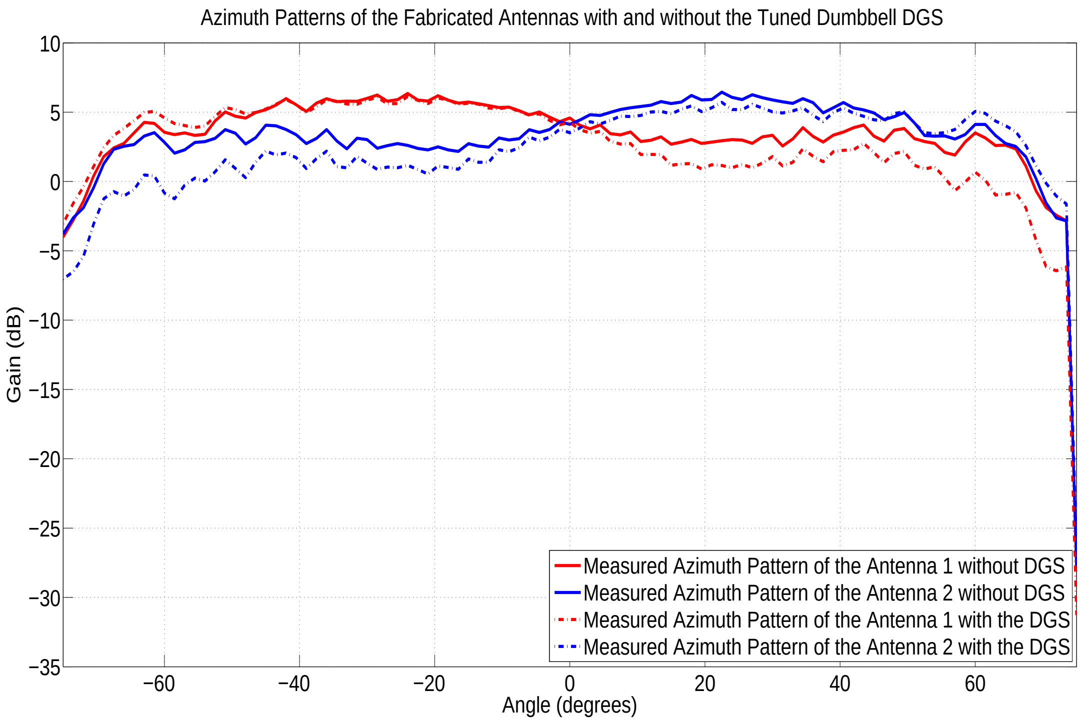

Figure 2.77: Azimuth patterns of the fabricated antennas with and without the tuned dumbbell DGS.

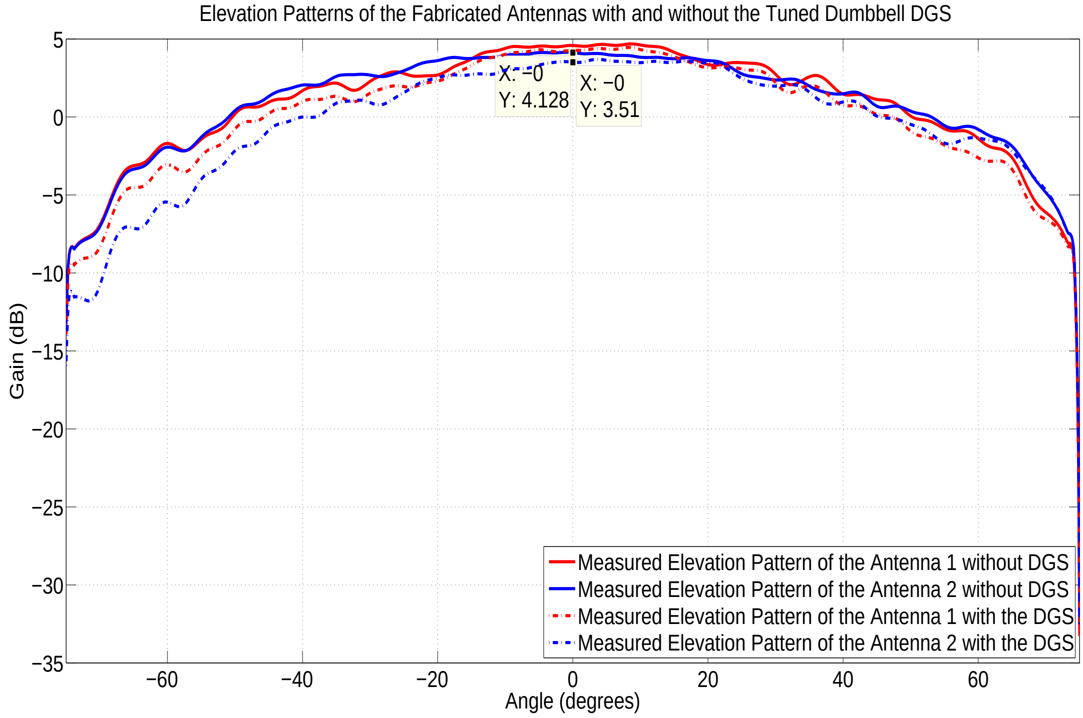

Figure 2.78: Elevation patterns of the fabricated antennas with and without the dumbbell DGS.

azimuth pattern measurements of the first and the second antennas in the presence and absence of the tuned dumbbell DGS while Fig. 2.78 shows the elevation pattern measurements of the first and the second antennas in the presence and absence of the tuned dumbbell DGS. It is seen from Fig. 2.75 and 2.76 that although the beamwidths of the fabricated and simulated antennas are very close to each other, gain of the both azimuth and elevation pattern of the fabricated antennas are 1.3 dB to 1.5 dB less than the gain of the simulated antennas. Furthermore, it is seen from Fig. 2.77 and Fig. 2.78 that addition of the dumbbell DGS causes a decrease in the gain of the antennas up to 0.6 dB, and narrows the 3 dB beamwidth up to 10 degrees. The 0.5 dB decrease in the gain is not important (it may be a measurement error as well). However, a 10 degree decrease in the beamwidth is important. One reason may be the change in the current distribution of the patches after the tuned dumbbell is introduced.

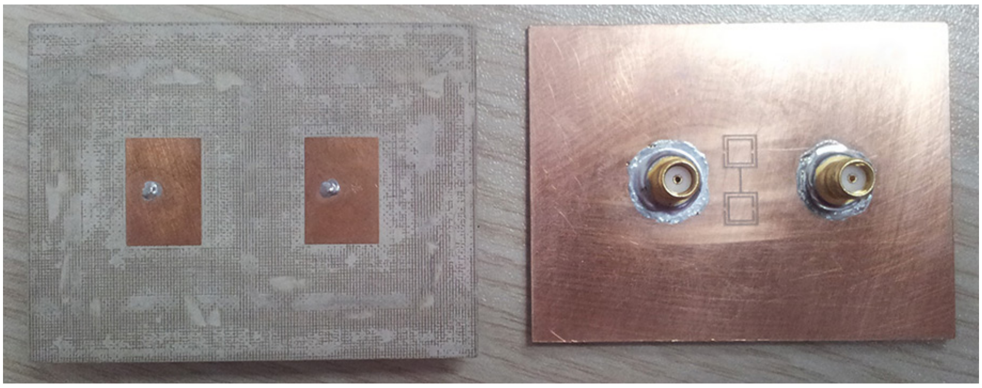

(a) (b)

Figure 2.79: a) Top view of the fabricated two microstrip antennas on ARLON TC600 with a single SCSRR DGS. (b) Back view of the fabricated antennas with a single SCSRR DGS.

2.4.4 Measurement Results of Two Microstrip Patch Antennas Fabricated on ARLON TC600: SCSRR DGS Case

The fourth fabrication is the two microstrip antennas with the SCSRR etched to the ground plane in between the microstrip patch antennas to form the DGS on ARLON TC600 (ϵ_r = 6.15 and tanδ = 0.002). The dimensions of the board outline, the thickness of the dielectric material, the height and width of the patch antennas, the feed location of the antennas and the edge-to-edge separation between the antennas are kept the same. The dimensions of the SCSRR are L = 4.7 mm, ws = 0.22 mm, ls = 3.86 mm, g = 0.5 and a = b = 0.22 mm.

Fig. 2.80 shows the magnitude of the return loss ($|S_{11}|$and $|S_{22}|$ in dB) of the simulated and the fabricated antennas versus frequency in the presence of the SCSRR DGS. Similarly, Fig. 2.81 shows the magnitude of the mutual coupling ($|S_{21}|$ in dB) results of the simulated and the fabricated antennas versus frequency with the SCSRR DGS. As seen in Fig. 2.80, the resonance frequency of the fabricated patch antennas are shifted more than 78 MHz toward the high frequency side and the resonance frequency of the stop band of the fabricated

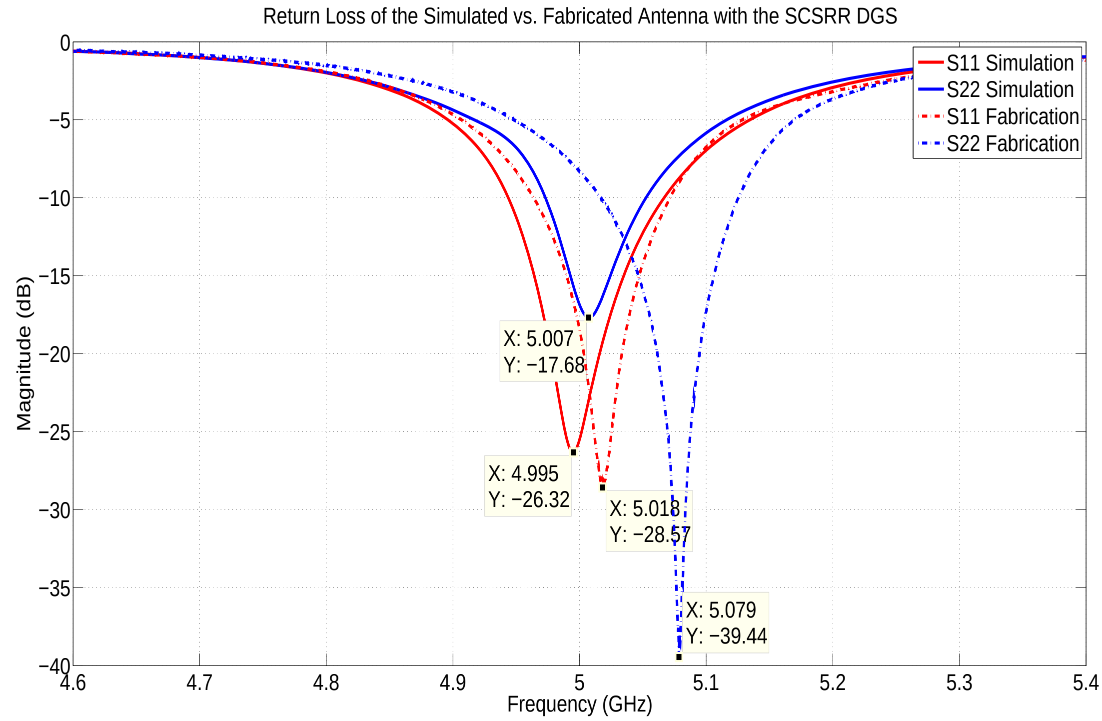

Figure 2.80: Return loss ($|S_{11}|$ and $|S_{22}|$ in dB) results of the simulated and the fabricated antennas with the SCSRR DGS.

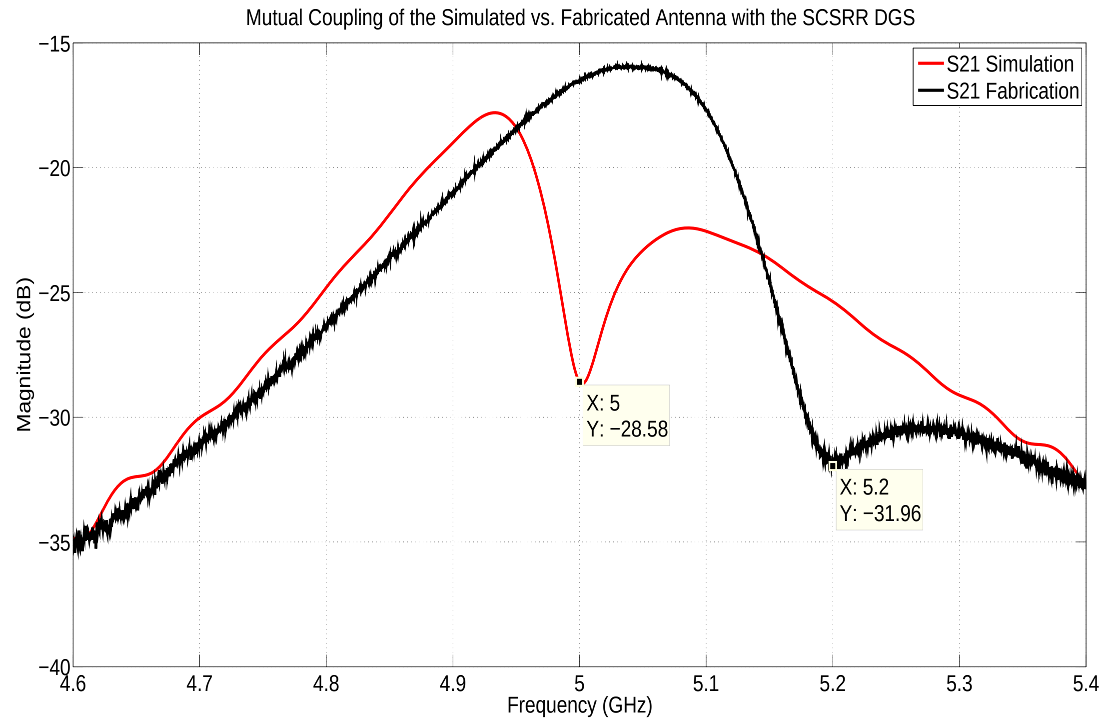

Figure 2.81: Mutual coupling ($|S_{21}|$ in dB) results of the simulated and the fabricated antennas with the SCSRR DGS.

SCSRR DGS is shifted about 200 MHz toward the high frequency side compared to the simulations. To compensate the extra 200 MHz shift, the resonance frequency of the stop band of SCSRR DGS is reduced by modifying (i.e., fine tuning) the SCSRR dimensions.

2.4.5 Measurement Results of the Two Microstrip Patch Antennas Fabricated on ARLON TC600: Tuned SCSRR DGS Case

The final production of this chapter is the two microstrip antennas with the tuned SCSRR etched to the ground plane in between the microstrip patch antennas on ARLON TC600. All substrate and antenna related geometrical and electrical parameters are kept the same. However, the dimensions of the SCSRR are tuned so that the new dimensions of the SCSRR are $L = 5.3$ mm ,$ws = 0.3$ mm, $ls = 3.78$ mm , $g = 0.5$ and $a = b = 0.3$ mm.

Fig. 2.82 shows the magnitude of the return loss ($|S_{11}|$and $|S_{22}|$ in dB) of the simulated and the fabricated antennas versus frequency in the presence of the tuned SCSRR DGS. Similarly, Fig. 2.83 shows the magnitude of the mutual coupling ($|S_{21}|$ in dB) results of the simulated and the fabricated antennas versus frequency with the tuned SCSRR DGS. In addition to those, Fig. 2.84 indicates the magnitude of the mutual coupling ($|S_{21}|$ in dB) of all the fabricated antennas. It is seen from Fig. 2.82 that the resonance frequencies of the fabricated patch antennas are nearly same as the simulated ones. However, Fig. 2.83 indicates that after the modification made on the SCSRR DGS , the resonance frequency of the stop band of the SCSRR DGS is shifted back to 5 GHz and it is seen from Fig. 2.84 that there is a 5.3 dB mutual coupling suppression at 5 GHz.

Fig. 2.85 shows the simulated and the measured azimuth patterns of the first and second antennas with the tuned SCSRR DGS and Fig. 2.86 shows the same

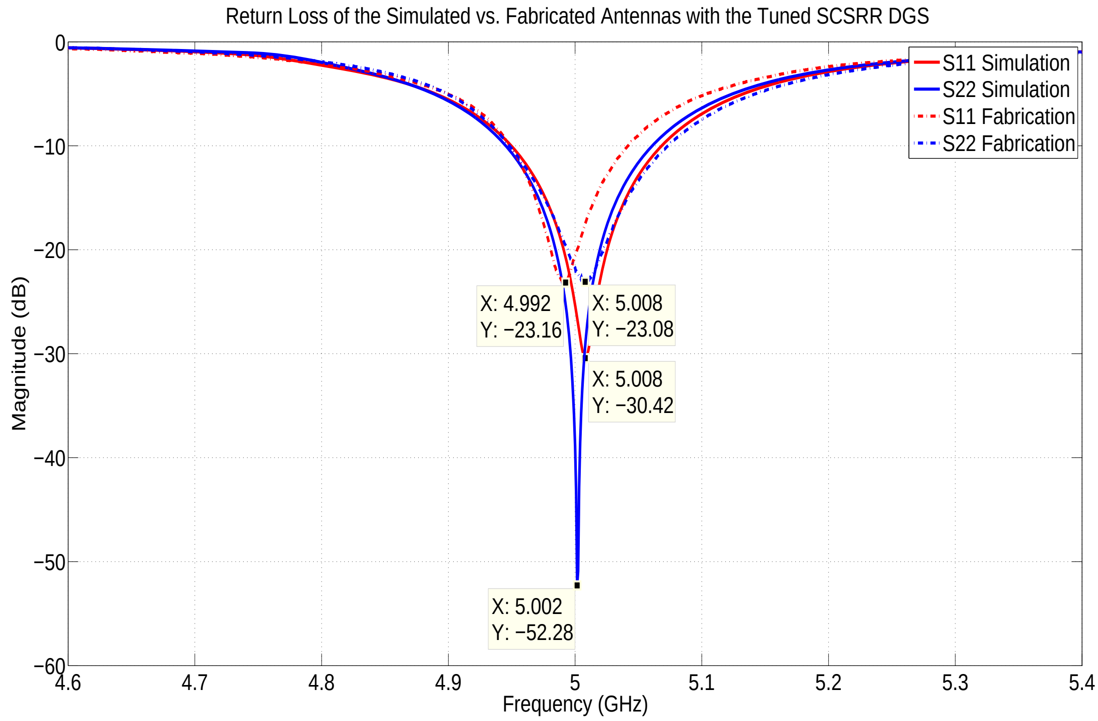

Figure 2.82: Return loss ($|S_{11}|$ and $|S_{22}|$ in dB) results of the simulated and the fabricated antennas with the tuned SCSRR.

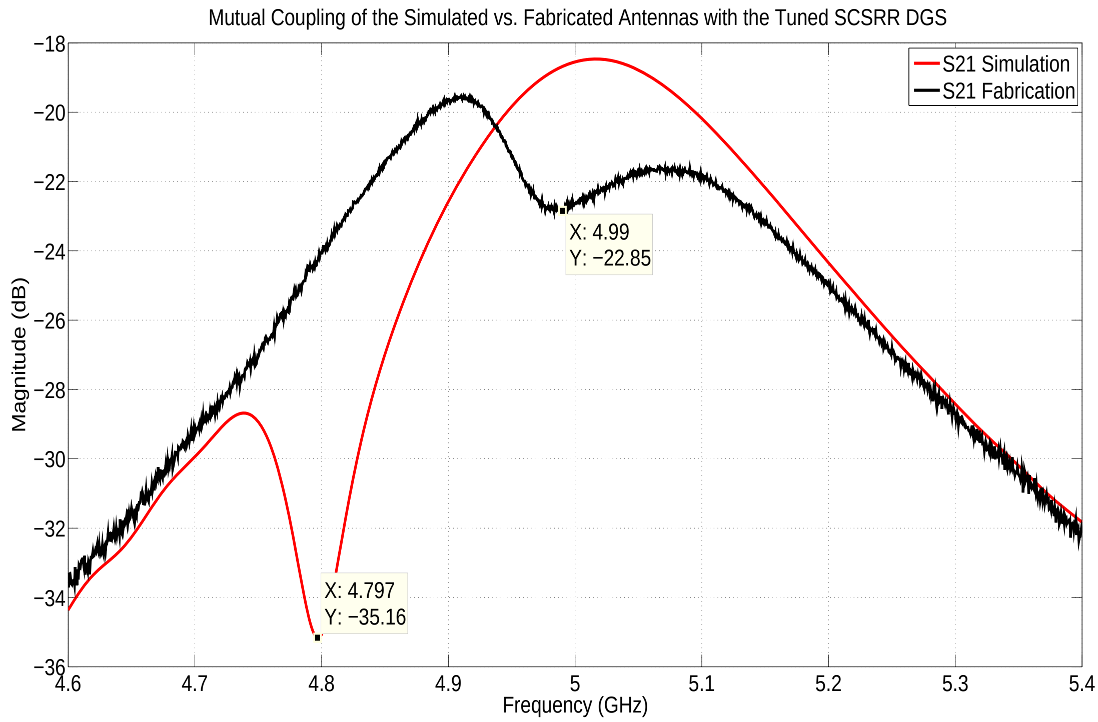

Figure 2.83: Mutual coupling ($|S_{21}|$ in dB) results of the simulated and the fabricated antennas with the tuned SCSRR.

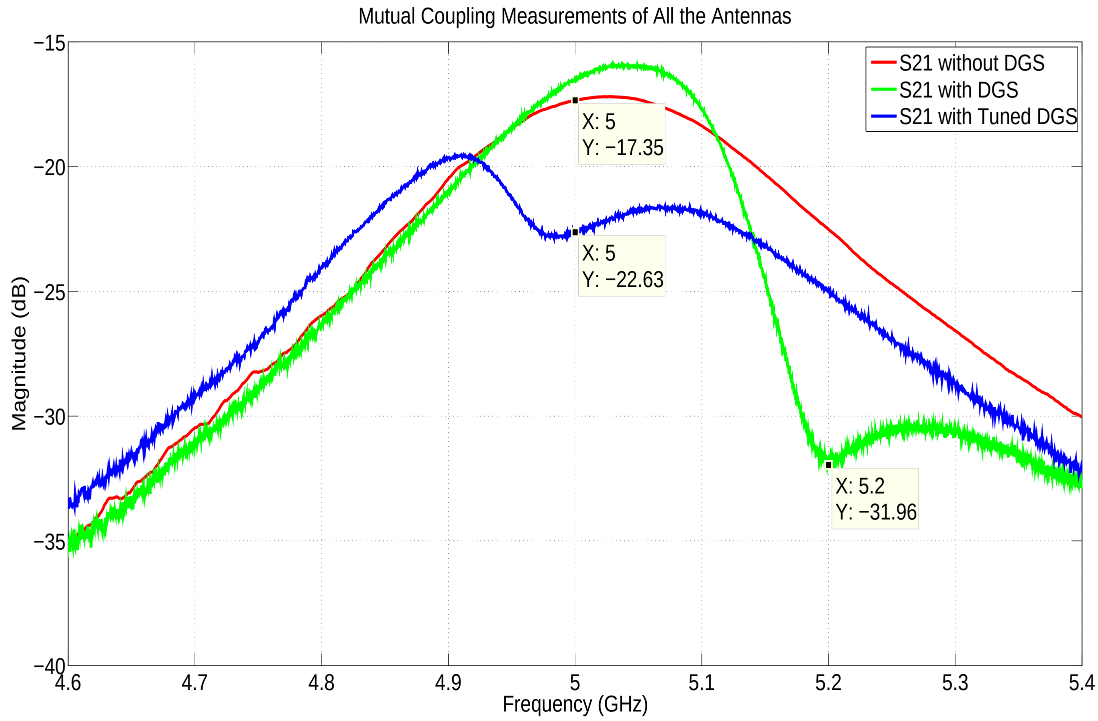

Figure 2.84: Mutual coupling ($|S_{21}|$ in dB) results of all the fabricated antennas with and without the SCSRR DGS.

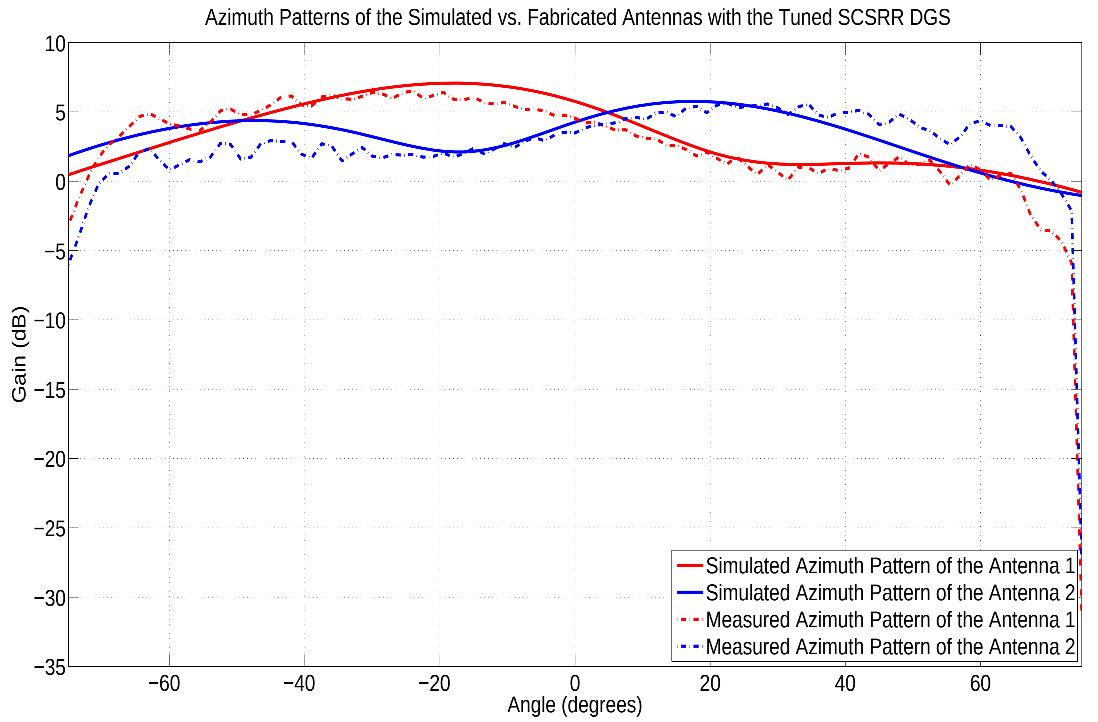

Figure 2.85: Azimuth patterns of the simulated and the fabricated antennas with the tuned SCSRR DGS.

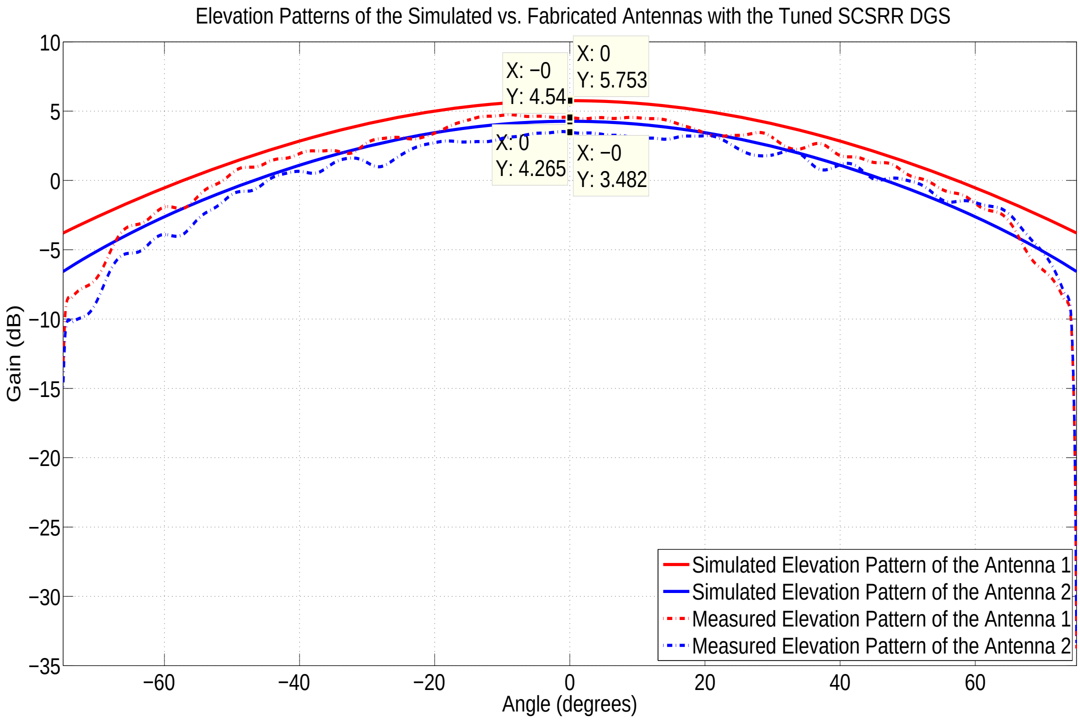

Figure 2.86: Elevation patterns of the simulated and the fabricated antennas with the tuned SCSRR DGS.

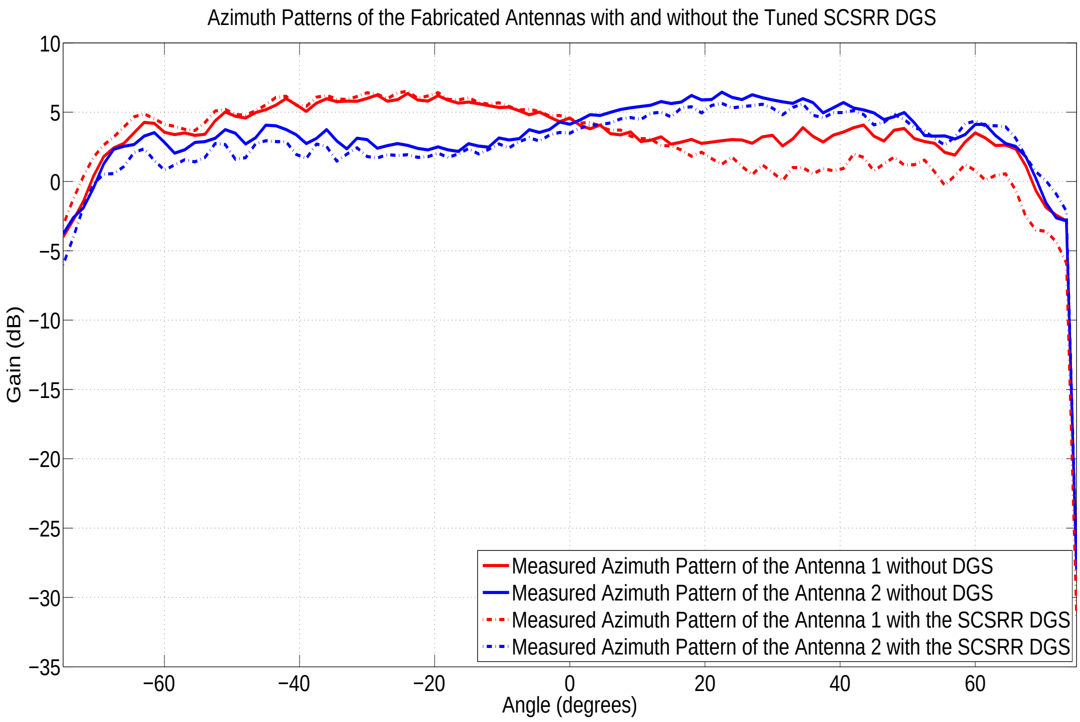

Figure 2.87: Azimuth patterns of the fabricated antennas with and without the tuned SCSRR DGS.

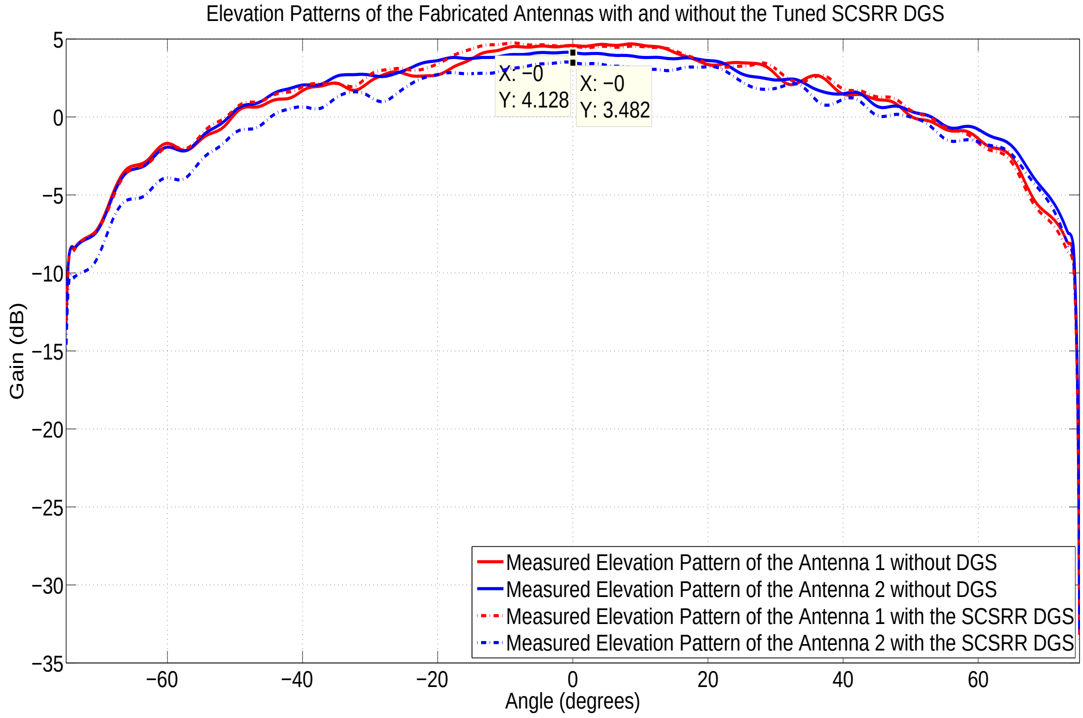

Figure 2.88: Elevation patterns of the fabricated antennas with and without the tuned SCSRR DGS.

results for the elevation patterns. Additionally, Fig. 2.87 illustrates the azimuth pattern measurements of the first and the second antennas in the presence and absence of the tuned SCSRR DGS while Fig. 2.88 shows the same results for the elevation pattern measurements. It is seen from Figs. 2.85 and 2.86 that although the beamwidths of the produced and the simulated antennas are very close to each other, gain of the both azimuth and elevation pattern of the fabricated antennas are 0.8 dB to 1.3 dB less than the gain of the simulated antennas, which is acceptable. Furthermore, it is seen from Fig. 2.87 and Fig. 2.88 that addition of the tuned SCSRR DGS does not change the azimuth and/or elevation patterns of the first antenna although the gain of the second antenna decreases about 0.7 dB, and the 3 dB beamwidth of the second antenna is changed 5 to 9 degrees compared to the fabricated antennas without the SCSRR DGS. Similar to the dumbbell DGS case such a change in the 3 dB beamwidth may be due to the change in the current distribution on the patches after the SCSRR DGS is introduced.

Chapter 3

Addition of a Reflector and a Cavity to Two-Element Microstrip Antenna Array in the Presence of the Dumbbell DGS

One main problem observed in the presence of DGSs (that use dumbells or SCSRRs) is the increase in the backlobe radiation levels and increase in the beamwidth of the backlobe as seen in Chapter 2. Increased backlobe radiation and the increase in the beamwidth of the backlobe give rise to some significant problems such as power loss in the direction of radiation (i.e., main lobe direction) undesired multipath signal propagation and the interference generated by the backlobe radiation [13],[14].

There are two mechanisms that cause these backlobe problems when DGS is used to reduce the mutual coupling between two microstrip antennas. One of them is the reflected surface waves due to the DGS. Although their effect is more pronounced to the input impedance of the antennas as well as their

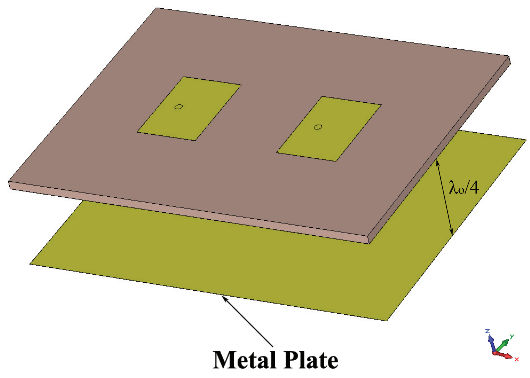

Figure 3.1: Metal plate, installed under the two element microstrip antenna array, acting as reflector.

resonance frequencies, they also affect the radiation patterns in particular the elevation pattern. On the other hand, the second mechanism is the dominant one and it is based on the fact that etched geometries on the ground plane act like microstrip slot antennas and they directly create the backlobes. Therefore, in this chapter, we introduce methods to eliminate the second (and the dominant) backlobe mechanism for our two-element microstrip antenna array designs in the presence of dumbbell DGS since they provide a better mutual coupling reduction.

There are different methods to reduce the backlobe radiation. First one is placing a metal plate under the microstrip patch antenna that acts like a reflector and hence, it will be referred to as reflector throughout this thesis. Reflector is placed directly under the two-element microstrip patch antenna array where the backlobe radiation exists, and the space between the antenna and the reflector is set to quarter wavelength as seen in Fig. 3.1. Consequently, making use of the image theory, the back radiation (due to the etched elements) is eliminated, and the directly radiated waves and the waves reflected from the reflector reinforce each other in the forward direction [14],[12],[15]. However, note that the reflector is not infinitely large and a part of the diffracted rays from the edges of the reflector contributes to the back radiation.

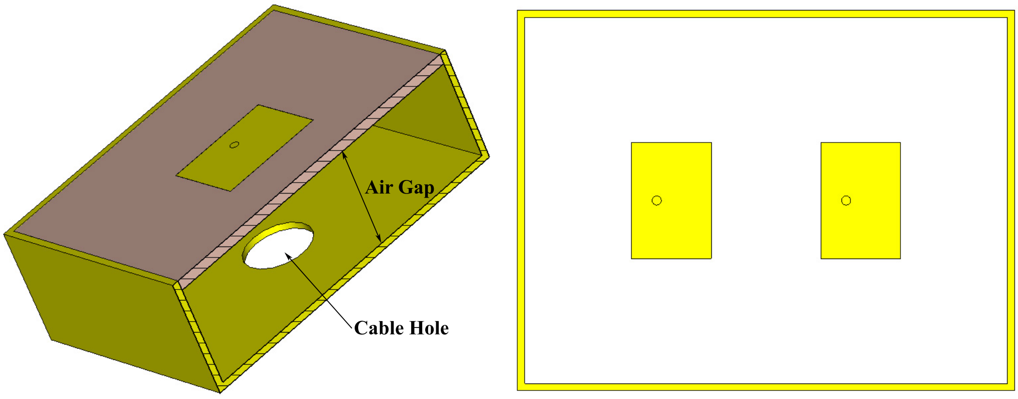

(a) (b)

Figure 3.2: (a) Cross-section of the two-element microstrip antenna array with a cavity. (b) Top view of the two-element microstrip antenna array with a cavity.

The second method to reduce the backlobe radiation is making use of a cavity [14] as shown in Fig. 3.2. The suppression of the backward radiation in the aperture coupled microstrip antennas has been reported before [16], [17]. Besides, cavities may act as a heat sink for high-power transmission systems, and they can reduce surface waves thereby increase the isolation between microstrip antennas [18]. However, special care is required in using a cavity together with a microstrip structure with a DGS. First of all, there must be some air-gap between the bottom metal that forms the cavity and the ground plane in order not to short the DGS structure. Secondly, feeding of the antennas may become challenging. Either, the SMA connectors (connected to the cavity wall via wire) are elongated or we open wide enough holes for cables to get through the cavity so that they can be connected to the antennas via SMA connectors. However, too wide holes can degrade the backlobe suppression.

A third method is making use of slotted-ground-chokes where the ground plane is etched from each edge to open rectangular slots as shown in Fig. 3.3 [13]. These chokes maintain the distribution of the surface currents to be stronger at the slots and decrease the backward radiation.

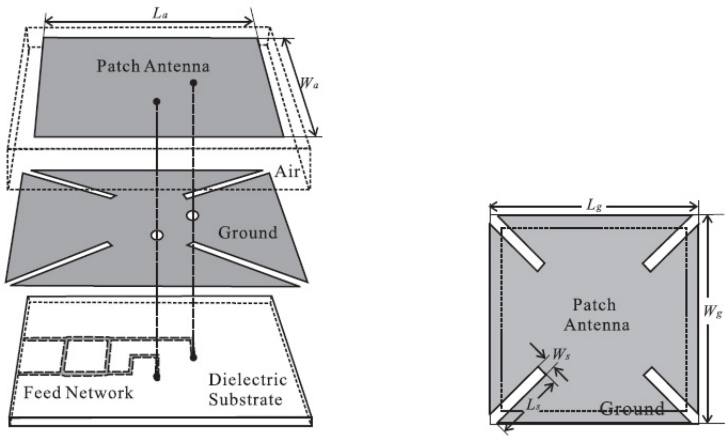

(a) (b)

Figure 3.3: (a) The geometry of the microstrip patch antenna with the slotted ground choke (b) Top view of the patch antenna with the slotted choke.

In this work, we have combined the first two methods to reduce the backlobe radiation. Namely, we enclose the antenna with a cavity and keep the length of the air-gap between the two-element microstrip antenna array and the cavity to $\lambda_o/4$. Moreover, we introduce holes for feeding cables that get through the cavity so that the antenna can be fed properly. In the next sections, numerical investigations and fabrication results will be presented.

3.1 Numerical Investigation of the Effects of $\lambda_o/4$ Spaced Reflector to the Two-Element Microstrip Antenna with a DGS

Effects of the reflector to the performance merits of the two-element microstrip antenna array with the dumbbell DGS is analysed for the array on ARLON TC600 (ϵ_r=6.15, tanδ=0.002) with the same geometrical parameters used for the fabrication. Briefly, dimensions of the board outline is 66 mm $\times$ 50 mm, the patch sizes: 15.86 mm $\times$ 10.91 mm, the feeding location: 2 mm away from center of each antennas along its width direction and at the middle of each antenna

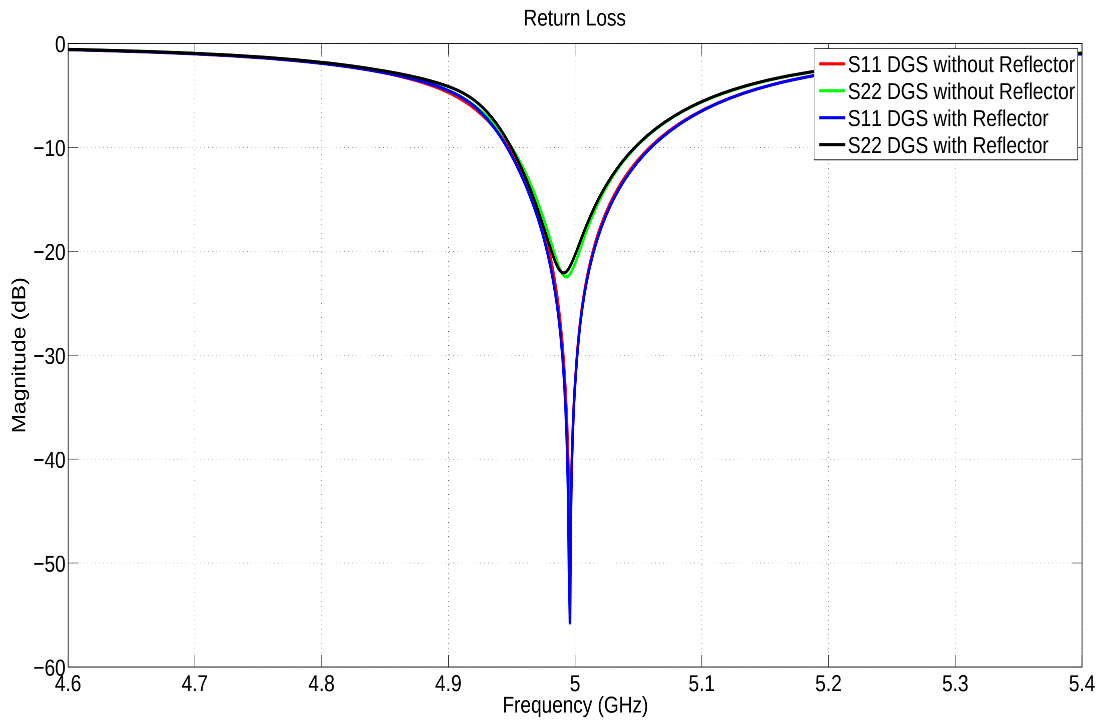

Figure 3.4: Simulated return loss results ($|S_{11}|$ and $|S_{22}|$ in dB) of the antennas with and without the reflector versus frequency in the presence of the dumbbell DGS

along its length direction. Finally, the edge-to-edge and separation between the patches: $\lambda_o/4 = 15$ mm at 5 GHz. Dimensions of the dumbbells etched to the ground are $dl = 6.5$ mm, $s = 0.4$ mm and $w = 2.5$ mm. Reflector is installed 15 mm under the array as in Fig. 3.1. Dimensions of the reflector is 66 mm $\times$ 50 mm and its thickness is 0.017 mm.

Fig. 3.4 shows the magnitude of the return loss ($|S_{11}|$ and $|S_{22}|$ in dB) of the antennas versus frequency in the presence and absence of the reflector while the dumbbell DGS is present in between the patch antennas. Similarly, Fig. 3.5 shows the magnitude of the mutual coupling ($|S_{21}|$ in dB) between the antennas versus frequency with and without the reflector while the dumbbell DGS is present in between the patch antennas. Fig. 3.4 indicates that the return loss is not affected from the installation of the metallic plate under the array. Moreover, as seen from Fig. 3.5, the insertion losses are improved about 1 dB at 5 GHz.

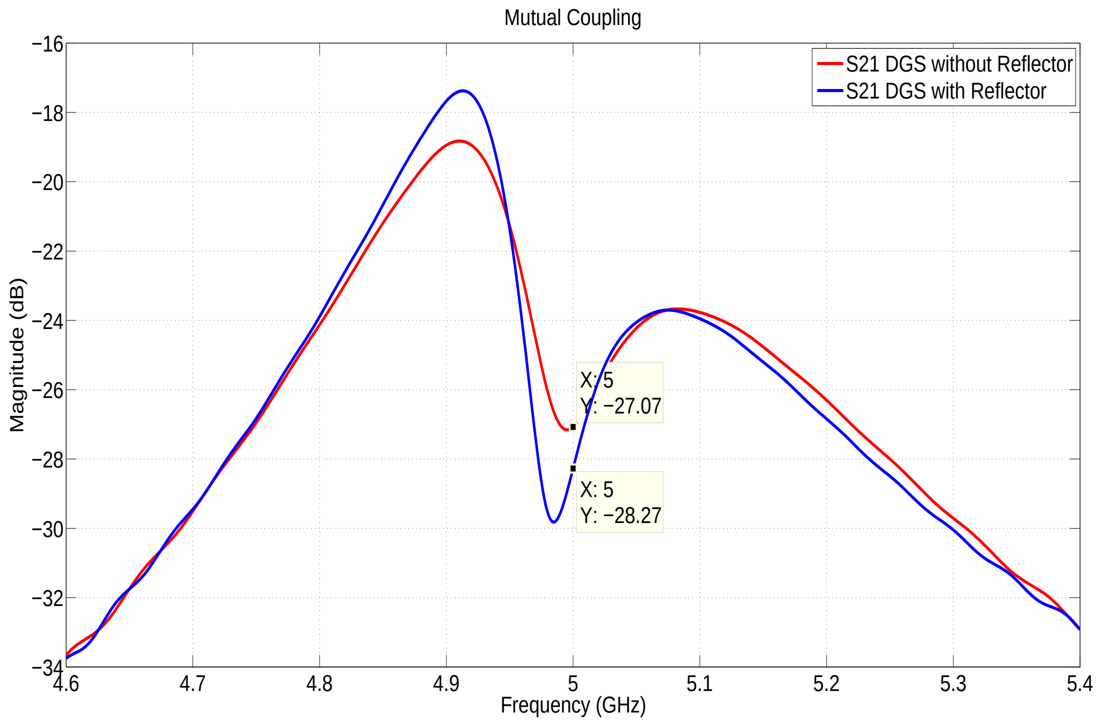

Figure 3.5: Simulated mutual coupling results ($|S_{21}|$ in dB) between the antennas with and without the reflector versus frequency in the presence of the dumbbell DGS.

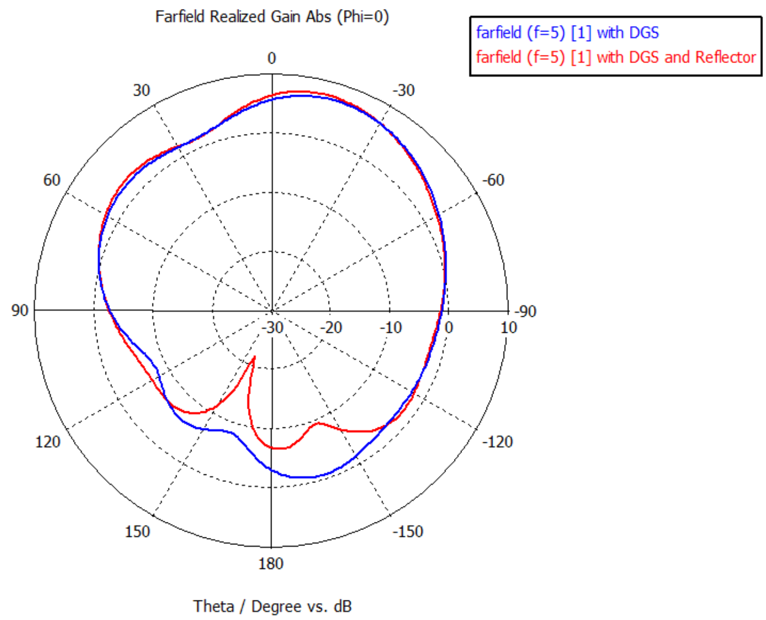

Figure 3.6: Simulated azimuth pattern of the first antenna with and without the reflector in the presence of the dumbbell DGS.

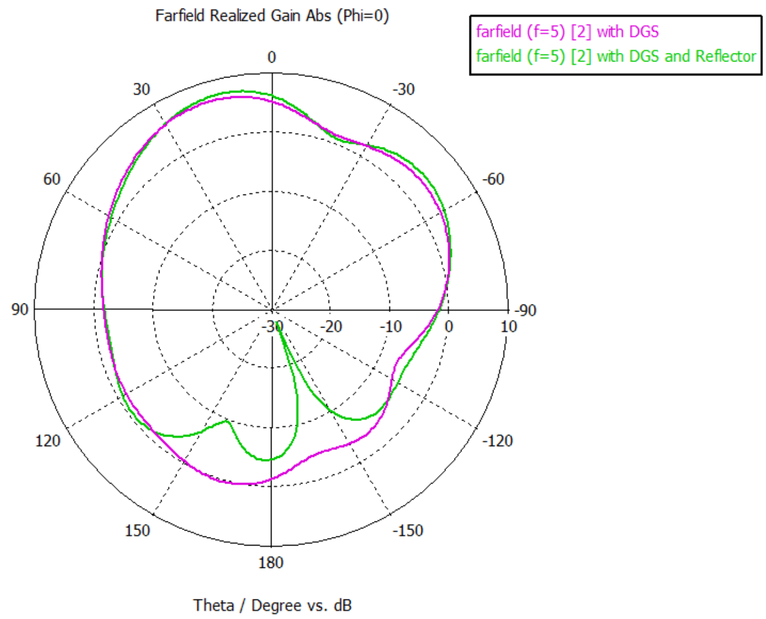

Figure 3.7: Simulated azimuth pattern of the second antenna with and without the reflector in the presence of the dumbbell DGS.

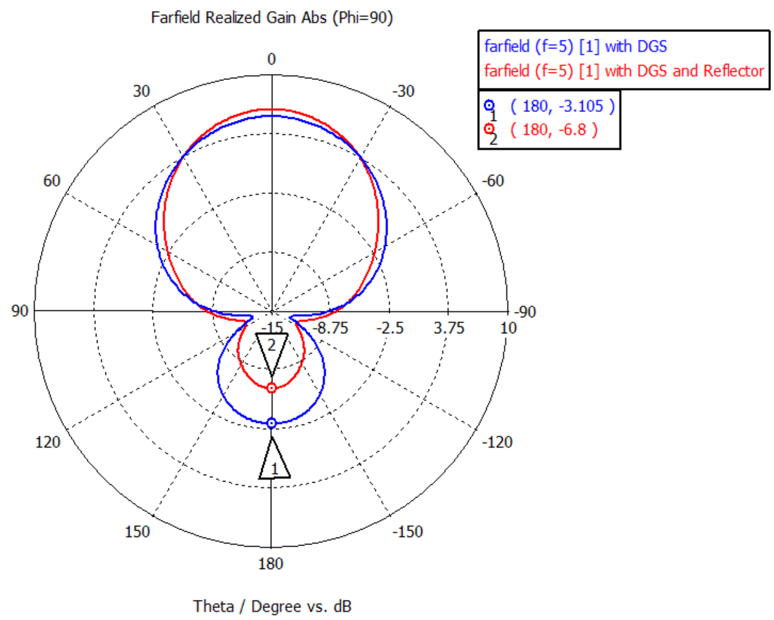

Figure 3.8: Simulated elevation pattern of the first antenna with and without the reflector in the presence of the dumbbell DGS.

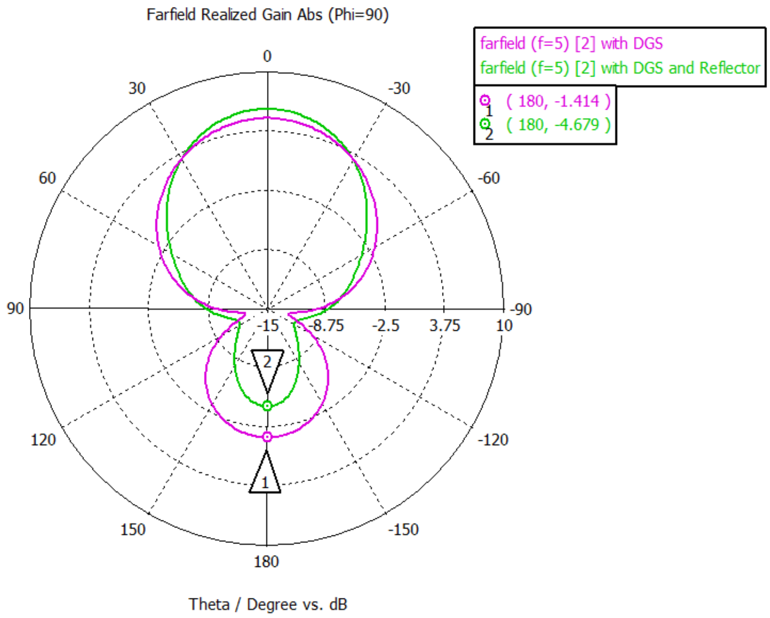

Figure 3.9: Simulated elevation pattern of the second antenna with and without the reflector in the presence of the dumbbell DGS.

Fig. 3.6 and Fig. 3.7 show the simulated azimuth patterns of the first and the second antennas, respectively, with and without the reflector in the presence of the dumbbell DGS. Similarly, Fig. 3.8 and Fig. 3.9 show the simulated elevation patterns of the first and the second antennas, respectively, with and without the reflector in the presence of the dumbbell DGS. Fig. 3.6-Fig. 3.9 show that the backlobe radiation levels of the antennas are reduced by 3.7 dB (at the 1st antenna) and 3.2 dB (at the 2nd antenna), respectively, in the both elevation and azimuth patterns. Both s-parameters and farfield results suggest that installation of the reflector improves the backward radiation without affecting the antenna performance in terms of matching and resonance frequency.

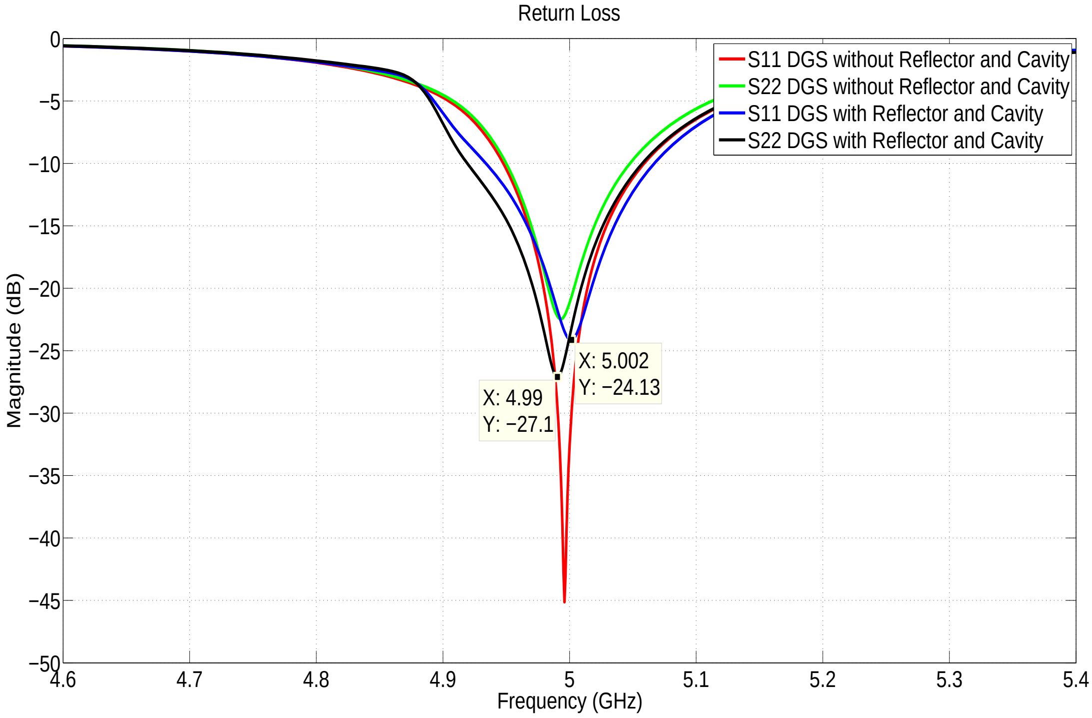

Figure 3.10: Simulated return loss results ($|S_{11}|$ and $|S_{22}|$ in dB) of the antennas with and without the reflector and the cavity versus frequency in the presence of the dumbbell DGS.

3.2 Numerical Investigation of the Effect of Both the $\lambda_o/4$ Spaced Reflector and the Cavity on the Performance Merits of the Two-Element Microstrip Antenna with a DGS

In this section, the same antenna configuration, as in Section 3.1 is used, and the reflector is replaced with a cavity enclosing the whole array with DGS. The cavity has a 1 mm wall thickness. Notice that bottom part of the cavity acts like a reflector. Hence, the air-gap of the cavity is set to $\lambda_o/4$. Dimensions of the cavity are 52 mm $\times$ 68 mm $\times$ 17.541 mm, and the radius of the holes for wires to get thorough is 5 mm.

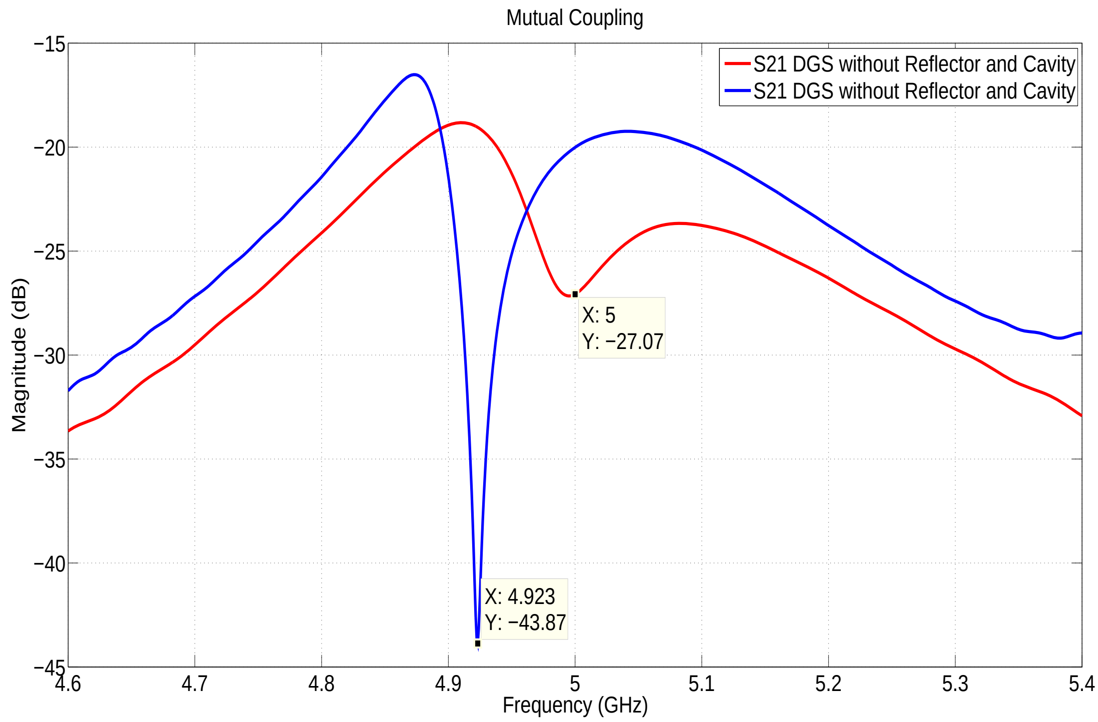

Figure 3.11: Simulated mutual coupling results ($|S_{21}|$ in dB) between the antennas with and without the reflector and the cavity versus frequency in the presence of the dumbbell DGS.

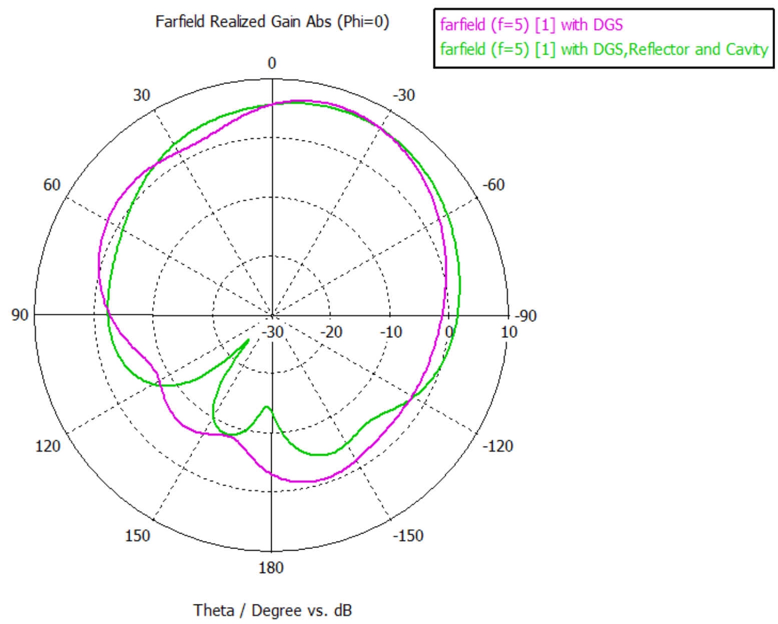

Figure 3.12: Azimuth pattern of the first antenna with and without the reflector and the cavity in the presence of the dumbbell DGS.

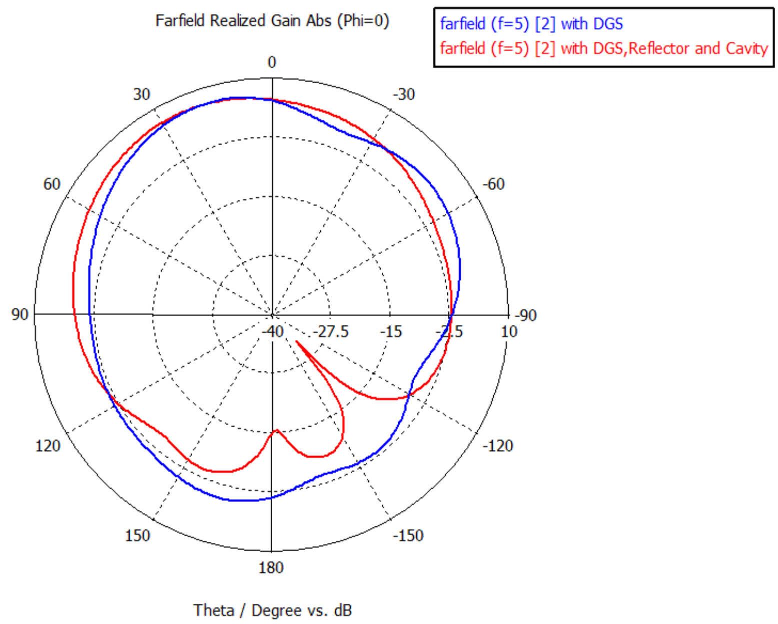

Figure 3.13: Azimuth pattern of the second antenna with and without the reflector and the cavity in the presence of the dumbbell DGS.

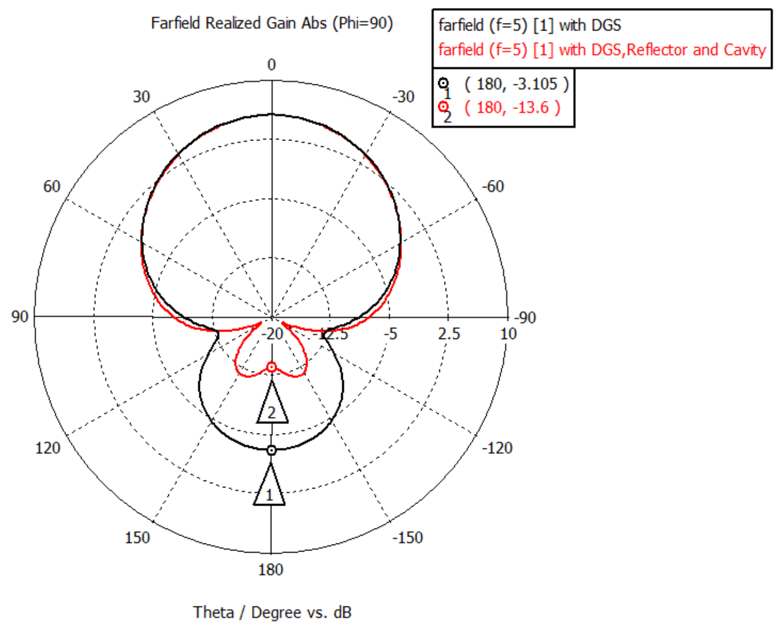

Figure 3.14: Elevation pattern of the first antenna with and without the reflector and the cavity in the presence of the dumbbell DGS.

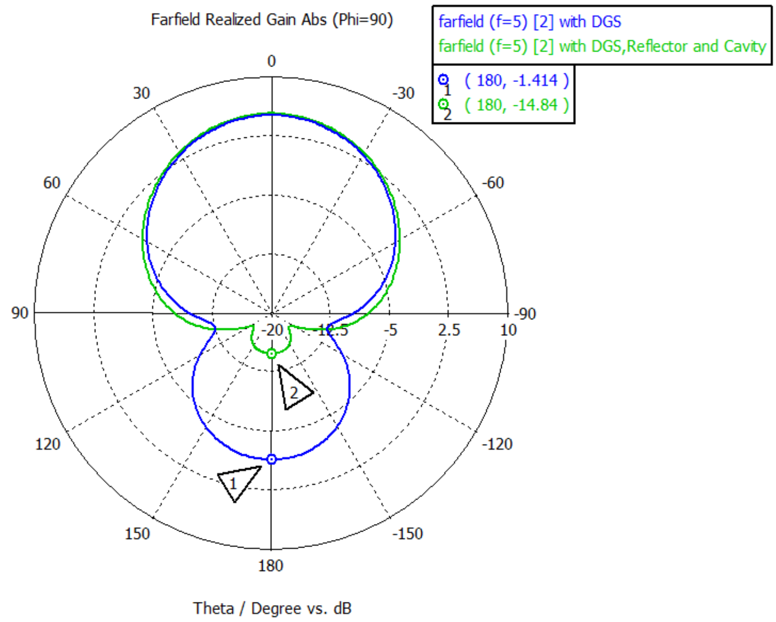

Figure 3.15: Elevation pattern of the second antenna with and without the reflector and the cavity in the presence of the dumbbell DGS.

Fig. 3.10 shows the magnitude of the return loss ($|S_{11}|$ and $|S_{22}|$ in dB) of the antennas versus frequency in the presence and absence of the reflector and the cavity while the dumbbell DGS is present in between the patch antennas. Similarly, Fig. 3.11 shows the magnitude of the mutual coupling ($|S_{21}|$ in dB) between the antennas versus frequency with and without the reflector and the cavity while the dumbbell DGS is present. It is seen from the results of Fig. 3.10 and Fig. 3.11 that although the return loss of the antennas are not affected significantly, the resonance frequency of the suppression band is shifted about 70 MHz.

Fig. 3.12 and Fig. 3.13 show the simulated azimuth patterns of the first and second antennas, respectively, with and without the reflector and the cavity in the presence of the dumbbell DGS. Similarly, Fig. 3.14 and Fig. 3.15 show the simulated elevation patterns of the first and second antennas, respectively, with and without the reflector and the cavity in the presence of the dumbbell DGS. It is seen from the farfield pattern of the first antenna in Fig. 3.12 and Fig. 3.14 that the backlobe radiation is reduced by 10.5 dB. Moreover, Fig. 3.13 and

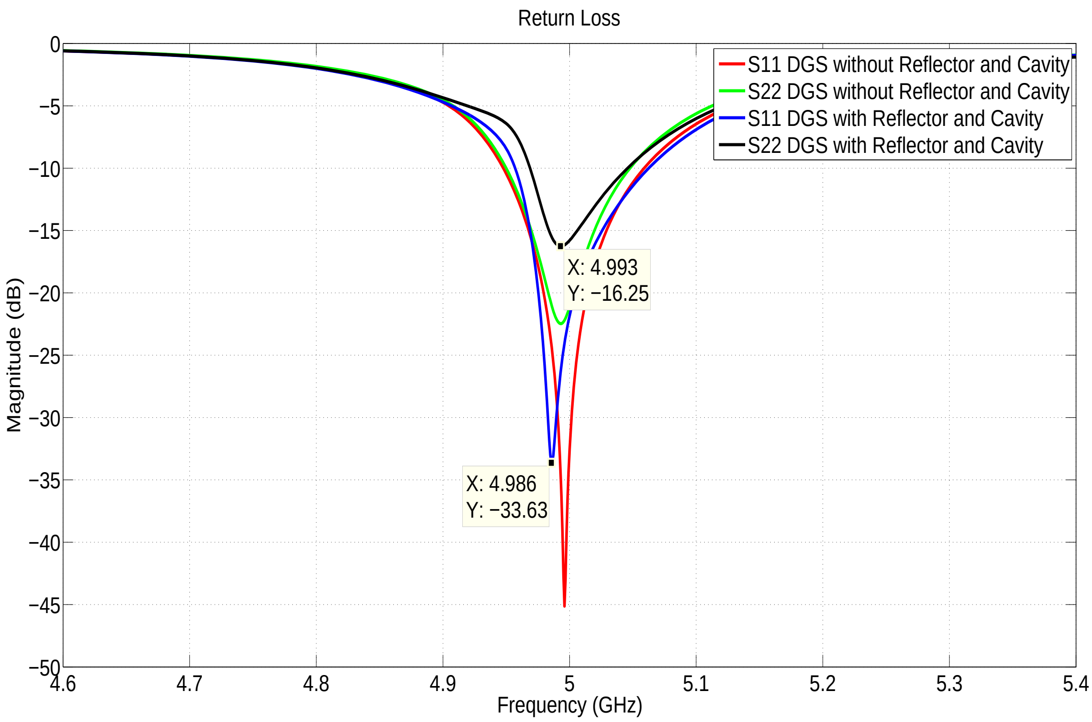

Figure 3.16: Simulated return loss results ($|S_{11}|$ and $|S_{22}|$ in dB) of the antennas with and without the reflector and the cavity versus frequency in the presence of the tuned dumbbell DGS.

Fig. 3.15 indicate that in the second antenna there is a 13.4 dB reduction in the backlobe levels . However, since the center frequency of the suppression band of the dumbbell DGS is shifted by 70 MHz due to the addition of the reflector and the cavity to the system, isolation between the antennas resonating at 5 GHz is degraded. It should be noted that because of such a frequency shift, the mutual coupling reduction at 5 GHz is minimal and the two-element microstrip antenna array behaves as if there is no DGS at this frequency. Therefore, the backlobe radiation is nearly minimized. However, these results do not reflect the real improvements in the backlobe radiation. In order to provide the mutual coupling reduction between the antennas at 5 GHz, the initial DGS etched between the microstrip patch antennas has been modified. The tuned dumbbell dimensions are as follows: $dl = 6.21$ mm, $s = 0.4$ mm and $w = 2.5$ mm. The following results are obtained with the tuned dumbbell DGS:

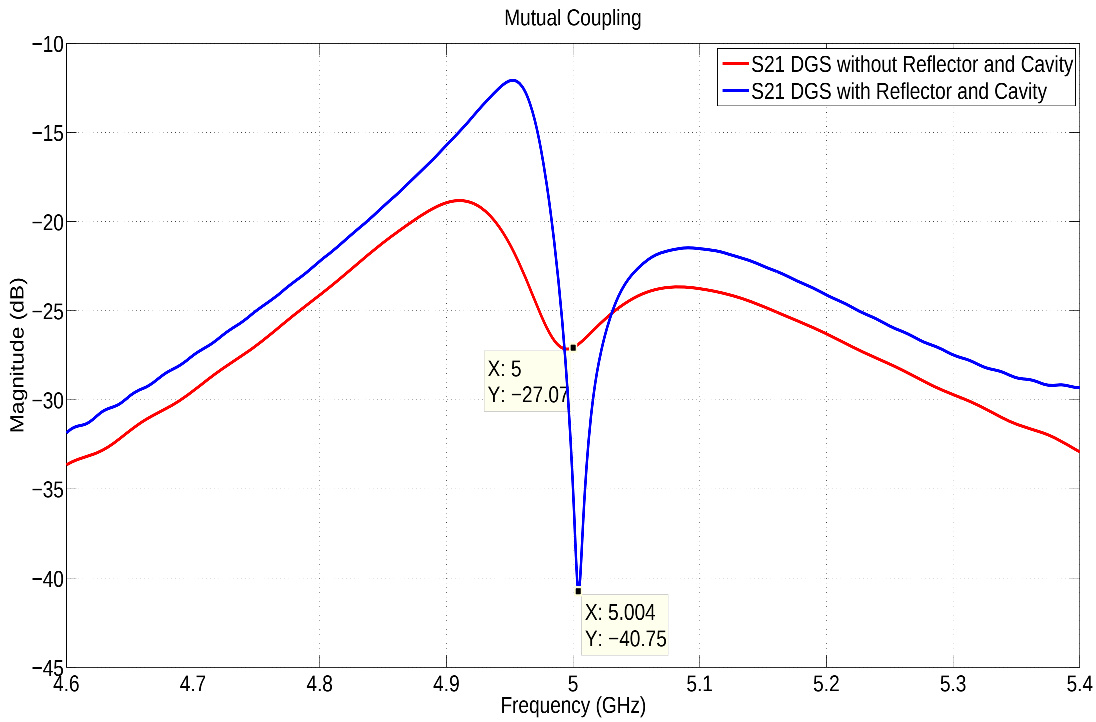

Figure 3.17: Simulated mutual coupling results ($|S_{21}|$ in dB) between the antennas with and without the reflector and the cavity versus frequency in the presence of the tuned dumbbell DGS.

Fig. 3.16 shows the magnitude of the return loss ($|S_{11}|$ and $|S_{22}|$ in dB) of the antennas versus frequency in the presence and absence of the reflector and the cavity while the tuned dumbbell DGS is present in between the patch antennas. Similarly, Fig. 3.17 shows the magnitude of the mutual coupling ($|S_{21}|$ in dB) between the antennas versus frequency with and without the reflector and the cavity while the tuned dumbbell DGS is present in between the patch antennas. It is seen from the Fig. 3.16 that although the matching of the antennas are deteriorated by 10 dB, the matching can still be considered as acceptable and the shift in center frequency of the microstrip patch antennas is less than 15 MHz. Fig. 3.17 shows that the mutual coupling at 5 GHz is enhanced by 8 dB in spite of the fact that the bandwidth of the suppression is decreased.

Fig. 3.18 and Fig. 3.19 show the simulated azimuth patterns of the first and second antennas, respectively, with and without the cavity and the reflector in the presence of the tuned dumbbell DGS. Similarly, Fig. 3.20 and Fig. 3.21 show the

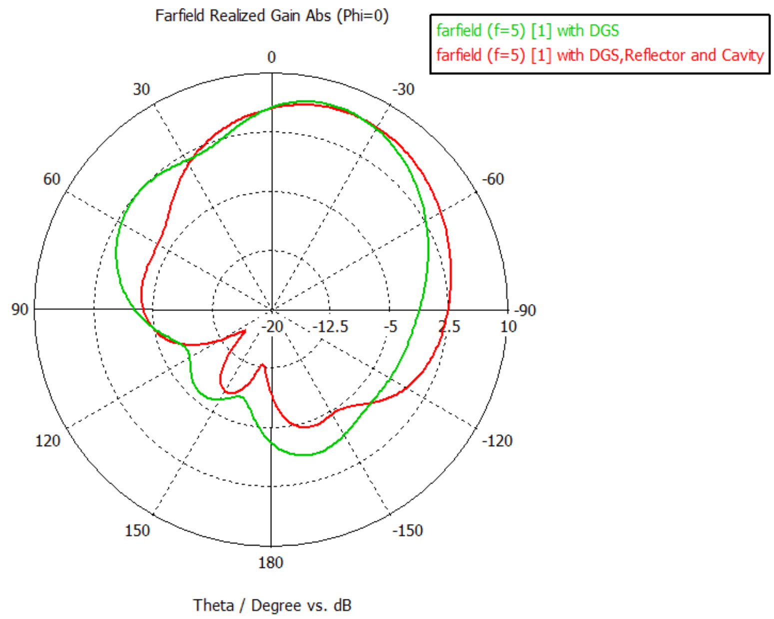

Figure 3.18: Simulated azimuth pattern of the first antenna with and without the reflector and the cavity in the presence of the tuned dumbbell DGS.

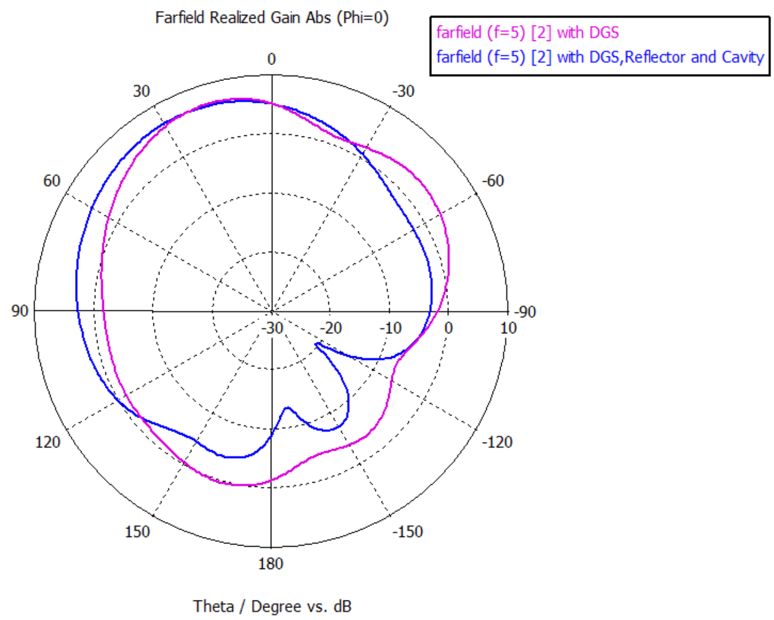

Figure 3.19: Simulated azimuth pattern of the second antenna with and without the reflector and the cavity in the presence of the tuned dumbbell DGS.

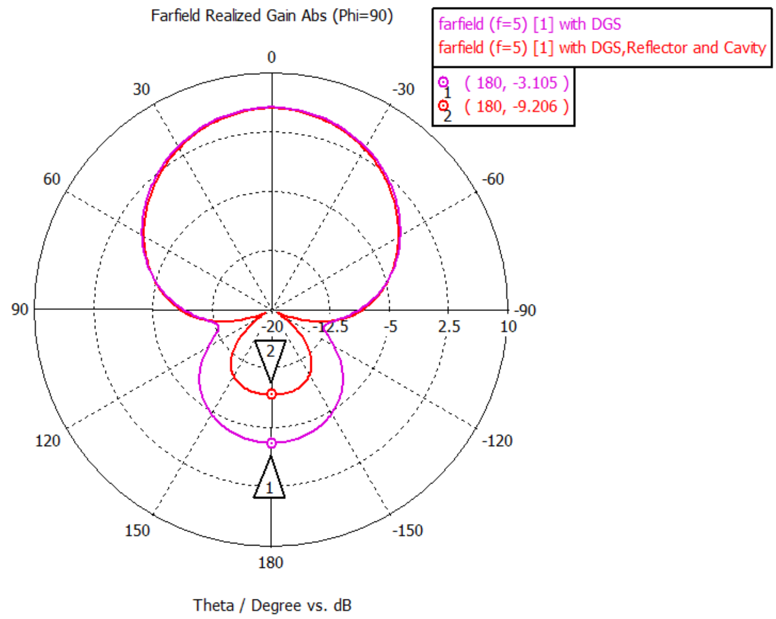

Figure 3.20: Simulated elevation pattern of the first antenna with and without the reflector and the cavity in the presence of modified the dumbbell DGS.

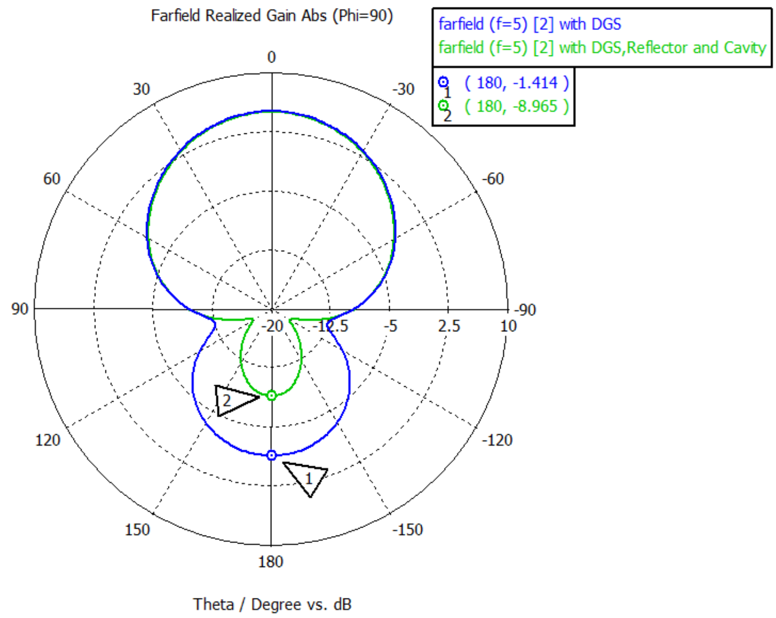

Figure 3.21: Simulated elevation pattern of the second antenna with and without the reflector and the cavity in the presence of the tuned dumbbell DGS.

Figure 3.22: (a) Top view of the cavity (b) Bottom view of the cavity

simulated elevation patterns of the first and second antennas, respectively, with and without the cavity and the reflector in the presence of the tuned dumbbell DGS. Fig. 3.18-Fig. 3.21 indicate that for the first and second antennas, 6 dB and 7.5 dB backlobe level reduction is obtained, respectively, with the tuned dumbbell DGS configuration. Once again, it should be noted that these results indicate the real improvements in the backlobe radiation since the mutual coupling reduction is achieved at 5 GHz. Hence, baclobe level reduction is less than the previous case since the DGS radiates more at 5 GHZ in this case than the previous case

3.3 Fabrication Results

The dimensions of the cavity are kept the same as that of the final design. Basically, these dimensions are as follows: width $\times$ length = 68 mm $\times$ 52 mm, height = 17,542 mm. There are two 10 mm wide holes away from center of the cavity by -10.86 mm and 15.04 mm, respectively, as seen in Fig. 3.22.

Fig. 3.23 shows the magnitude of the return loss ($|S_{11}|$ and $|S_{22}|$ in dB) of the simulated and the fabricated antennas versus frequency in the presence of the reflector and the cavity while the dumbbell DGS is etched to the ground plane of

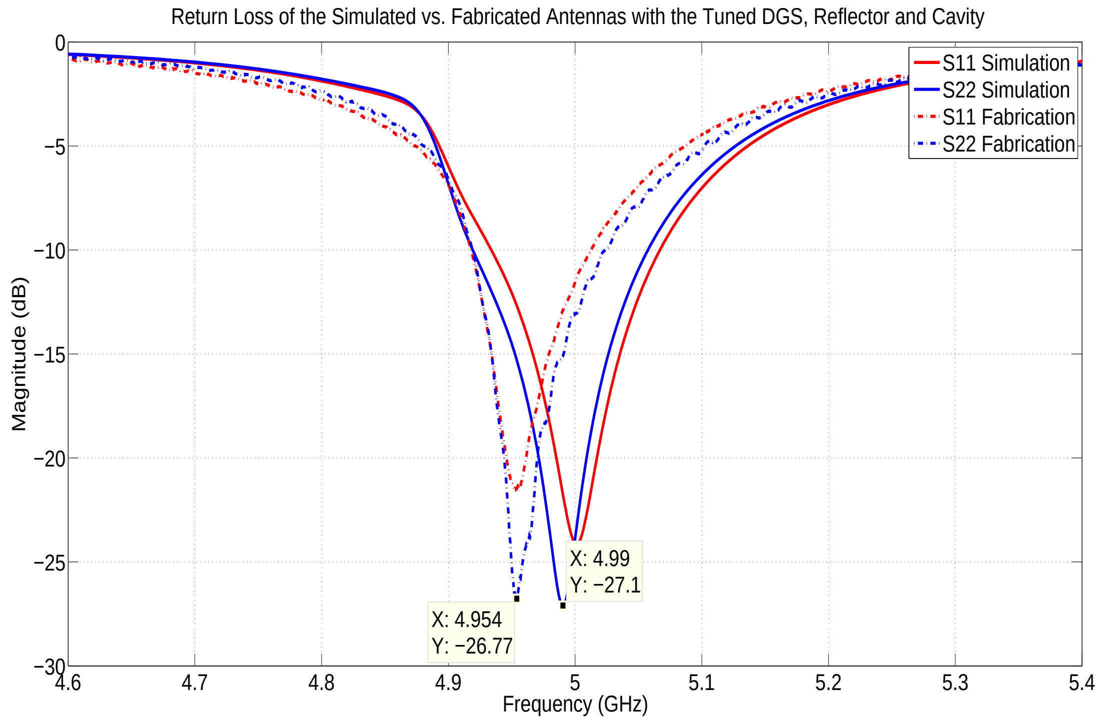

Figure 3.23: Return loss ($|S_{11}|$ and $|S_{22}|$ in dB) results of the simulated and the fabricated antennas with the cavity and the reflector while the dumbbell DGS is present.

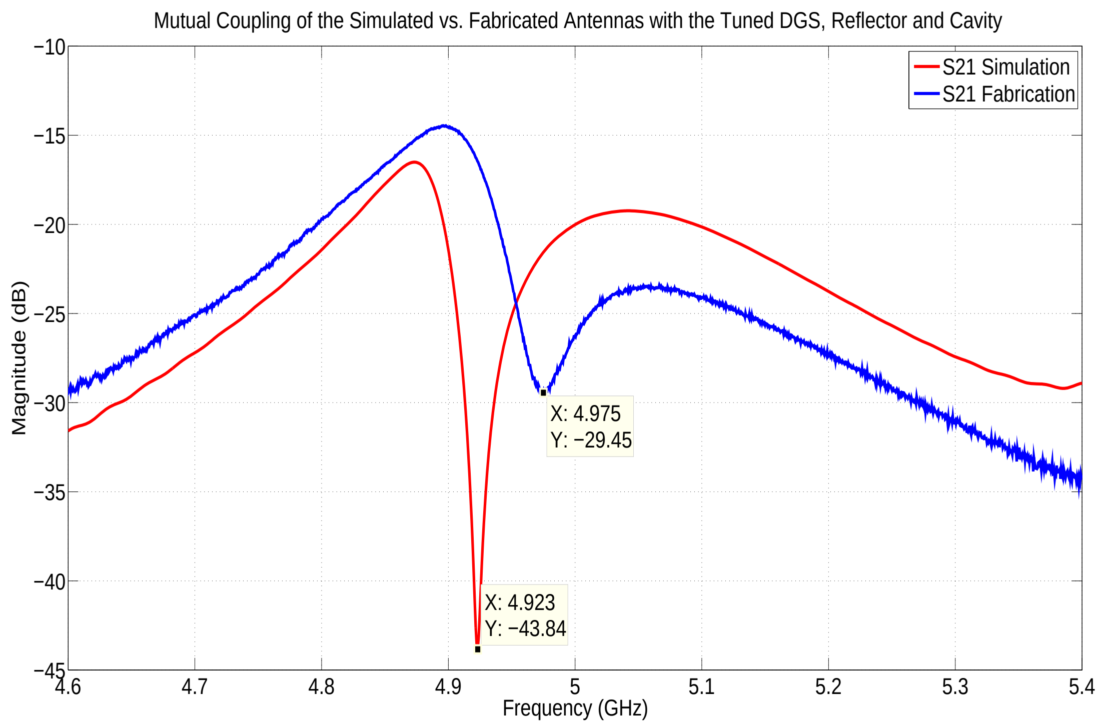

Figure 3.24: Mutual coupling ($|S_{21}|$ in dB) results of the simulated and the fabricated antennas with the reflector and the cavity while the dumbbell DGS is present.

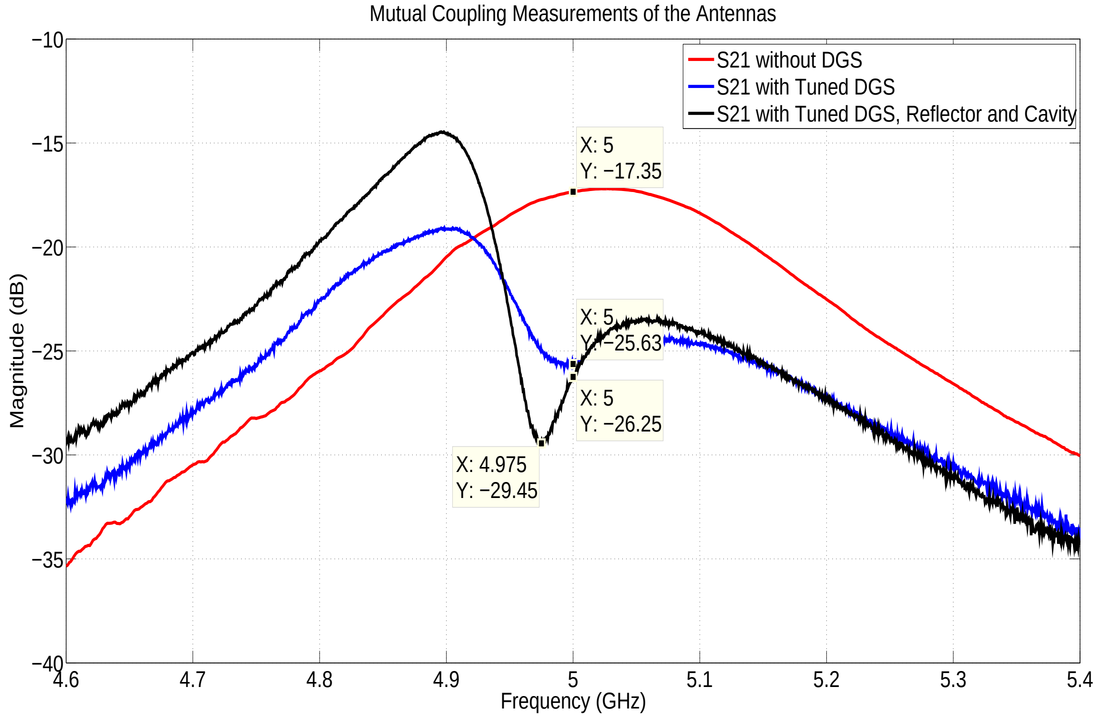

Figure 3.25: Mutual coupling ($|S_{21}|$ in dB) results of all the fabricated antennas.

the two-element microstrip antenna array. On the other hand, Fig. 3.24 shows the magnitude of the mutual coupling ($|S_{21}|$ in dB) results of the simulated and the fabricated antennas versus frequency in the presence of the reflector and the cavity while the dumbbell DGS is present. It is seen from Fig. 3.23 that the center frequency of the patch elements in the two-element microstrip antenna array is 40 MHz shifted when compared with the simulation results. Although there is a frequency shift between the simulated and the measured results, the mutual coupling suppression frequency of the measurements is closer to the design frequency (i.e., 5GHz) as seen in Fig. 3.24. Mismatches are mainly due to the mechanical inhomogeneity in the wall thickness of the cavity, which also explains the frequency shifts in return loss of the fabricated antennas (compared to the simulation results) in Fig. 3.23.

Figure 3.25 shows the measured mutual coupling results ($|S_{21}|$ in dB) of the antennas with no dumbbell DGS, with the dumbbell DGS and with the dumbbell DGS plus reflector and the cavity. As seen in Fig. 3.25, when the dumbbell DGS

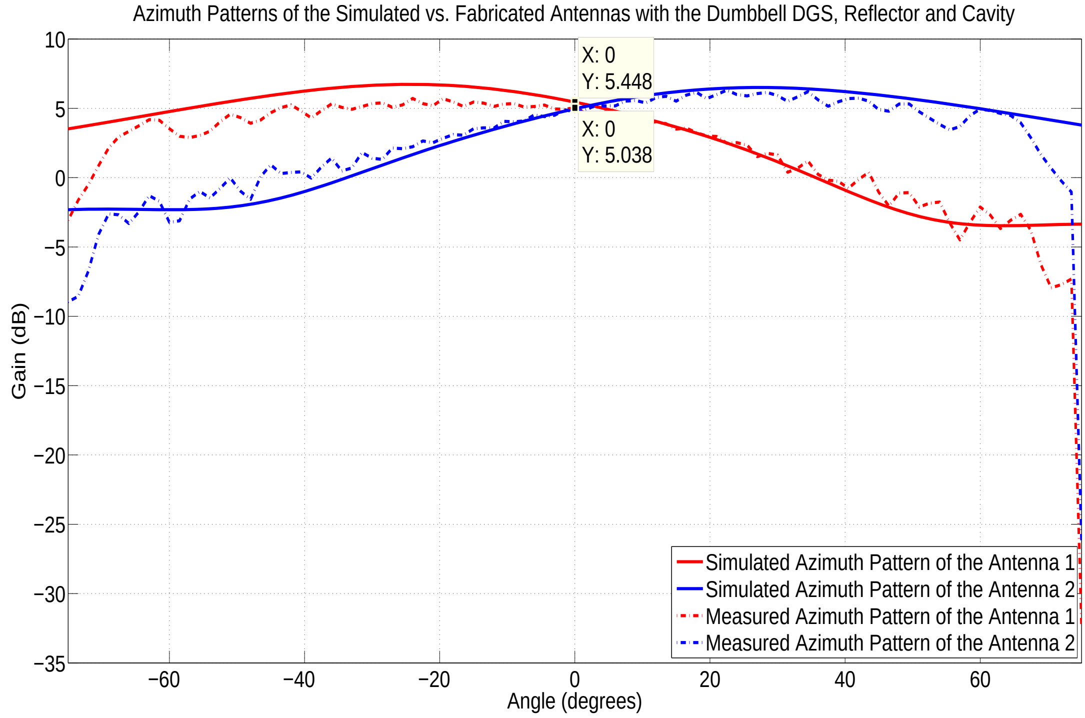

Figure 3.26: Azimuth patterns of the simulated and the fabricated antennas with the dumbbell DGS plus reflector and the cavity.

is introduced between the two-element microstrip antenna array, although the center frequency is slightly shifted by 40 MHz and it continues to shift when the reflector and the cavity are added, a significant mutual coupling reduction (approximately 8 dB) is achieved with the dumbbell DGS, and an additional suppression of 5 dB at 4.975 GHz is obtained when the reflector and the cavity are added.

Fig. 3.26 shows the simulated and the measured azimuth patterns of the first and second antennas as well as Fig. 3.27 shows the same results for the elevation patterns of the first and second antennas with the dumbbell DGS, the reflector and the cavity. As seen from these figures, the simulated and measured results agree well with each other. On the other hand, Fig. 3.28 and Fig. 3.29 illustrate the azimuth pattern measurements of the first and second antennas in the absence and presence of the dumbbell DGS and in the presence of the dumbbell DGS, the reflector and the cavity, while Fig. 3.30 and Fig. 3.31 show the same results for the elevation pattern. These figures indicate that the gain

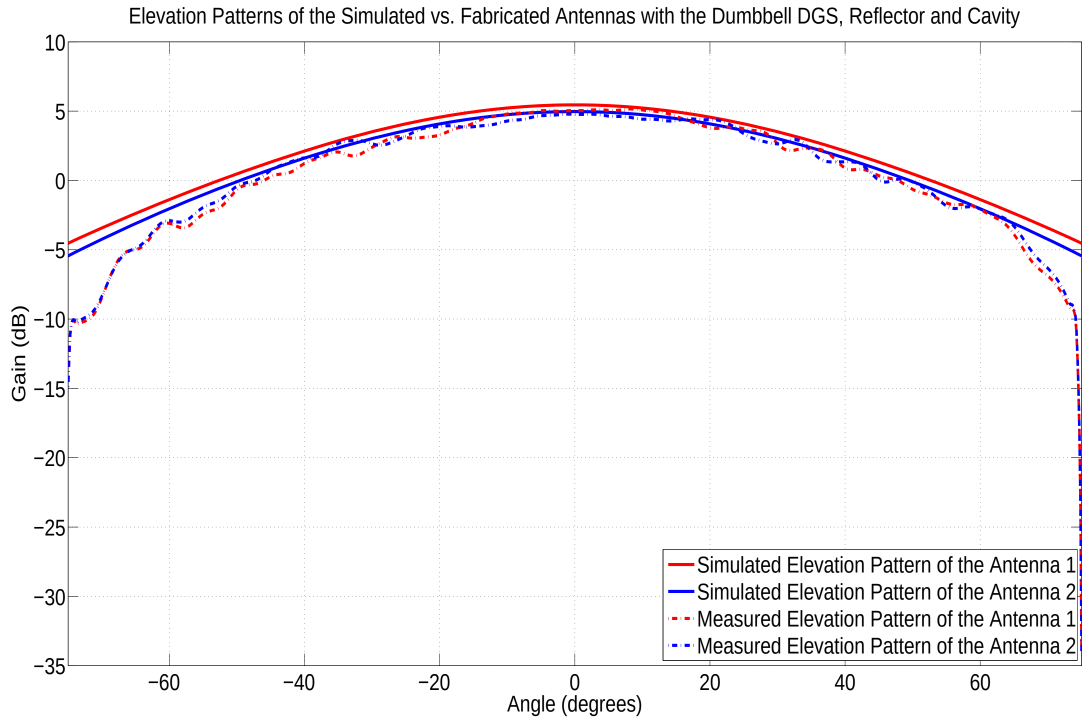

Figure 3.27: Elevation patterns of the simulated and the fabricated antennas with the dumbbell DGS, the reflector and the cavity.

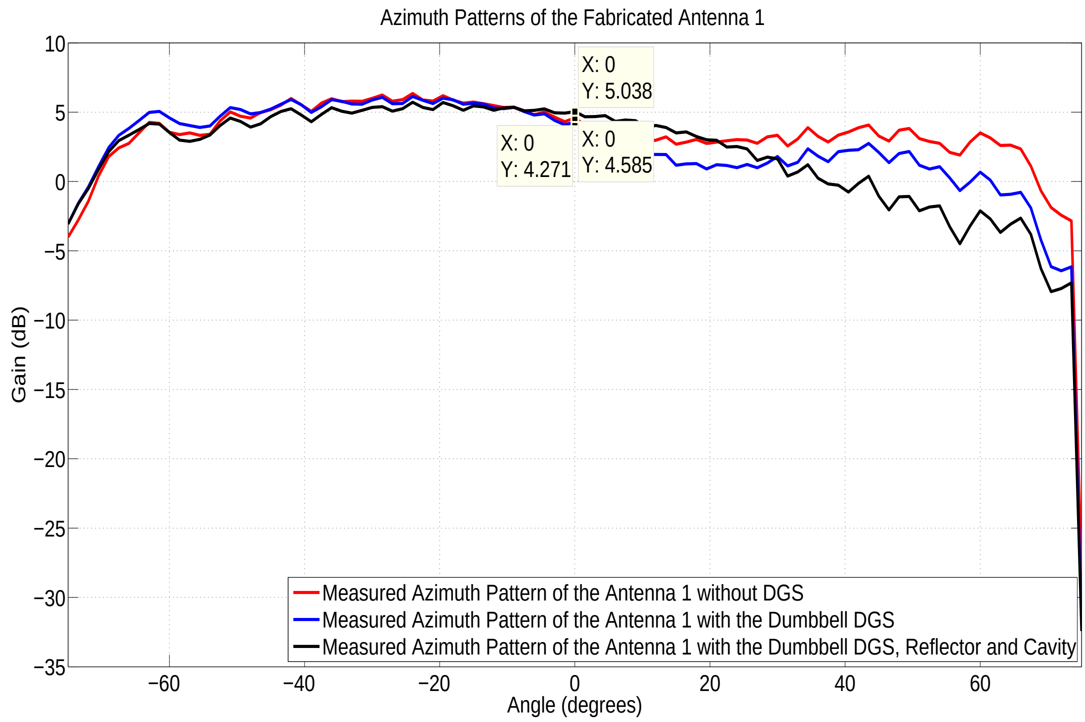

Figure 3.28: Measurements of the azimuth patterns of antenna 1 without DGS, with the dumbbell DGS and with the dumbbell DGS, the reflector and the cavity.

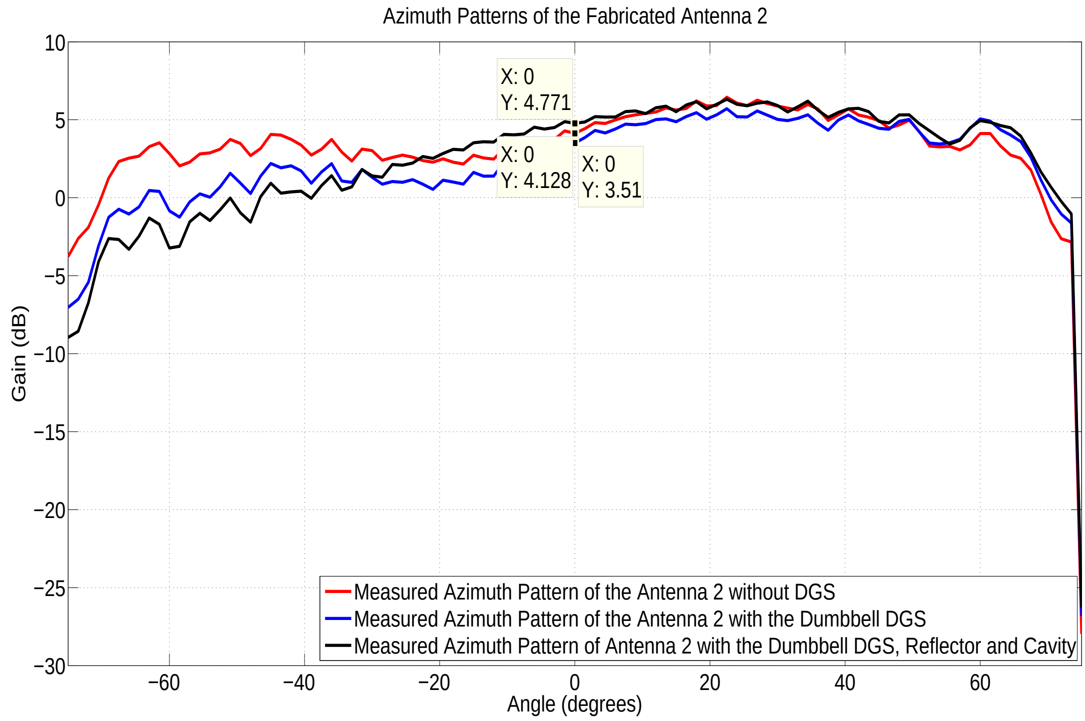

Figure 3.29: Measurements of the azimuth patterns of antenna 2 without DGS, with the dumbbell DGS and with the dumbbell DGS, the reflector and the cavity.

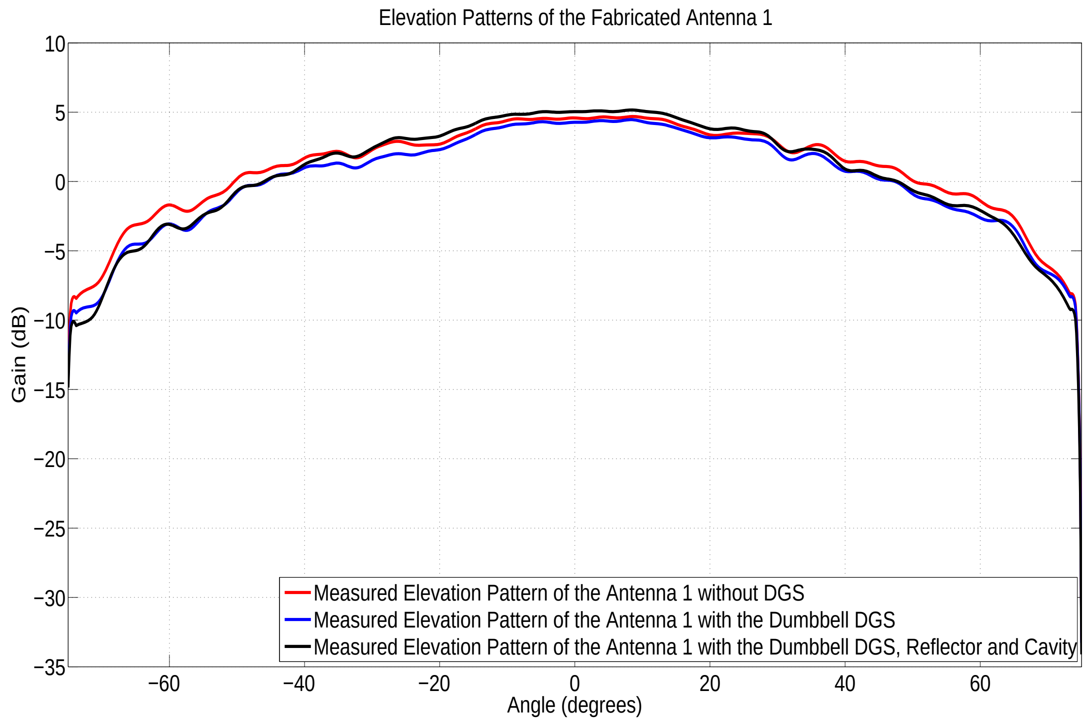

Figure 3.30: Measurements of the elevation patterns of antenna 1 without DGS, with the dumbbell DGS and with the dumbbell DGS, the reflector and the cavity.

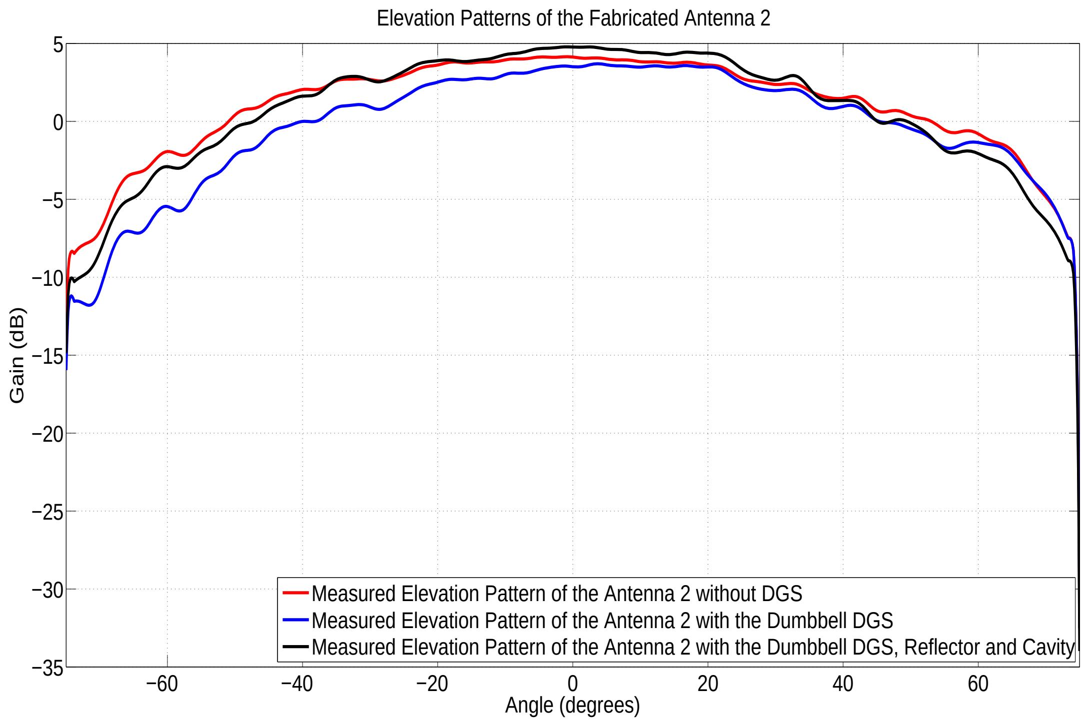

Figure 3.31: Measurements of the elevation patterns of antenna 2 without DGS, with the dumbbell DGS and with the dumbbell DGS, the reflector and the cavity.

of the fabricated antennas 1 and 2 with dumbbell DGS improves about 0.7 dB to 1.2 dB, respectively, after the introduction of the reflector and the cavity. Besides, the 3 dB beamwidth of the elevation patterns of both antennas narrow down approximately 5 degrees as seen in Fig. 3.30 and Fig. 3.31.

Chapter 4

Design, Analysis and Fabrication of a 2×2 Microstrip Array with the Dumbbell DGS, Reflector and Cavity

4.1 Introduction

In this chapter we focus on the effect of dumbbell DGS on the performance of the 2×2 microstrip antenna array in the presence of both the reflector and the cavity. As mentioned before, the main aim is to enhance the farfield performance of the 2×2-microstrip antenna array by diminishing both the mutual coupling between the microstrip patch antennas (via utilizing the dumbbell DGS) and to suppress the backlobe radiation with the help of the reflector and cavity. Note that, we continue to work with ARLON TC600 (ϵ_r = 6.15 and tanδ= 0.002) as the substrate.

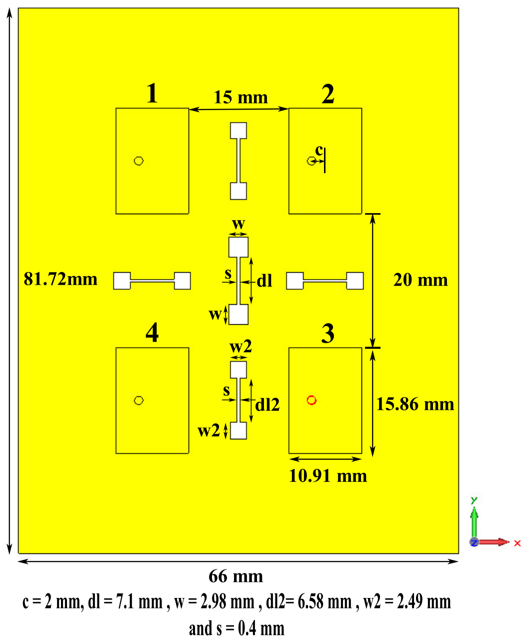

Figure 4.1: Illustration of the 2×2 microstrip antenna array with five-dumbbell DGS.

Initially, five dumbbells are etched to the ground plane to form a DGS as shown in Fig. 4.1. One of the dumbbells is in the middle of all four patch antennas, two are in between the patches along the H-plane, and the remaining two are in between the patches along the E-plane (see Fig. 4.1). However, in this configuration, the dumbbells are very close to each other. Therefore, strong mutual coupling among them degrades their performance and requires significant amount of work for tuning. On the other hand, the main aim of using a DGS is to suppress the surface waves. Because the surface waves are stronger along the E-plane, the dumbbells etched between the two antennas along the H-plane are cancelled, and the number of dumbbells is reduced to three.

In this chapter, first a brief summary of the results corresponding to the five-dumbbell DGS are given. Then, fabrication results are presented when the number of dumbbells is reduced to three.

4.2 Fabrication Results

4.2.1 Summary of the Simulation and Fabrication Results of the 2×2 Microstrip Antenna Array on Substrate ARLON TC600 in the Absence of the Dumbbell DGS

The simulated 2×2 microstrip antenna array in the absence of the dumbbell DGS is fabricated on substrate ARLON TC600 (ϵ_r = 6.15, tanδ= 0.002) with a thickness of 1.524 mm. All the substrate and the antenna dimensions are the same for simulations and fabrications. Basically, the dimensions of the board outline are 66 mm × 81.72 mm. The horizontal edge-to-edge separation between the patch antennas is $\lambda_o/4$ (15 mm), and the vertical edge-to-edge separation between the antennas is $\lambda_o/3$ (20 mm). The separation along the H-plane is kept larger as we want to eliminate the space wave coupling as much as possible since they are dominant in this plane. The length and width of the patch antennas are 15.86 mm × 10.91 mm, respectively, and their feeding point is 2 mm away from the center of the patch antennas along the width direction and at the center along the length direction. The front and back view of the fabricated 2×2 microstrip antenna array is given in Fig. 4.2.

Fig. 4.3 shows the magnitude of the return loss ($|S_{11}|$, $|S_{22}|$, $|S_{33}|$ and $|S_{44}|$ in dB) of the simulated and the fabricated array versus frequency in the absence of the dumbbell DGS. Additionally, Fig. 4.4 shows the magnitude of the mutual coupling ($|S_{21}|$, $|S_{43}|$, $|S_{31}|$, $|S_{42}|$, $|S_{41}|$ and $|S_{32}|$ in dB) results of the simulated and the fabricated antennas in the absence of the dumbbell DGS. It is seen from Fig. 4.3 that the resonance frequency of the fabricated patch antennas is about 20 MHz less than that of the simulated results. Besides, matching of the fabricated antennas are about 8 dB worse than matching of the simulated

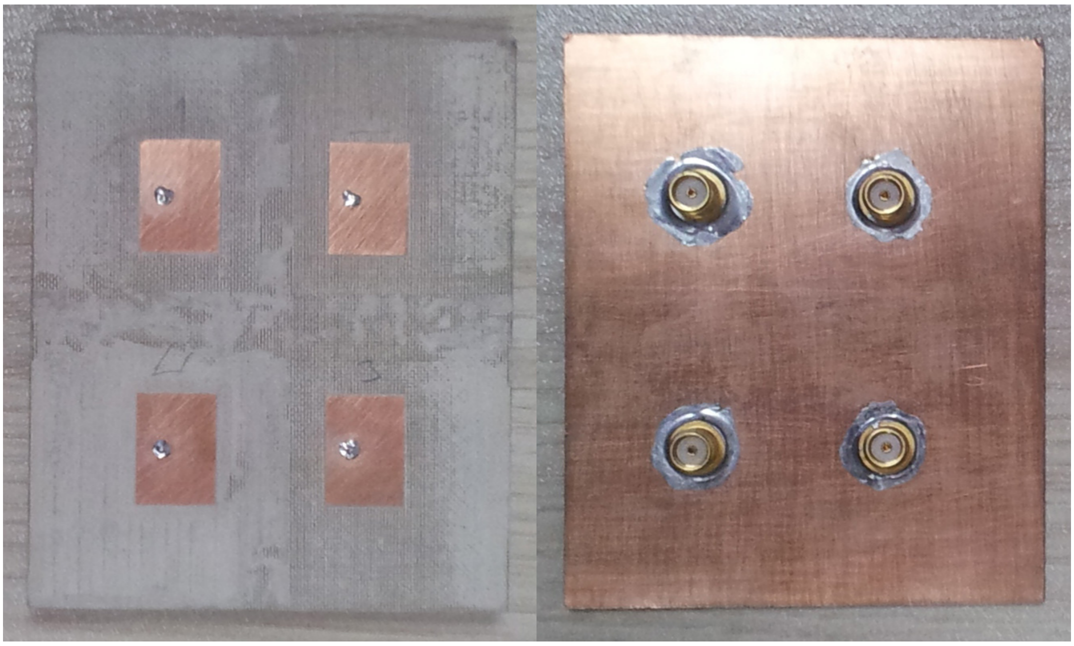

(a) (b)

Figure 4.2: (a) Frontview of the fabricated 2×2 microstrip antenna array without the dumbbell DGS. (b) Backview of the fabricated 2×2 microstrip antenna array without the dumbbell DGS.

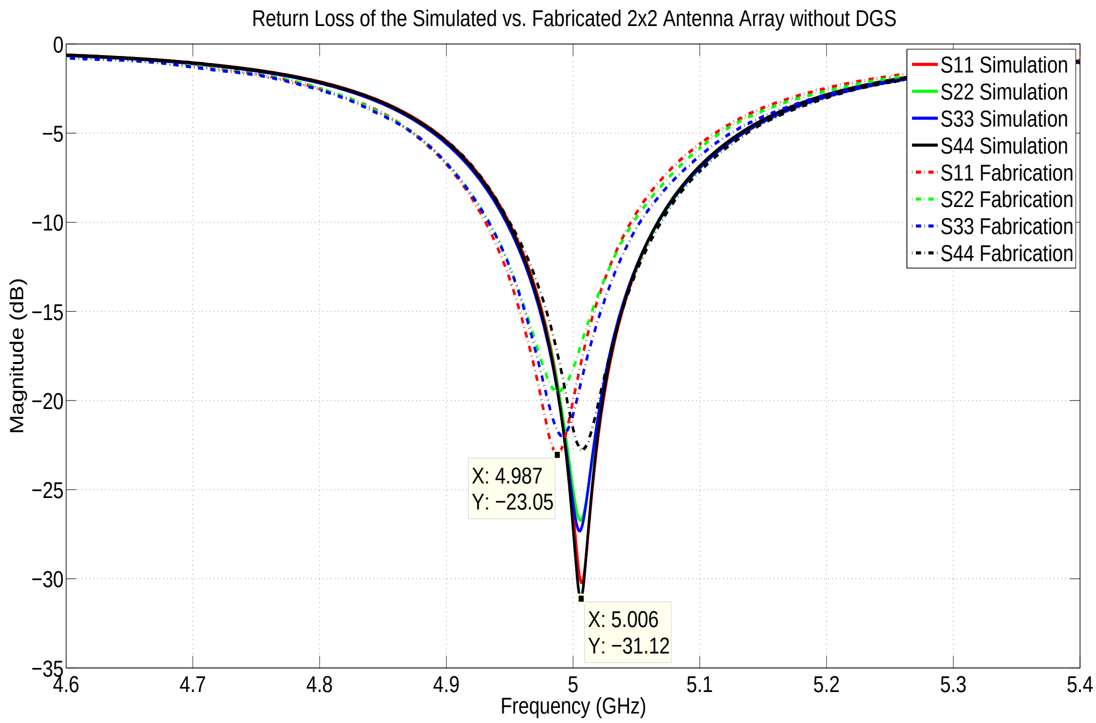

Figure 4.3: Return loss ($|S_{11}|$, $|S_{22}|$, $|S_{33}|$ and $|S_{44}|$ in dB) results of the simulated and the fabricated antennas in the absence of the dumbbell DGS.

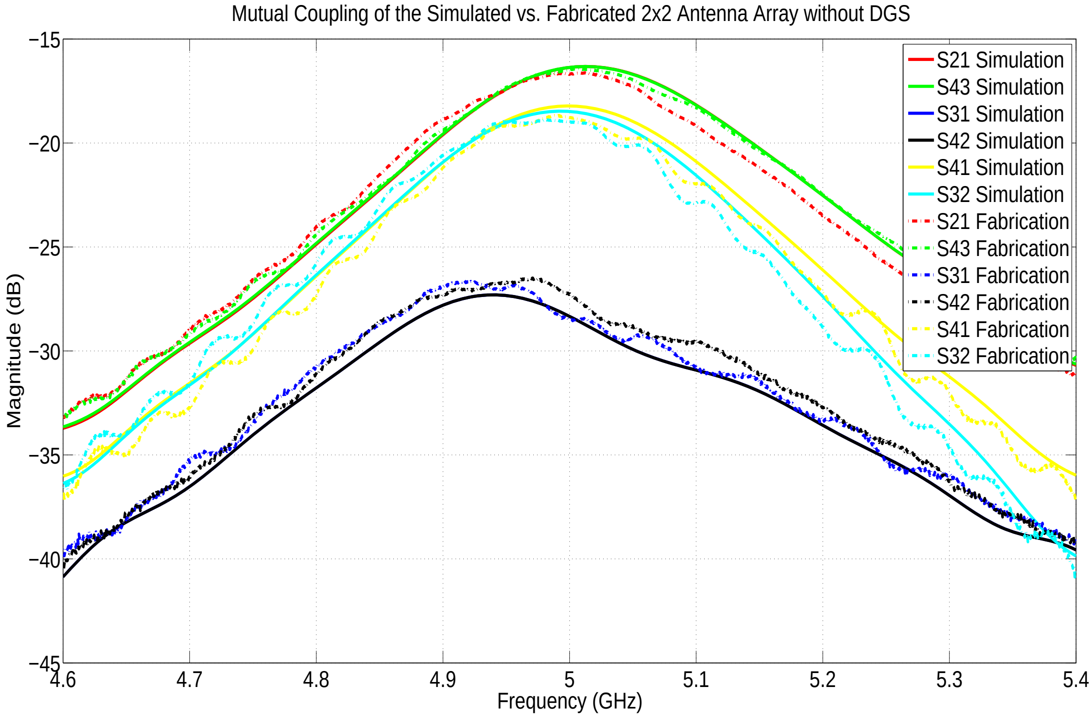

Figure 4.4: Mutual coupling ($|S_{21}|$, $|S_{43}|$, $|S_{31}|$, $|S_{42}|$, $|S_{41}|$ and $|S_{32}|$ in dB) results of the simulated and the fabricated antennas in the absence of the dumbbell DGS.

antennas. On the other hand, notice that the simulated and fabricated mutual coupling results agree with each other very well as indicated in Fig. 4.4. Besides, $|S_{21}|$ and $|S_{43}|$, $|S_{41}|$ and $|S_{32}|$ as well as $|S_{31}|$ and $|S_{42}|$ are close to each other due to the symmetry in the array and the feed positions.

The main difference between the simulated and the fabricated results in Figs. 4.3 and 4.4 are due to the fabrication process that involves sanding the edges of the antennas in order to get rid of the copper chips around the antennas, which also degrades the matching.

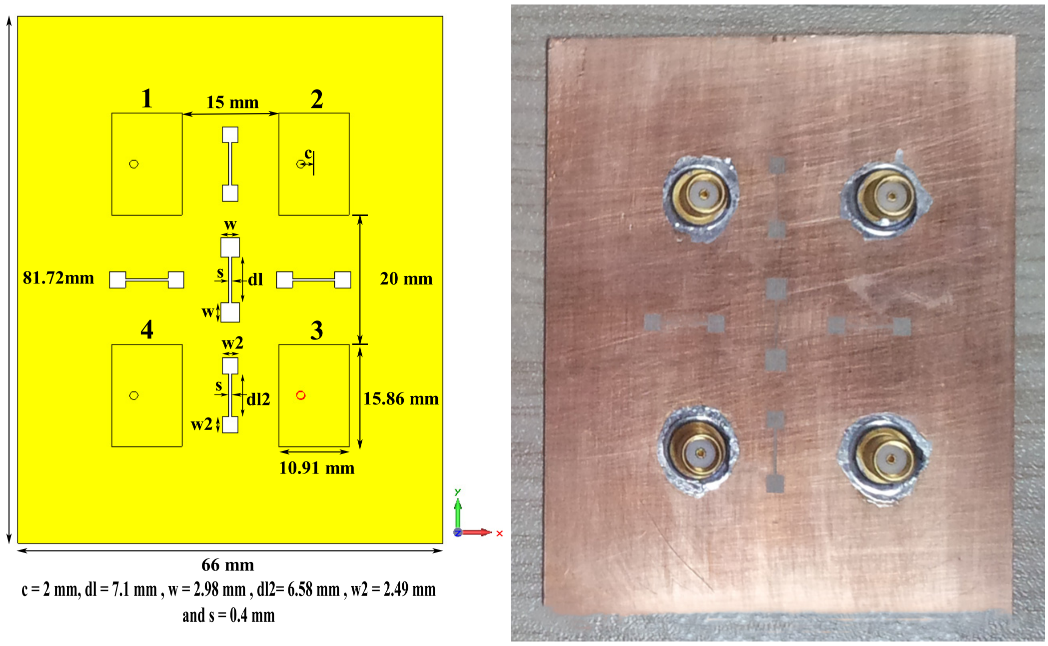

(a) (b)

Figure 4.5: (a) Top view of the simulated 2×2 microstrip antenna array with the five-dumbbell DGS. (b) Backview of the fabricated 2×2 microstrip antenna array with the five-dumbbell DGS.

4.2.2 Summary of the Simulation and Fabrication Results of the 2×2 Microstrip Antenna Array with the Five-Dumbbell DGS on Substrate ARLON TC600

The 2×2 microstrip antenna array together with the etched five dumbbells that form the DGS is simulated and fabricated on substrate ARLON TC600 (ϵ_r = 6.15, tanδ= 0.002) that has a thickness of 1.524 mm. All the substrate, antenna and dumbbell dimensions are the same for both simulations and fabrications. Basically, the dimensions of the board outline are 66 mm × 81.72 mm. The horizontal edge-to-edge separation between the patch antennas is $\lambda_o/4$ (15 mm), and the vertical edge-to-edge separation between the antennas is $\lambda_o/3$ (20 mm). The length and width of the patch antennas are 15.86 mm × 10.91 mm, respectively, and their feeding point is 2 mm away from the center of the patch antennas along

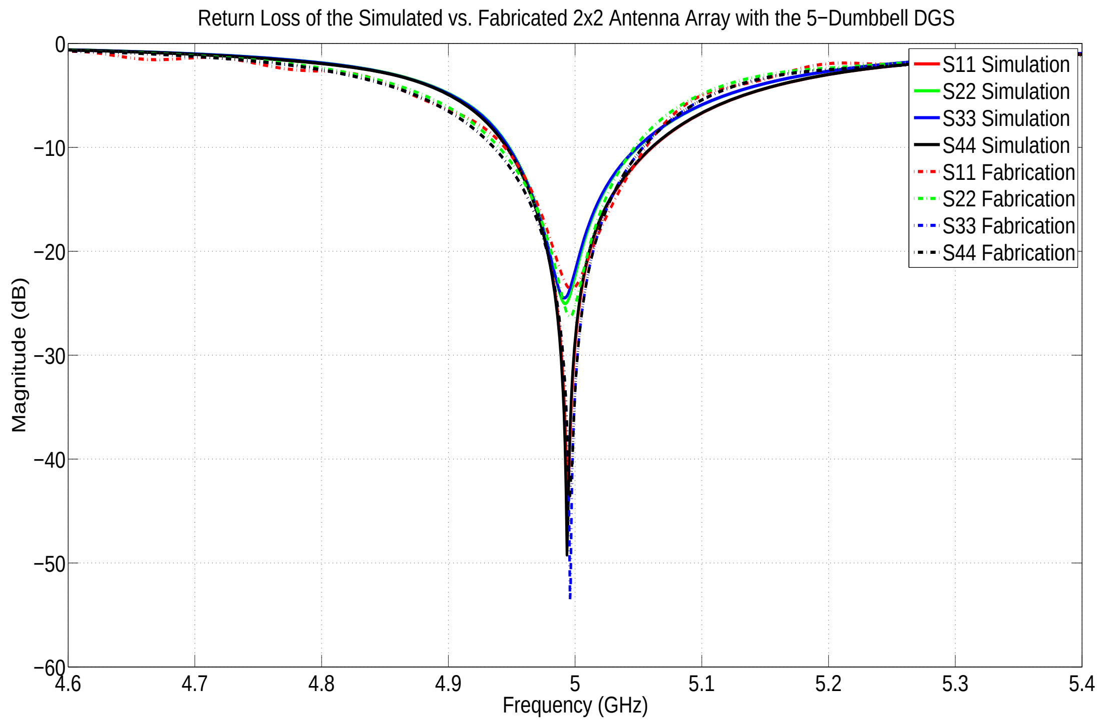

Figure 4.6: Return loss ($|S_{11}|$, $|S_{22}|$, $|S_{33}|$ and $|S_{44}|$ in dB) results of the simulated and the fabricated antennas in the presence of the five-dumbbell DGS

the width direction and at the center along the length direction. In addition, dimensions of dumbbell that is at the middle of the array are dl = 7.1 mm, s = 0.4 mm and w = 2.98 mm while the dimensions of the other dumbbells are $dl2$ = 6.58 mm, s = 0.4 mm and w = 2.49 mm as illustrated in Fig. 4.5(a). The backview of the fabricated array with the etched five dumbbells (that form DGS) is shown in Fig. 4.5(b).

Fig. 4.6 shows the magnitude of the return loss ($|S_{11}|$, $|S_{22}|$, $|S_{33}|$ and $|S_{44}|$ in dB) of the simulated and the fabricated antennas versus frequency in the presence of the five-dumbbell DGS. Similarly, Fig. 4.7 shows the magnitude of the mutual coupling ($|S_{21}|$, $|S_{31}|$ and $|S_{41}|$ in dB) results of the simulated and the fabricated antennas after the introduction of five-dumbbell DGS as shown in Fig. 4.5. As seen from Fig. 4.6, the fabricated return loss results of the antennas agree well with simulation results. However, Fig. 4.7 indicates that there is a 250 MHz frequency shift at the resonance frequency of the stop band between the antennas 1 and 2 when the measured $|S_{21}|$ is compared with the simulated

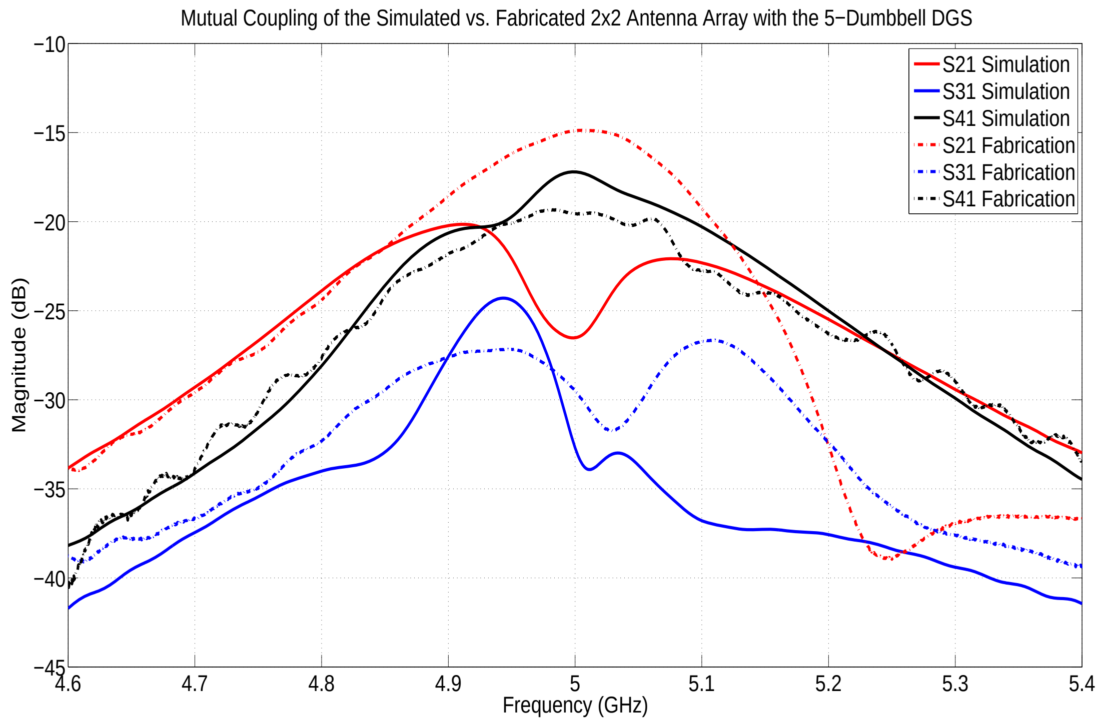

Figure 4.7: Mutual coupling ($|S_{21}|$, $|S_{31}|$ and $|S_{41}|$ in dB) results of the simulated and the fabricated antennas in the presence of the five-dumbbell DGS.

$|S_{21}|$. Recall that the same problem was also observed in the 2-element antenna array in Chapter 2, and resolved by tuning the dimensions of the dumbbell.

4.2.3 Fabrication Results of the 2×2 Microstrip Antenna Array with the Three-Dumbbell DGS on Substrate ARLON TC600

In order to avoid the 250 MHz frequency shift in the fabrication results, the dimensions of the dumbbell between the antennas 1 and 2, as well as the one between 4 and 3 are modified. Moreover, considering the fact that the dumbbells are used to suppress the surface waves, the dumbbells between 1 and 4, and 2 and 3 (the dumbbells along the H-plane) are cancelled. Thereby, complexity of the design is reduced.

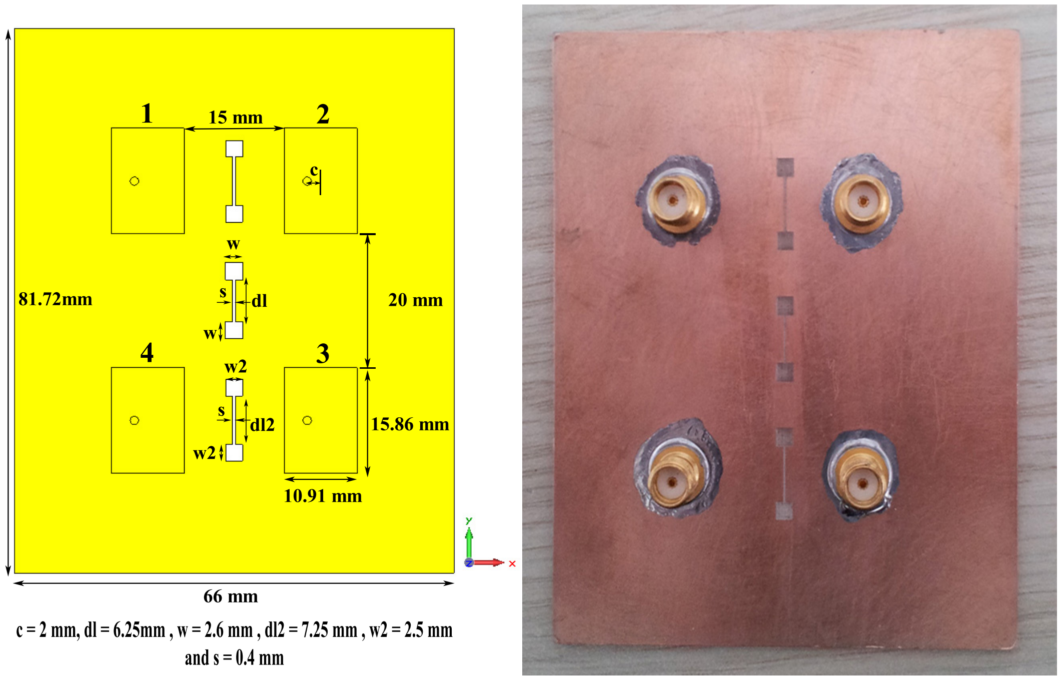

(a) (b)

Figure 4.8: (a) Top view of the simulated 2×2 microstrip antenna array with the three-dumbbell DGS. (b) Backview of the fabricated 2×2 microstrip antenna array with the three-dumbbell DGS.

Similar to the previous cases, the array is designed on ARLON TC600 ($\epsilon_r =$ 6.15, tanδ= 0.002 and thickness s = 1.524 mm). All dimensions are kept the same except the dimensions of the dumbbells. The dimensions of dumbbell that is in the middle of the array are dl = 6.25 mm, s = 0.4 mm and w = 2.6 mm and the dimensions of the other dumbbells are $dl2$ = 7.25 mm, s = 0.4 mm and $w2$ = 2.5 mm. The details of the geometry as well as the backview of the fabricated array with the three-dumbbell DGS are given in Fig. 4.8.

Fig. 4.9 shows the magnitude of the return loss ($|S_{11}|$, $|S_{22}|$, $|S_{33}|$ and $|S_{44}|$ in dB) results of the simulated and the fabricated antennas versus frequency in the presence of three-dumbbell DGS whereas Fig. 4.7 shows the magnitude of the mutual coupling ($|S_{21}|$, $|S_{31}|$, $|S_{43}|$ and $|S_{42}|$ in dB) results of the simulated and the fabricated antennas after the insertion of three-dumbbell DGS as illustrated in Fig. 4.8(a). Fig. 4.9 shows that the measured return loss results of the

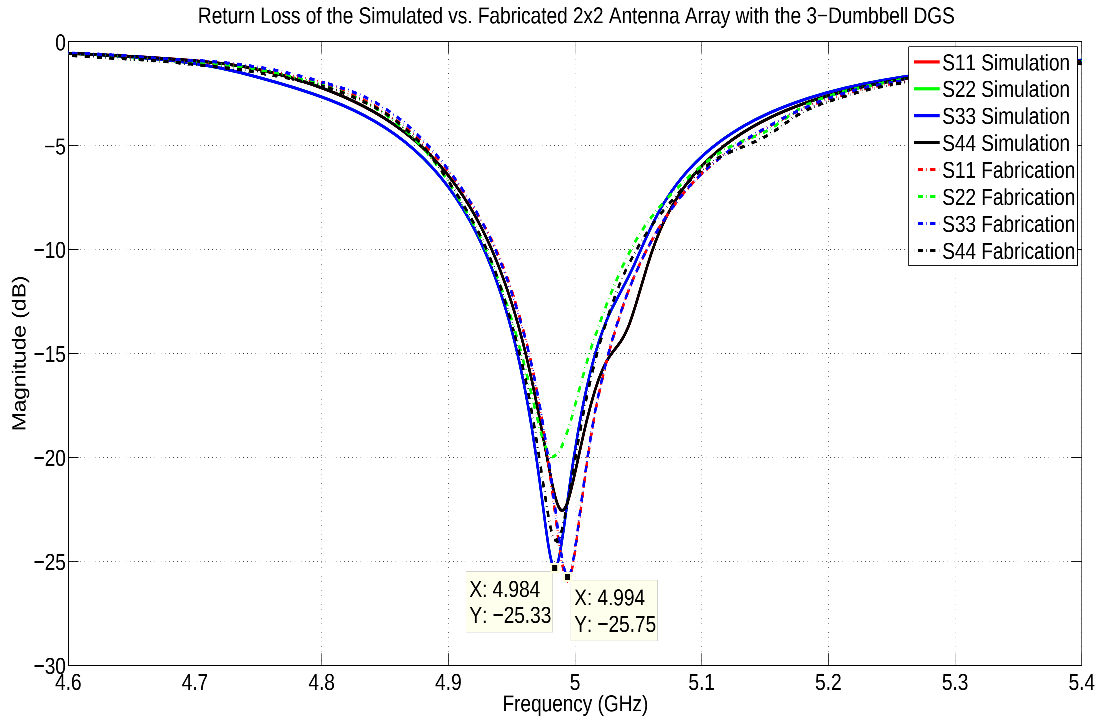

Figure 4.9: Return loss ($|S_{11}|$, $|S_{22}|$, $|S_{33}|$ and $|S_{44}|$ in dB) results of the simulated and the fabricated antennas with the three-dumbbell DGS.

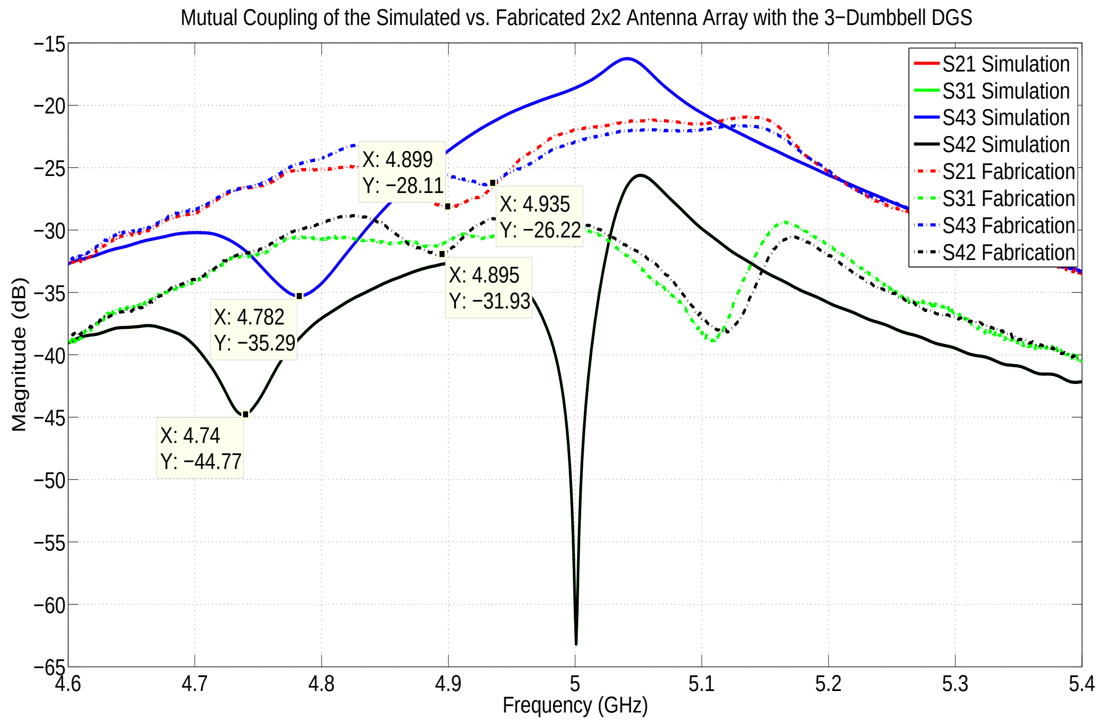

Figure 4.10: Mutual coupling ($|S_{21}|$, $|S_{31}|$, $|S_{43}|$ and $|S_{42}|$ in dB) results of the simulated and the fabricated antennas with the three-dumbbell DGS.

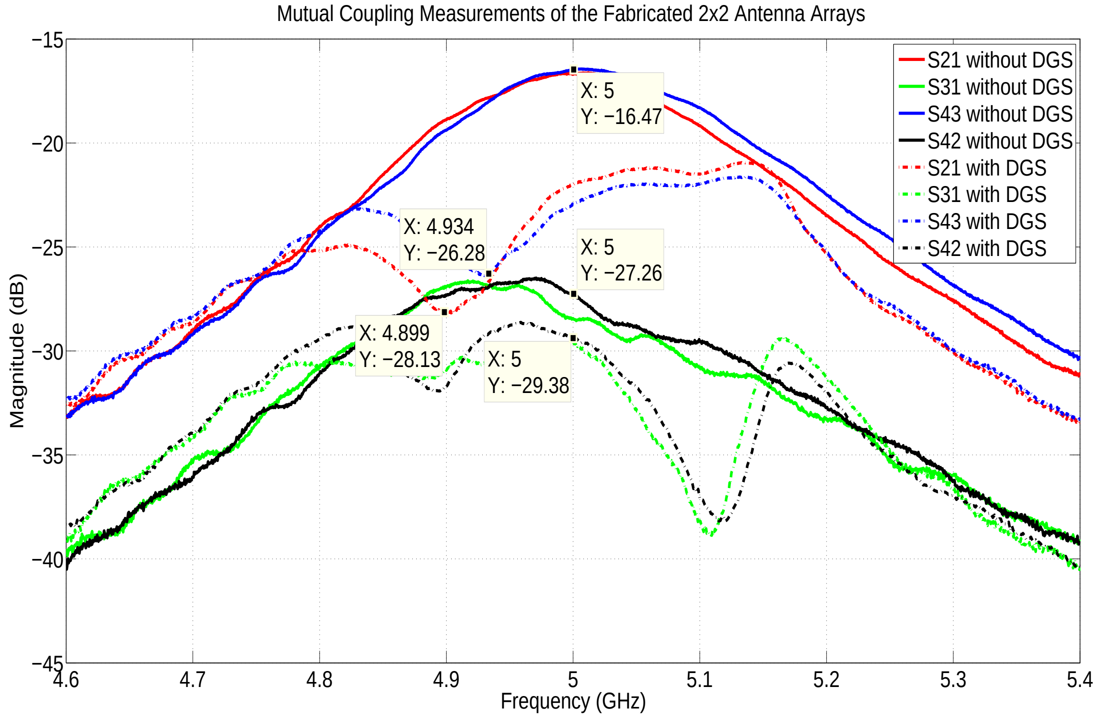

Figure 4.11: Mutual coupling ($|S_{21}|$, $|S_{31}|$, $|S_{43}|$ and $|S_{42}|$ in dB) results of the 2×2 antenna array in the absence and presence of the three-dumbbell DGS.

fabricated patch antennas are in good agreement with that of the simulated results where the shift in resonance frequency is less than 10 MHz. However, as seen from Fig. 4.10, a frequency shift at the resonance frequency of the stop band of the dumbbell DGS still exists. Regarding $|S_{21}|$ and $|S_{43}|$, there is a 100 MHz frequency shift, and regarding $|S_{31}|$ and $|S_{42}|$, the shift is about 150 MHz. These results still indicate a production error. At this stage instead of fabricating a new 2×2 array, dumbbells are tuned using a copper tape.

4.2.4 Fabrication Results of the Tuned 2×2 Microstrip Antenna Array with the Three-Dumbbell DGS on Substrate ARLON TC600

Similar to the previous three-dumbbell DGS case, all antenna dimensions are kept the same except the two dumbbells at the top and the bottom of the antennas. If

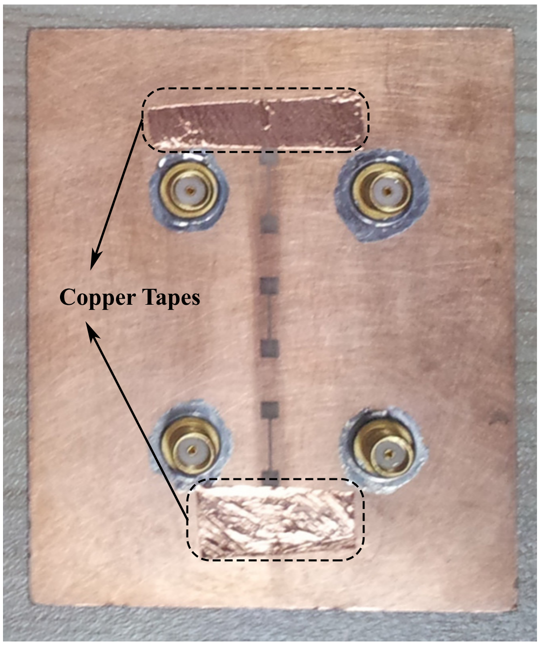

Figure 4.12: Backview of the tuned 2×2 microstrip antenna array with the three-dumbbell DGS.

we were to modify the dumbbell in the middle of the array, modifications would also affect the dumbbells on the top and the bottom of the array. In order to tune the two dumbbells, two pieces of copper tapes are used in such a way that one of them is pasted to the upper dumbbell so that the vertical length of the upper square head of the dumbbell (w) is decreased, and the second one is pasted to the lower dumbbell so that the vertical length of the lower square head of the dumbbell is reduced as shown in Fig. 4.12. Consequently, by reducing the area of the dumbbells mutual coupling reduction between the antenna couples 1-2 and 4-3 is maximized around 5 GHz.

Fig. 4.13 shows the magnitude of the return loss ($|S_{11}|$, $|S_{22}|$, $|S_{33}|$ and $|S_{44}|$ in dB) of the fabricated antennas versus frequency in the presence of the tuned dumbbell DGS and in the absence of DGS. Additionally, Fig. 4.14 shows the magnitude of the mutual coupling ($|S_{21}|$, $|S_{31}|$, $|S_{43}|$, $|S_{42}|$, $|S_{41}|$ and $|S_{32}|$ in dB) versus frequency in the presence of the tuned dumbbell DGS and in the absence of DGS. As seen in Fig. 4.13, after the tuning process, matching of the patch antennas are enhanced significantly. Moreover, Fig. 4.14 reveals that there is 9

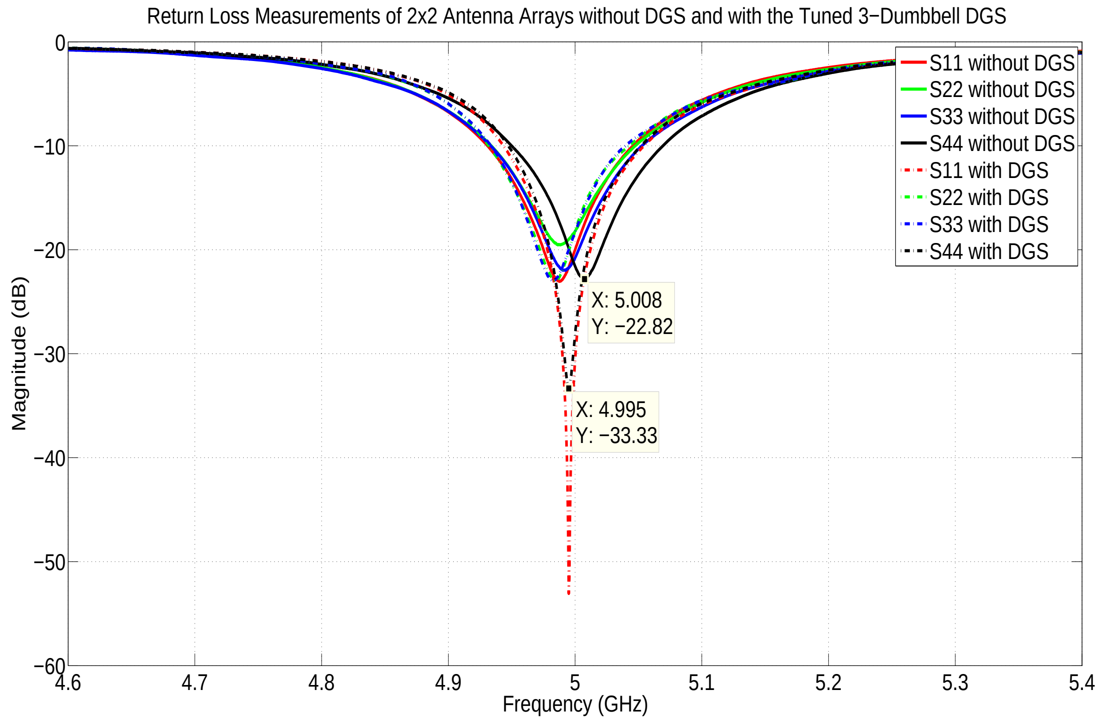

Figure 4.13: Return loss ($|S_{11}|$, $|S_{22}|$, $|S_{33}|$ and $|S_{44}|$ in dB) measurements of the 2×2 antenna array without DGS and with the tuned dumbbell DGS.

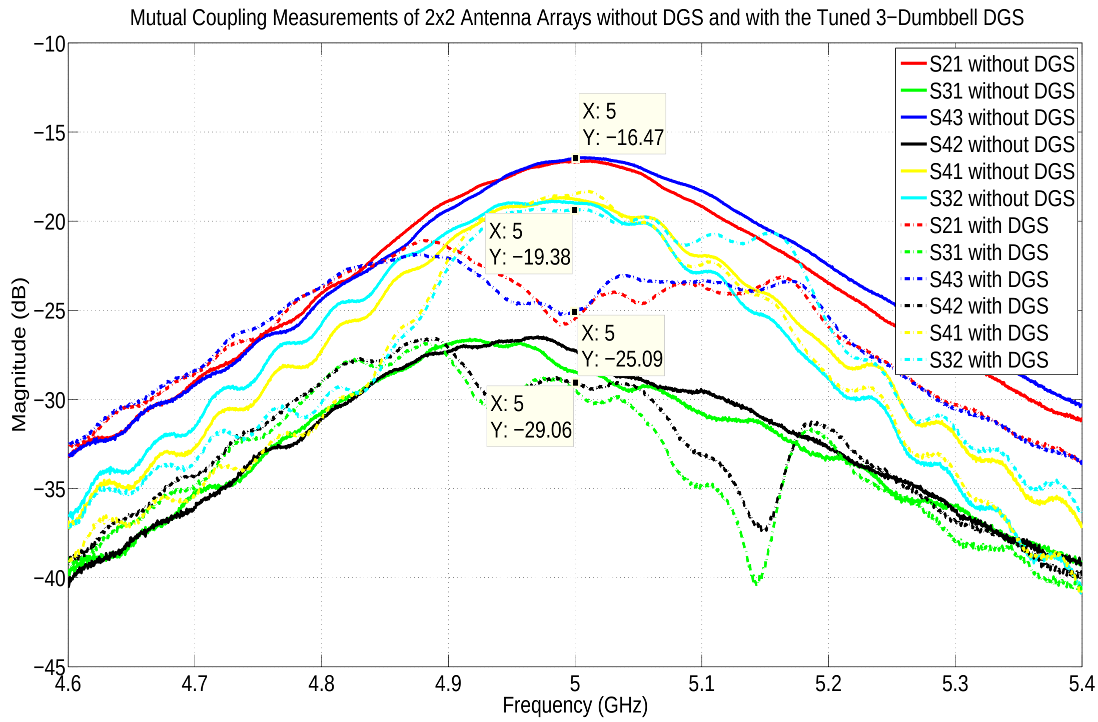

Figure 4.14: Mutual coupling ($|S_{21}|$, $|S_{31}|$, $|S_{43}|$, $|S_{42}|$, $|S_{41}|$ and $|S_{32}|$ in dB) measurements of the 2×2 antenna array without DGS and with the tuned DGS.

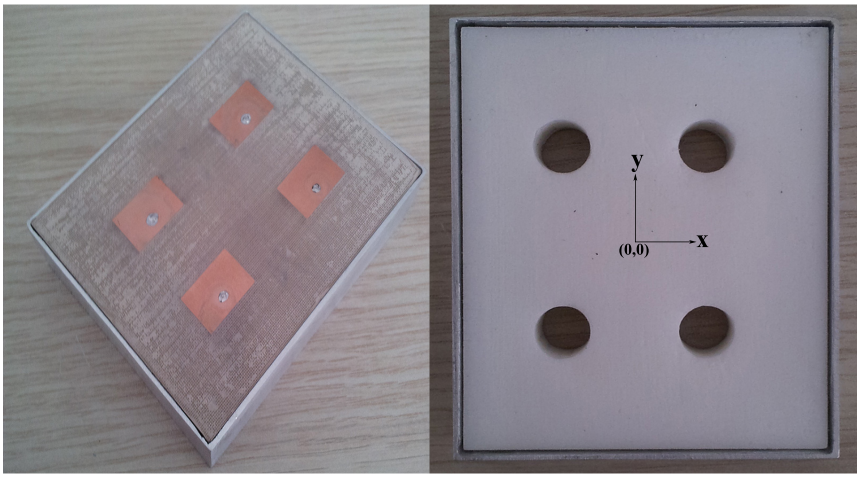

(a) (b)

Figure 4.15: (a) Perspective view of the 2×2 microstrip antenna array with the three-dumbbell DGS and the reflector and cavity combination. (b) Front view of the reflector and cavity combination.

dB mutual coupling reduction at 5 GHz in between the antenna couples 1-2 and 3-4. Besides, the mutual coupling reduction between the antenna couples 3-1 and 4-2 is about 2 dB at 5 GHz whereas there is no mutual coupling reduction between antenna couples 4-1 and 3-2 at 5 GHz.

4.2.5 Fabrication Results of the Tuned 2×2 Microstrip Antenna Array with the Three-Dumbbell DGS, the Reflector and the Cavity on Substrate ARLON TC600

The tuned 2×2 microstrip antenna array presented in the previous subsection is combined with a reflector and a cavity. The dimensions of the cavity are as follows: width × length = 69 mm × 84.72 mm, height = 19.41 mm and the wall thickness is 1.5 mm. Besides, there are four 10 mm wide holes located (-14.955 mm, 17.93 mm), (10.955 mm, 17.93 mm), (-10.955 mm, 17.93 mm) and (-14.955 mm, -17.93 mm), respectively, from the center of the cavity. Note that (x,y)

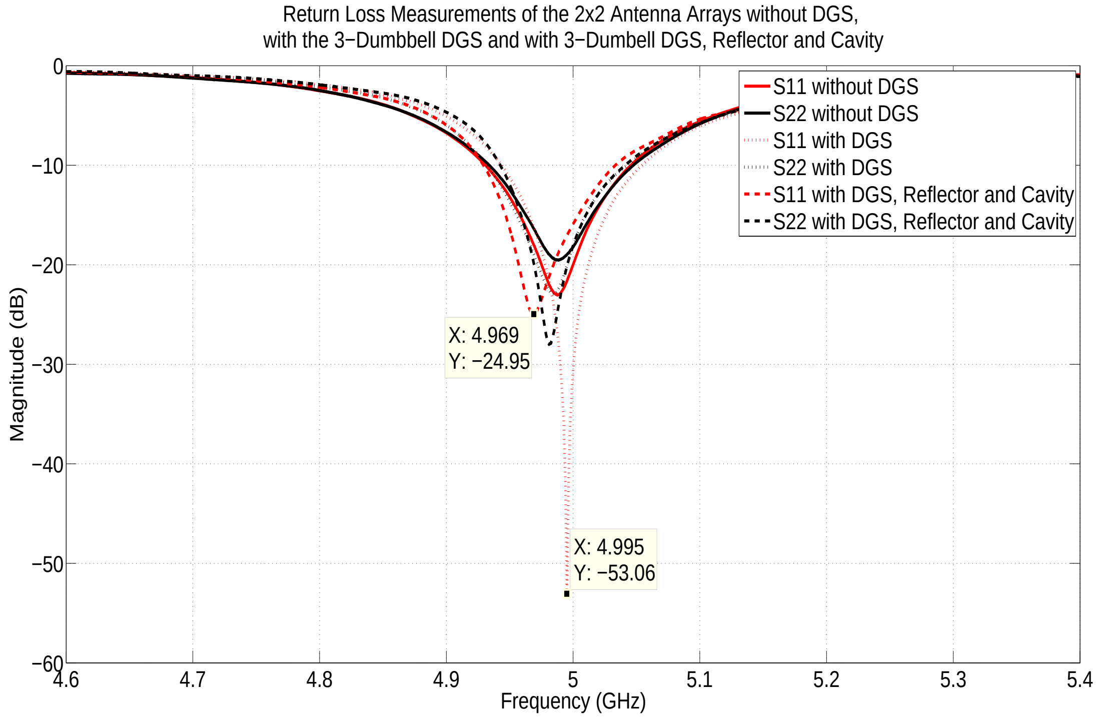

Figure 4.16: Return loss ($|S_{11}|$ and $|S_{22}|$ in dB) measurements of the 2×2 antenna arrays without DGS, with tuned DGS and tuned DGS, reflector and cavity.

represents the × and y axis locations of the each hole assuming that (0,0) is the center of the array.

Figs. 4.16 and 4.17 show the magnitude of the return loss ($|S_{11}|$, $|S_{22}|$, $|S_{33}|$ and $|S_{44}|$ in dB) of the fabricated antennas versus frequency in the presence and the absence of the tuned dumbbell DGS and in the presence of the tuned dumbbell DGS, reflector and the cavity combination. Figs. 4.18, 4.19 and 4.20 show the magnitude of the mutual coupling ($|S_{21}|$, $|S_{43}|$, $|S_{31}|$, $|S_{42}|$, $|S_{41}|$ and $|S_{32}|$ in dB) versus frequency in the presence and the absence of the tuned dumbbell DGS and in the presence of the tuned dumbbell DGS, reflector and the cavity combination. Figs. 4.16 and 4.17 indicate that the frequency shift in the return loss results of the antennas with the three-dumbbell DGS, the reflector and the cavity combination are less than 25 MHz and return losses are enhanced (up to 15 dB). On the other hand, Fig. 4.18 shows that although insertion of the reflector and the cavity combination does not affect the mutual coupling reduction much at 5 GHz, it narrows the suppression bandwidth of the mutual coupling.

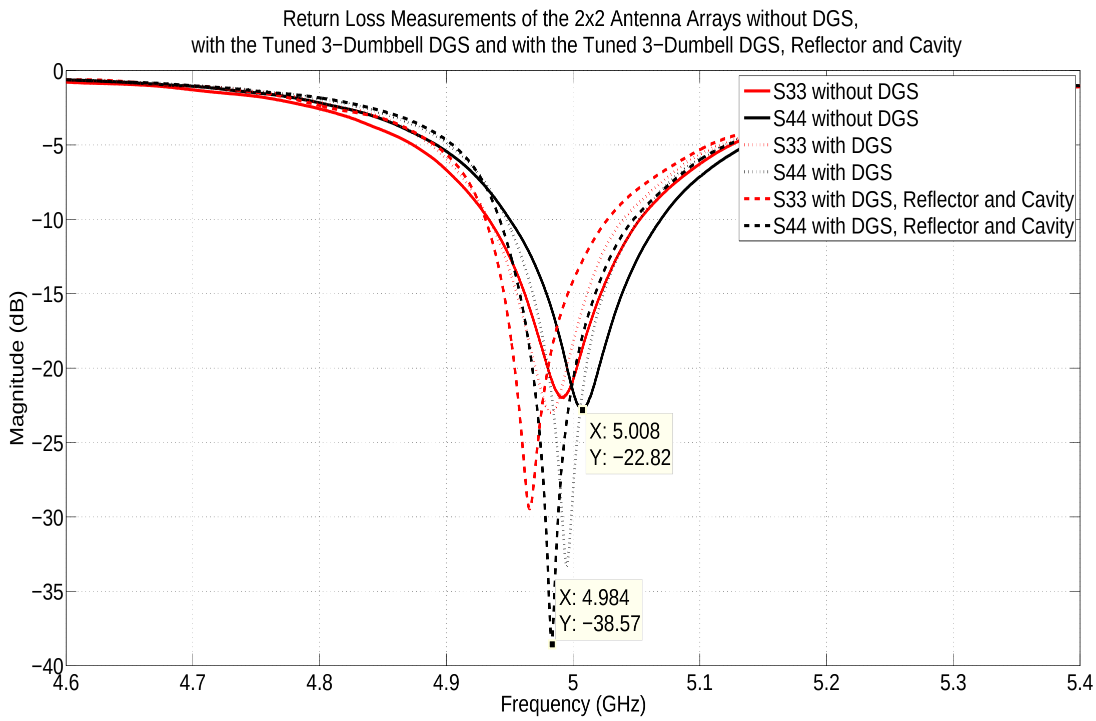

Figure 4.17: Return loss ($|S_{33}|$ and $|S_{44}|$ in dB) measurements of 2×2 antenna arrays without DGS, with tuned DGS and tuned DGS, reflector and cavity.

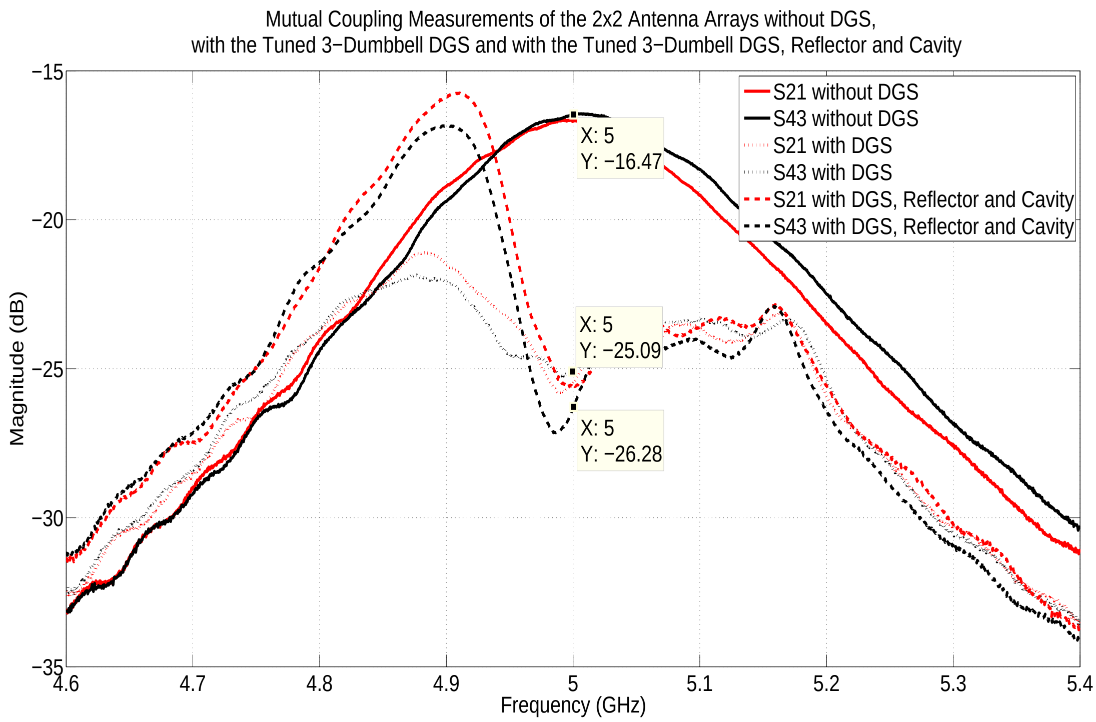

Figure 4.18: Mutual coupling ($|S_{21}|$ and$|S_{43}|$) measurements of 2×2 antenna arrays without DGS, with tuned DGS and tuned DGS plus reflector and cavity.

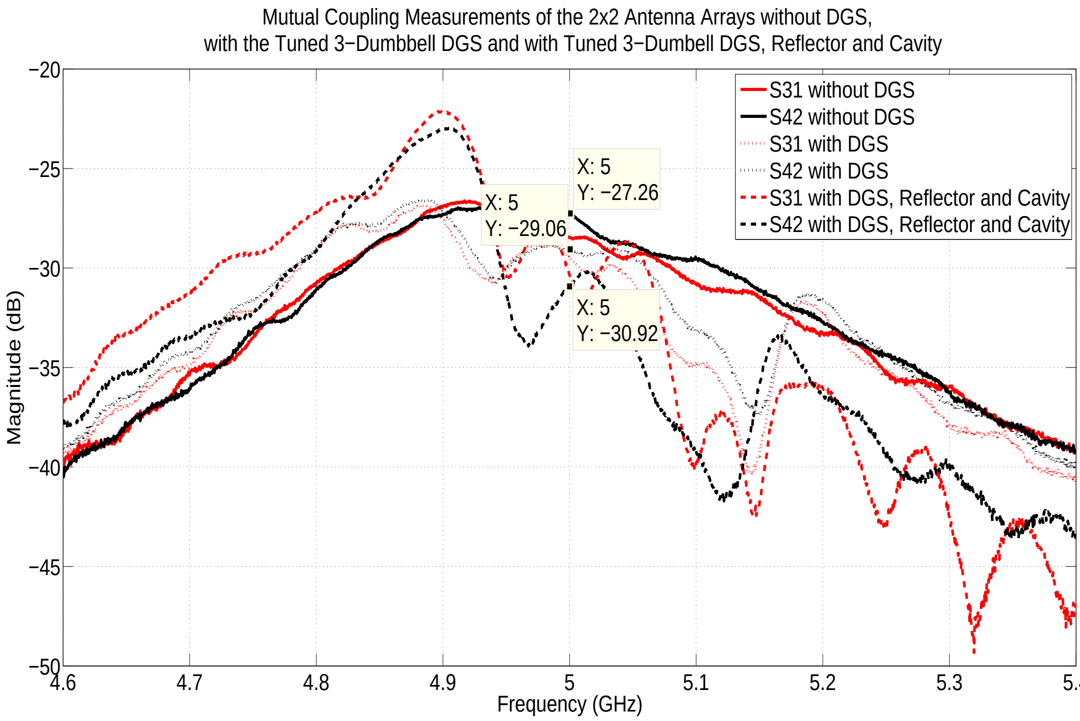

Figure 4.19: Mutual coupling ($|S_{31}|$ and $|S_{42}|$ in dB) measurements of 2×2 antenna arrays without DGS, with the tuned DGS and the tuned DGS plus reflector and cavity.

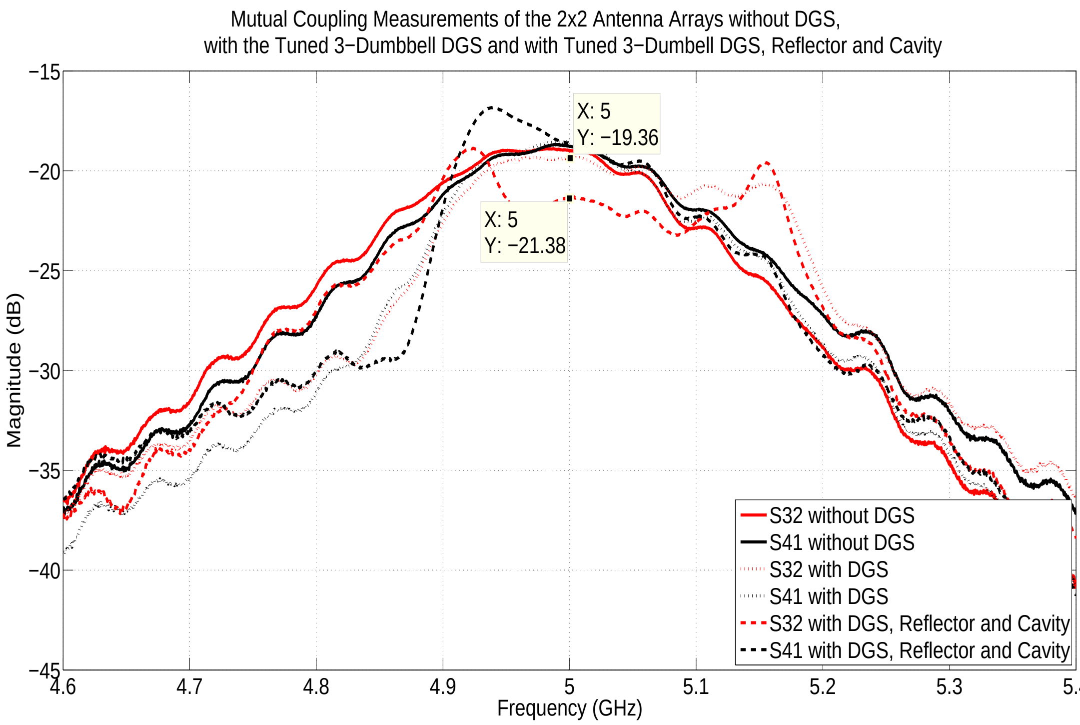

Figure 4.20: Mutual coupling ($|S_{41}|$ and $|S_{32}|$ in dB) measurements of 2×2 antenna arrays without DGS, with the tuned DGS and the tuned DGS plus reflector and cavity.

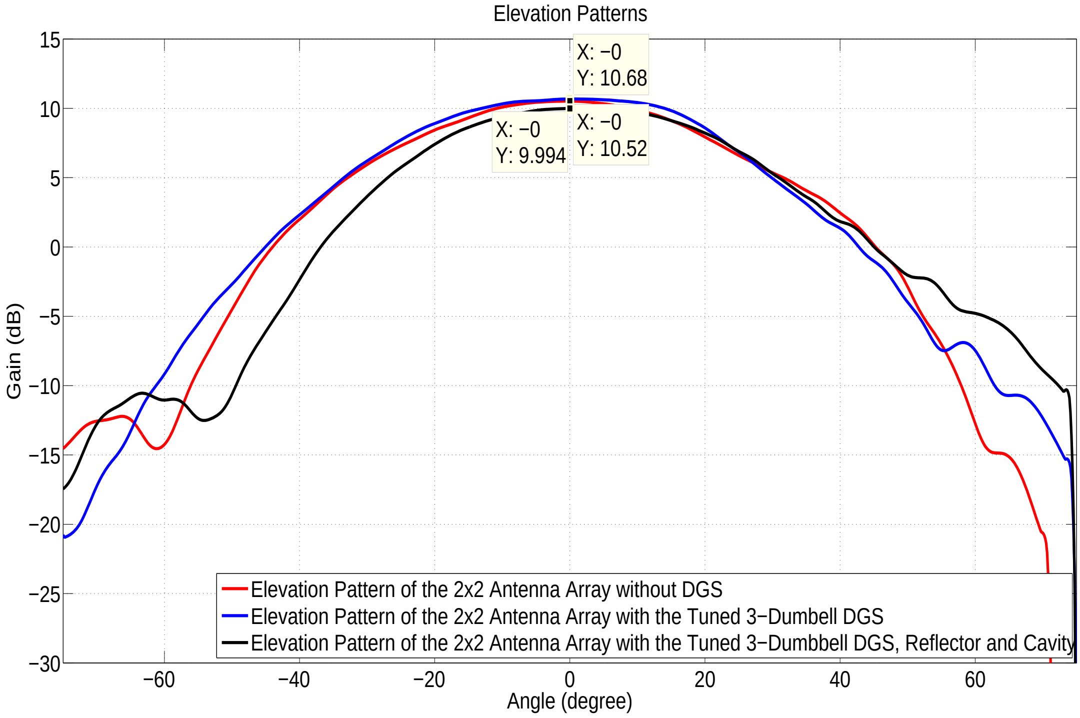

Figure 4.21: Measured elevation patterns of the 2×2 arrays when all patch antennas are fed identically.

Regarding Fig. 4.19, the addition of the reflector and the cavity combination to the array enhances the mutual coupling reduction for frequencies higher than 5 GHz, whereas it increases the mutual coupling for frequencies lower than 5 GHz whereas it only causes minor changes on mutual coupling along H-plane as seen in Fig. 4.20.

Finally, Fig. 4.21 shows the measured elevation patterns of all the 2×2 arrays while Fig. 25 shows the measured azimuth patterns of all the 2×2 arrays. It is seen from the Fig. 4.21 that the gain and the 3-dB beamwidth of the 2×2 antenna array with the three-dumbbell DGS (10.68 dB) and the 2×2 antenna array without DGS (10.52 dB) are very close to each other. Insertion of the reflector and the cavity combination to the antenna does not affect the antenna performance much. Furthermore, Fig. 4.22 indicates that although the gain of the antenna arrays (without DGS, with only three-dumbbell DGS and with the three-dumbbell DGS, reflector and cavity) are close to each other, 3-dB beamwidth of the antenna array becomes 10 degrees smaller. The main reason

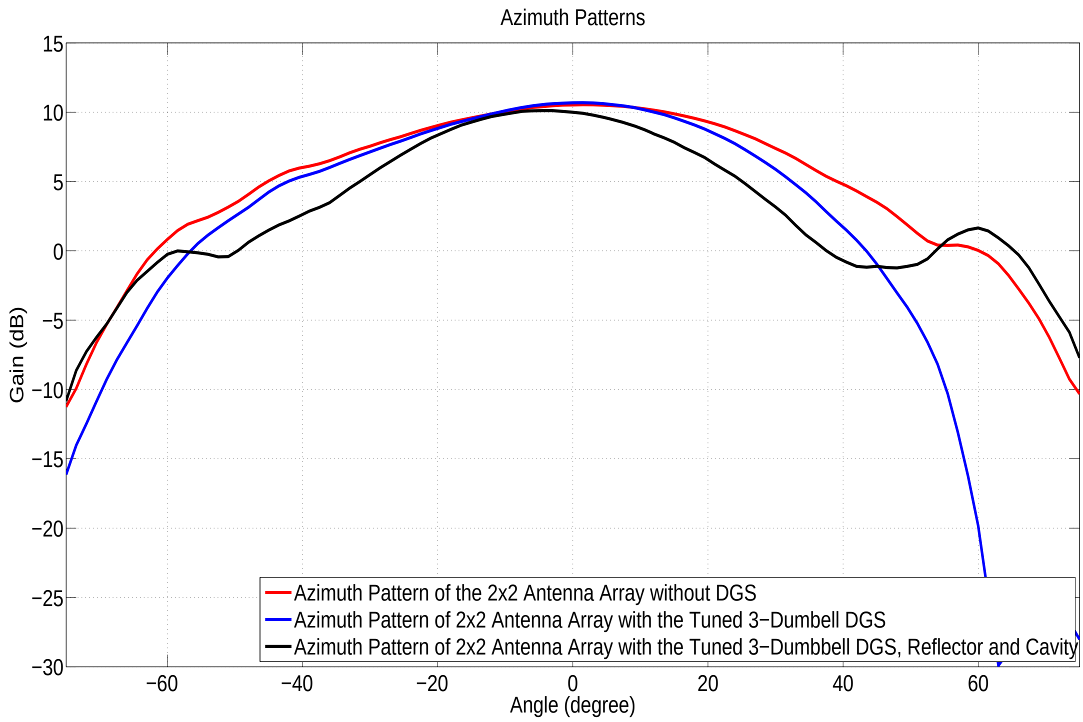

Figure 4.22: Measured azimuth patterns of the 2×2 arrays when all patch antennas are fed identically.

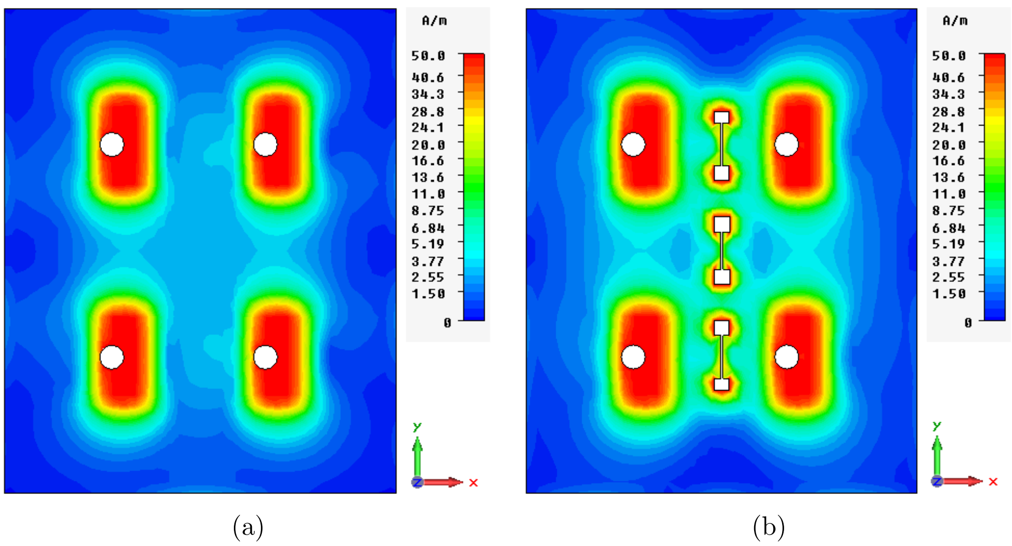

Figure 4.23: (a)Surface current distribution on the ground plane of the antenna array without the DGS. (b)Surface current distribution on the ground plane of the antenna array with the three-dumbbell DGS.

behind it is probably the change in the surface current distribution on the ground plane of the array after the DGS is introduced as seen in Fig. 4.23. Moreover, the cavity and the reflector combination changes the current distribution more and forces it to radiate in main beam direction.

Chapter 5

Conclusions

In this thesis, effects of two types of defected ground structures (DGS), namely the slotted complementary split ring resonator (SCSRR) and the dumbbell on the mutual coupling reduction in the microstrip antenna arrays have been studied extensively.

In Chapter 2, firstly, the band rejection characteristics of the dumbbell and the SCSRR DGS have been investigated by performing parametric studies in the form of simulations. Then, mutual coupling reduction in between two adjacent microstrip patch antennas by using dumbbell and SCSRR DGS has been investigated and fabrication results of these DGSs have been provided. Based on the measurements, it has been observed that introduction of the DGS does not affect the front lobe of the farfield patterns. However, since we did not have the adequate antenna measurement capabilities, we could not measure backlobe of the farfield patterns. Therefore, based on the simulation results, introduction of a DGS to a microstrip antenna causes a significant increase in the backlobe radiation levels since the DGS acts like a microstrip slot antenna.

In Chapter 3, a reflector and a cavity have been introduced to decrease the backlobe radiation level, and the fabrication results for this new structure have been provided. It has been shown that, addition of a reflector and a cavity to the array with the dumbbell DGS does not affect the front lobe of the farfield patterns. Moreover, although we were not able to measure the backlobe of the farfield patterns, a 10 dB reduction in the backlobe radiation is expected based on the simulation results.

In Chapter 4, the final fabricated structure, optimized for the two adjacent microstrip patch antennas, has been extended to a 2×2 microstrip antenna array. Both simulation and fabrication results have been provided regarding some of the array performance merits. It has been demonstrated that although significant amount of mutual coupling reduction has been achieved by using the dumbbell DGS, the reflector and the cavity, no improvement has been observed in the farfield performance merits of the 2×2 microstrip antenna array.

This work indicates that significant mutual coupling reduction can be achieved by using a dumbbell or a SCSRR DGS in the expense of the increased backlobe radiation that may cause undesired multipath signal propagation and interference in RF systems. Although, we have tried to decrease the backlobe radiation by introducing the reflector and the cavity combination to the antenna array with the dumbbell DGS, we do not have any reliable fabrication results on backlobe radiation. As a future work, in order to have more accurate fabrication results, antennas can be fabricated using a Laser LPKF machine instead of a plain LPKF machine and antennas can be measured in a nearfield system that has the ability to measure the backlobe pattern of the antennas.

Bibliography

[1] R. Garg, P. Bhartia, I. Bahl, and A. Ittipiboon, *Microstrip Antenna Design Handbook*. Artech House Antennas and Propagation Library, Boston, MA, 2000.

[2] T. Arima and T. Uno, "Reducing electromagnetic coupling for bistatic subsurface radar using ebg structures," *Antenna Technology, 2009. iWAT 2009. IEEE International Workshop*, pp. 1–4, March 2009.

[3] G. Dadashzadeh, A. Dadgarpour, F. Jolani, and B. Virdee, "Mutual coupling suppression in closely spaced antennas," *Microwaves, Antennas and Propagation, IET*, vol. 5, no. 1, pp. 113–125, January 2011.

[4] M. Bait-Suwailam, O. Siddiqui, and O. Ramahi, "Mutual coupling reduction between microstrip patch antennas using slotted-complementary split-ring resonators," *Antennas and Wireless Propagation Letters, IEEE*, vol. 9, pp. 876–878, 2010.

[5] F. Yang and Y. Rahmat-Samii, "Microstrip antennas integrated with electromagnetic band-gap (ebg) structures: A low mutual coupling design for array applications," *IEEE Trans. Antennas Propagat.*, vol. 51, p. 2939–2949, October 2003.

[6] E. Rajo-Iglesias, O. Quevedo-Teruel, and L. Inclan-Sanchez, "Mutual coupling reduction in patch antenna arrays by using a planar ebg structure and

a multilayer dielectric substrate," *Antennas and Propagation, IEEE Transactions*, vol. 56, no. 6, pp. 1648–1655, June 2008.

[7] M. Salehi, A. Motevasselian, A. Tavakoli, and T. Heidari, "Mutual coupling reduction of microstrip antennas using defected ground structure," *Communication systems, 2006. ICCS 2006. 10th IEEE Singapore International Conference*, vol. 56, no. 6, pp. 1–5, October 2008.

[8] D.-B. Hou, S. Xiao, B.-Z. Wang, J. Jiang, L.; Wang, and W. Hong, "Elimination of scan blindness with compact defected ground structures in microstrip phased array," *Microwaves, Antennas and Propagation, IET*, vol. 3, no. 2, pp. 269–275, March 2009.

[9] D. N. Elsheakh, H. A. Elsadek, E. A. Abdallah, M. F. Iskander, and H. Elhenawy, "Low mutual coupling 2x2 microstrip patch array antenna by using novel shapes of defect ground structure," *Microwave and Optical Technology Letters*, vol. 52, no. 5, pp. 1208–1215, May 2010.

[10] M. Mandal and S. Sanyal, "A novel defected ground structure for planar circuits," *Microwave and Wireless Components Letters, IEEE*, vol. 16, no. 2, pp. 93–95, February 2006.

[11] G. Breed, "An introduction to defected ground structure in microstrip circuit," *High Frequency Electronics*, pp. 50–54, November 2008.

[12] C. A. Balanis, *Antenna Theory: Analysis and Design, 3rd Edition.* John Wiley and Sons Publication, 2005.

[13] W. Lim, H. Jang, and J. Yu, "New method for back lobe suppression of microstrip patch antenna for gps," *Microwave Conference (EuMC), 2010 European*, pp. 679–682, September 2010.

[14] Z. Aijaz and S. Shrivasta, "Tecniques to reduce backlobe of microstrip antenna.," 2010.

[15] A. Kuchar, *Aperture-Coupled Microstrip Patch Antenna Array.* PhD thesis, Technische Universitaet Wien, 1996.

[16] I. Navarro and C. Kai, “A ka-band cavity-enclosed aperture-coupled circular patch antenna and array for millimeter-wave circuit integration.,” *Antennas and Propagation Society International Symposium, 1992. AP-S. 1992 Digest. Held in Conjuction with: URSI Radio Science Meeting and Nuclear EMP Meeting., IEEE*, vol. 1, pp. 313–316, July 1992.

[17] J. Baracco and P. Brachat, “Shielded microstrip subarray with large bandwidth and low cross polarization,” *Antennas and Propagation Society International Symposium, 1992. AP-S. 1992 Digest. Held in Conjuction with: URSI Radio Science Meeting and Nuclear EMP Meeting.*, vol. 1, pp. 293–296, July 1992.

[18] N. Karmakar, “Investigations into a cavity-backed circular-patch antenna,” *Antennas and Propagation, IEEE Transactions*, vol. 50, no. 12, pp. 1706–1715, December 2002.